Send Orders for Reprints to reprints@benthamscience.ae

Current Topics in Medicinal Chemistry, 2015, *15*, 328-344

Soft Matter Assemblies as Nanomedicine Platforms for Cancer Chemotherapy: A Journey from Market Products Towards Novel Approaches

Eliézer Jäger[1] and Fernando C. Giacomelli[2,*]

[1]*Institute of Macromolecular Chemistry, Academy of Sciences of the Czech Republic, Prague, Czech Republic;* [2]*Centro de Ciências Naturais e Humanas, Universidade Federal do ABC, Santo André, Brazil*

Abstract: The current review aims to outline the likely medical applications of nanotechnology and the potential of the emerging field of nanomedicine. Nanomedicine can be defined as the investigation area encompassing the design of diagnostics and therapeutics at the nanoscale, including nanobots, nanobiosensors, nanoparticles and other nanodevices, for the remediation, prevention and diagnosis of a variety of illnesses. The ultimate goal of nanomedicine is to improve patient quality-of-life. Because nanomedicine includes the rational design of an enormous number of nanotechnology-based products focused on miscellaneous diseases, a variety of nanomaterials can be employed. Therefore, this review will focus on recent advances in the manufacture of soft matter-based nanomedicines specifically designed to improve diagnostics and cancer chemotherapy efficacy. It will be particularly highlighted liposomes, polymer-drug conjugates, drug-loaded block copolymer micelles and biodegradable polymeric nanoparticles, emphasizing the current investigations and potential novel approaches towards overcoming the remaining challenges in the field as well as formulations that are in clinical trials and marketed products.

Keywords: Biodegradable nanoparticles, cancer therapy, liposomes, nanomedicine, polymer-drug conjugates, polymeric micelles, pre-clinical and clinical progress of nanomedicines, soft matter.

CANCER AND NANOMEDICINE

Cancer is a leading cause of death throughout the world. The World Health Organization (WHO) estimates that cancer caused and will cause the deaths of 84 million people between 2005 and 2015 [1]. Therefore, current investigations are focused on the discovery of novel, powerful anticarcinogenic compounds as well as the development of novel biomedical technologies to improve conventional therapies. The development of more effective therapies has become a multidisciplinary challenge incorporating materials science, biomedical engineering, life science and clinical practice. The central focus of current research is increasing survival time and enhancing patient quality-of-life. Conventional cancer treatments are currently based on chemotherapy. There are extremely powerful active agents marketed for clinical use, and due to the efficacy of the pharmacological compounds, tissue selectivity is of utmost importance. Unfortunately, for several treatments, a limited dosage reaches the desired tumor site, resulting in ineffective responses. Consequently, current research investigations are devoted to increasing the efficacy and selectivity of known chemotherapeutics rather than discovery of novel compounds. Therefore, it is important to understand tumor site pathophysiology and their distinct features compared with normal tissues. This knowledge is emerging as an alternative for overcoming the lack of specificity of conventional chemotherapeutic treatments. In the next subsection, a brief description of the particular features of tumor microenvironments will be provided, with special consideration given to tumor vasculature and physicochemical properties.

*Address correspondence to this author at the Centro de Ciências Naturais e Humanas, Universidade Federal do ABC, Santo André, Brazil;
Tel: + 55 11 4996 8361; Fax: + 55 11 4996 8361
E-mail: fernando.giacomelli@ufabc.edu.br

PARTICULAR FEATURES OF CANCER SITES

Tumor Vasculature

The cardiovascular system is responsible for the removal of waste metabolites as well as the delivery of nutrients, oxygen, blood and immune cells to all organs and tissues. The cardiovascular system develops through the vasculogenesis and angiogenesis processes. In pathological states, such as cancer and chronic inflammation, the rapid development of tumor cells requires the generation of new blood vessels to supply the necessary amounts of oxygen and nutrients [2]. In such conditions, the vasculature can be abnormally and irregularly activated. Generally, the blood vessel growth is poorly-aligned and has wide fenestrations. Furthermore, tumor tissues usually lack effective lymphatic drainage. Such structural differences compared with normal tissues modify fluid dynamics. The porosity and "leaky" vasculature enable the permeation and retention of macromolecular drugs and aggregates due to impaired lymphatic drainage within tumor sites. This phenomenon is known as the enhanced permeation and retention (EPR) effect. This enhanced retention is primarily caused by a lack of lymphatic vessels in the tissue surrounding tumor sites [3].

1568-0266/15 $58.00+.00

Physicochemical Aspects

In addition to the particular features of tumor vasculature, tumor sites can be distinguished from normal tissues, largely characterized by their slightly acidic extracellular pH (pH_e) and interstitial pressure gradient. The extracellular pH of tumor sites is slightly below 7.4 due to a lack of oxygen. This is caused by an insufficient blood supply because new blood vessel generation is generally not sufficiently rapid during tumor expansion. This leads to a hypoxic state where the tumor locality is deprived of an adequate oxygen supply. The hypoxic condition is generally followed by the production of higher lactic acid amounts, which contribute to the formation of an acidic microenvironment [4]. The pH_e in tumor sites usually ranges from 6.0 to 6.8 depending on the tumor aggressiveness. Conversely, tumor cell intracellular pH (pH_i) is usually similar to values observed in normal tissues, ranging from 4.5 in lysosomes up to 8.0 in mitochondria [5, 6]. Due to the wide pH range from pH_e to pH_i, pH-responsive polymer-based supramolecular assemblies with pK_a 5.0-8.0 are susceptible to drastic changes in their physicochemical properties as a function of pH when travelling from the extracellular to intracellular microenvironments. This knowledge is frequently considered during the development of pH-responsive systems [7-10].

Additionally, high interstitial fluid pressure is a typical feature of solid tumors. Generally, chemotherapeutics and high molecular weight nanocarriers are transferred from the bloodstream to tumor sites *via* convection, and the high interstitial fluid pressure of the tumor reduces the effectiveness of this process, which ultimately leads to a reduction of the uptake fraction of the active agent by the tumor site. Additionally, tumor sites generally maintain a negative interstitial pressure gradient, *i.e.*, the pressure in the tumor core is higher than the surrounding tissue. This property restricts the tumor's drug accumulation capacity because chemotherapeutics and high molecular weight nanocarriers will preferentially flow toward the low pressure region [11, 12].

TUMOR ACCUMULATION OF ACTIVE DRUGS AND NANOPARTICLES

The protection of chemotherapeutics using nanoparticle technology avoids the rapid degradation of active agents. The use of nanoparticles also reduces side-effects and provides higher therapeutic efficacy, sustained drug release and potentially specific accumulation and increased blood circulation half-life [13]. The permeation of active agents and supramolecular delivery systems into tumor sites is facilitated by their specific aforementioned features. Tumor accumulation may be achieved by passive or active targeting depending on the surface properties of the nanocarrier. Truly, active targeting can only occur after passive accumulation.

Passive Targeting and the EPR Effect

The blood vessels in solid tumors possess specific pathophysiological characteristics, such as extensive angiogenesis, irregular architecture with a discontinuous epithelium (hypervasculature), lack of a basal membrane, impaired lymphatic drainage and extensive production of numerous permeability mediators [11, 14]. Almost 30 years ago, two independent studies identified important principles for the selective accumulation of large molecules into tumors [15]. Firstly, the interesting fact that tumor vessels are hyperpermeable to large macromolecules compared with normal vessels [16], and secondly, the fact that large macromolecules can be retained within tumors due to poor clearance [17]. The tumor blood vessels are heterogeneous in their spatial distribution and are dilated, resulting in fenestrations in their capillaries. Depending on tumor type, these fenestrations can reach sizes from 10 nm to 2 μm [15, 18, 19]. Macromolecules and nanocarriers with appropriate dimensions (ranging from 10 to 200 nm) [20] are able to extravasate the large pores in the abnormal tumor vessels resulting in enhanced permeation. Additionally, lymphatic vessels are absent or non-functional in tumors, contributing to dysfunctional lymphatic drainage, resulting also in enhanced retention of permeated macromolecules. The extravasation, with enhanced permeation and retention of macromolecules, results in the mechanism known as the enhanced permeation and retention (EPR) effect, schematically depicted in Fig. (**1**). This phenomenon has been, to date, the basis of nanotechnology platforms for active agent delivery to tumors [21].

The pioneering investigations on this issue were performed by Matsumura and Maeda [17, 22, 23]. These studies were based on biodistribution observations of protein-polymer conjugates (SMANCS), chemical conjugates with a synthetic copolymer of styrene-co-maleic acid (SMA) and various radioactive (^{51}Cr-labeled) proteins of various molecular sizes (12 kDa - 160 kDa). The investigators observed a considerable time-dependent accumulation of SMANCS and plasma proteins with molecular weight greater than 60 kDa [17]. Furthermore, after an injection of a labeled albumin-dye complex (69 kDa), macromolecule accumulation was observed in normal and tumor tissues, with the retention of the complex only observed in tumor tissues.

This unique phenomenon of accumulation in solid tumors is considered a landmark for vectoring chemotherapeutics to tumors. Because these peculiarities are not observed in normal tissues, the discovery of the EPR effect is becoming a promising strategy for the further development of cancer therapies. As a result of the particular anatomical characteristics and pathophysiology of tumor tissues, the concentration of macromolecules and nanocarriers can reach values up to one hundred times higher than the concentration in normal tissues [17, 21, 23, 24]. Nevertheless, it is worth emphasizing that the EPR effect is a highly heterogeneous phenomenon, which can be substantially different from tumor to tumor and from patient to patient [11, 25, 26]. This effect is also time-dependent during treatment [27, 28], which has limited the progress of the development of therapies based on the EPR concept to date [29].

Active Targeting and Surface Functionalization

The term "active targeting" is generally related to the surface functionalization of nanoparticles with targeting ligands to allow binding to specific receptors overexpressed by tumor cells, tumor vasculature or tumor tissues [20, 25 , 30]. Active targeting is also called ligand-mediated targeting and is usually implemented to favor target cell recognition and target cell uptake. Therefore, it does not aim to improve

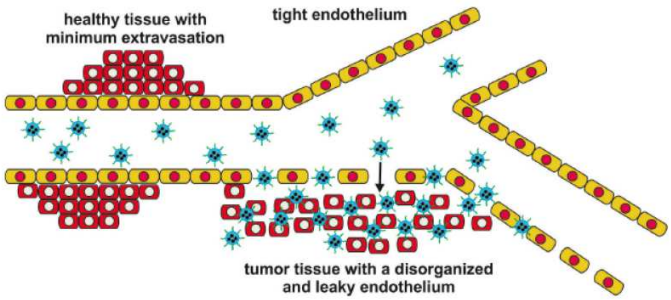

Fig. (1). Schematic representation of passive tumor nanoparticle accumulation due to the enhanced permeation and retention (EPR) effect.

overall tumor accumulation [31, 32]. Ligand-mediated targeting is particularly useful for the intracellular delivery of active agents unable to cross cellular membranes by themselves, such as siRNA and plasmid DNA [33-35]. Ideally, the receptors must be expressed homogeneously in all target cells, and the active-target nanoparticle must be in the tumor vicinity to enhance affinity [31, 36]. The nanoparticle binding affinity is dependent on the nanoparticle architecture, ligand specificity and ligand chemistry [30]. Physicochemical properties, such as size, shape and ligand density, may also possibly affect the efficacy of the active targeting strategy [37, 38].

The nanoparticle internalization is frequently important to increase the efficacy of antitumor agent delivery. The ligand nature is also important with regard to the mechanism of cell uptake. Long circulation times allow effective transport of the nanoparticles to tumor sites and nanoparticle accumulation *via* the EPR effect. Subsequently, specific ligands may contribute to an efficient endocytosis process. Effective internalization of nanoparticles generally leads to an increase in the therapeutic effect [39, 40].

Antibodies (monoclonal antibodies - mAbs or antibody fragments - scFv), proteins, peptides and other molecules, such as nucleic acids, carbohydrates, folate and aptamers, are amongst the most investigated ligands for nanoparticle surface functionalization (Fig. **2**). These categories are described in further detail below.

Antibodies: monoclonal antibodies (mAbs) have been extensively employed as targeting ligands for nanoparticle surface functionalization [20, 30, 41]. Since the first reports of mAb-functionalized liposomes [42, 43], several antibody-targeted NPs have been approved for use clinically [25, 30, 33]. Nevertheless, the manufacture of nanoparticles conjugated to mAbs remains challenging [44]. Because mAbs have a high molecular weight (~ 150 kDa), mAb-functionalization substantially increases the overall size of the nanoparticle (~ 30 nm), hampering their accumulation *via* the EPR effect [31]. Consequently, smaller antibodies and single-chain antibody fragments (scFv) have been investigated to reduce this undesirable effect. The most famous clinical examples to date are doxorubicin PEGylated liposomes (Doxyl®/Caelyx®) surface functionalized with a cetuximab (Erbitux®, anti-EGFR mAb) F(ab') antibody fragment [45]. The usage of scFv is currently preferred because they lack the Fc part of the antibody, preventing rapid recognition by immune system cells and increased clearance. Another example of scFv ligand-mediated targeting is the cationic liposomes SGT-53 developed for the treatment of solid tumors [46].

Peptides and proteins: Peptides have attracted scientific interest because of their smaller size compared with antibodies and also because of their high stability and simple conjugation process to nanoparticles. Small peptides (10-15 amino acids) are able to selectively bind proteins, cells and tissues. The most thoroughly investigated peptides are those containing the arginine-glycine-aspartic acid sequence (Arg-Gly-Asp or RGD). The RGD sequence is capable of binding overexpressed αvβ3 integrin in angiogenic vessels [34]. Cyclic or linear derivatives of the RGD sequence are the most

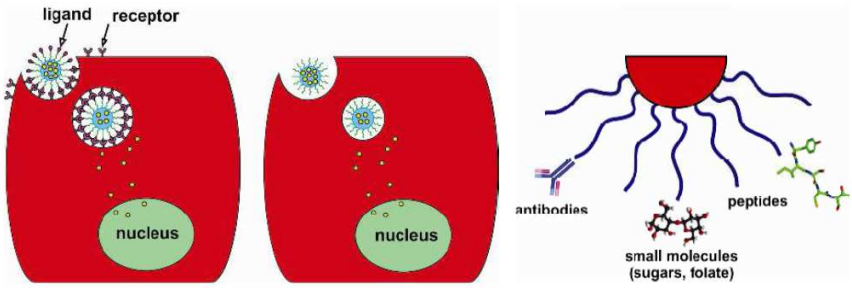

Fig. (2). Schematic representation of cell internalization by endocytosis *via* ligand-mediated targeting (left) and *via* passive targeting (middle). Schematic representation of commonly used targeting ligands for nanoparticle surface functionalization (right).

investigated peptides that can bind to endothelial αvβ3 integrins [25, 34]. Nevertheless, because αvβ3 integrin receptors are also expressed in normal cells and tissues, the main challenges are the isolation of peptides with higher specificity and affinity to antigens or tumor vasculatures. Subsequently, Asn-Gly-Arg (NGR)-containing oligopeptides are potentially interesting because they bind to aminopeptidase N (CD13) receptors present on tumor blood vessels, a receptor that is minimally expressed by the endothelial cells of normal blood vessels [47, 48]. Considering protein surface functionalization, Transferrin (Tf) is the most frequently used biomacromolecule because it strongly binds transferrin-receptors (TfR), which are overexpressed on the surface of cancer cells [30, 49].

Small molecules: small molecules can be easily conjugated to NPs. Moreover, the ligand density can be appropriately selected and there is less evidence of immunogenic effects due to their use *in vivo* [50, 51]. Folate has been widely employed as a targeting ligand because folate receptors are often expressed in a variety of tumor cells [44, 50-52]. Folate binds to folate receptors (FR) with high affinity enabling further nanoparticle internalization *via* receptor-mediated endocytosis [52]. The folate molecule has been used for the functionalization of polymer-drug conjugates [53], liposomes [52, 54], micelles [55] and dendrimers [56]. The main challenge with folate conjugation is that, again, folate receptors are also expressed in normal tissues, such as in the lung, intestine and kidneys [57]. Another limitation to folate conjugation is the density of folate molecules on the NPs surface. The high density of folate groups may reduce the circulation half-life of nanoparticles [54] due to the hydrophobic characteristics of the ligand. Sugars and carbohydrates have also received considerable attention in the field because they are abundant in nature, easily synthesized and have low molecular weight [58, 59]. Specific carbohydrates bind to cell membrane proteins (lectins). Carbohydrate ligands have high affinity, an effective endocytosis process after binding, and high biocompatibility, making them promising for the selective delivery of drugs and nucleic acids [58,60]. The presence of glucose [60], galactose [61] and galactosamine [62] has already been tested with potential success. The ACUPA moiety [63], targeted to prostate specific membrane antigen (PSMA) [64], is an example of the ligand-mediated targeting approach currently under clinical evaluation [65].

It is worth highlighting that the passive accumulation of nanoparticles and macromolecules in tumor sites *via* the EPR effect is the rate-limiting step for efficient ligand-mediated site-specific drug delivery because active targeting cannot occur without prior passive accumulation [25, 48]. Therefore, the antitumor effect of non-ligand-mediated targeting NPs may be further enhanced by the addition of targeting ligands to increase target cell specificity and internalization [20, 25, 30, 33]. For example, tumor models were treated with ~10 nm naked HPMA-based polymeric drug carriers or the same drug carrier functionalized with RGD or NGR. The results indicated that the functionalized assemblies bound rapidly and specifically to tumor blood vessels. However, the amount of drug delivered over time is higher *via* EPR-mediated passive targeting (employing the naked assemblies) [48]. The researchers point out that for long-circulating nanomedicine formulations, the potential of active over passive tumor targeting should not be overestimated.

Intracellular Delivery of Active Agents

Intracellular delivery is required for the therapeutic activity of macromolecules (particularly large and charged molecules, *i.e.*, siRNA, peptides) that cannot enter cells independently [20, 25]. Internalization can be mediated by the incorporation of different molecular classes onto the nanoparticle surface as described above. Ideally, nanomedicines must be able to deliver therapeutic agents into the target cells with minimal cytotoxicity. Subsequent to tumor accumulation and cell internalization, encapsulated therapeutic agents must be released into the pre-nuclear region of damaged cells. This drug release may occur *via* a slow diffusion process or, preferably, *via* an external stimuli or change in environmental condition, such as pH [66]. As previously mentioned, the pH of normal tissues (pH ~ 7.4) is progressively reduced to values near 6.5-6.0 in the extracellular region of tumor sites. High molecular weight nanocarriers are generally cell-internalized *via* endocytosis and during this process early endosomes gradually mature into late endosomes and eventually lysosomes [67]. Therefore, it is essential that the encapsulated therapeutic is released prior to lysosome formation, where the drug may be degraded. Endosome maturation is linked to a drastic reduction of the internal organelle pH to ~ 5.0. Therefore, polymer-based pH-responsive materials, which are susceptible to destabilization in acidic conditions, can ideally circulate in the slightly basic bloodstream and undergo further disintegration in the acidic organelle environment. Polymers containing amino groups with pKa ~ 5.0-7.4 demonstrate this behavior. The reduction in environmental pH may favor fast drug release, avoiding potential drug degradation. Endosomal escape is the most accepted mechanism for explaining the release of macromolecular drugs and high molecular weight nanocarriers from late endosomes due to the proton sponge effect, as outlined in Fig. (**3**).

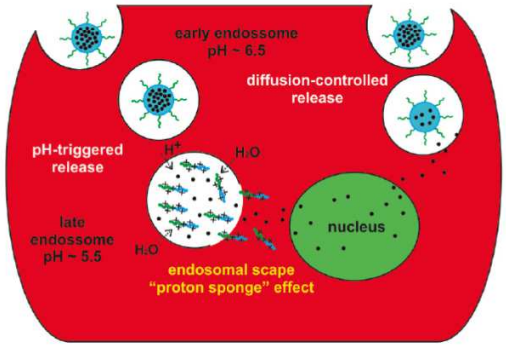

Fig. (3). Schematic representation of the intracellular delivery of active agents *via* diffusion-controlled (right) and pH-triggered (left) mechanisms.

During the proton sponge effect, agents that can be protonated subsidize the ionic concentration increase inside the organelles, stimulating osmotic swelling of late endosomes

causing further membrane rupturing and content release prior to its degradation. Polymers with amine groups have been demonstrated be efficient for the intracellular delivery of active agents and genes due to protonation in acidic environments [68].

CLASSES OF SOFT MATTER BASED NANOMEDICINES FOR CANCER THERAPY

Soft materials are generally susceptible to environmental conditions. Polymer-based nanomedicines can carry, either covalently linked or physically entrapped, an enormous variety of active agents, including drugs, contrast probes, proteins and nucleic acids. Therefore, they can be potentially employed in numerous biomedical applications. Specifically, polymeric assemblies have received substantial attention due their versatility and "smartness", as their structure can be modified *via* external stimuli (temperature, pH, light), allowing nanomedicines to be loaded with and deliver active molecules and contrast agents in a controlled fashion and, ideally, to desired sites.

Current investigations into the updated definition of soft matter based nanomedicines were begun decades ago by the convergence of polymer chemistry, materials engineering, biology and pharmacology. This convergence led to the development of numerous nanomedicines, including, initially, liposomes, followed by polymer-drug conjugates, drug-loaded block copolymer micelles and biodegradable polymeric nanoparticles. In this section, we will describe the most investigated classes of soft matter based nanomedicines and recent advances that have focused on cancer chemotherapy.

Liposomes

Liposomes are self-assembled, swollen vesicular nanostructures produced from amphiphilic phospholipids. The pioneers in the field described these swollen phospholipid systems in 1965 [69], initially naming them bangosomes. These structures were later conceptually established as drug delivery systems and were referred to as liposomes [70]. Liposomal nanostructures have a hydrophilic inner compartment, which made them suitable for hydrophilic cargo, such as DNA and therapeutic proteins [71, 72]. Moreover, hydrophobic agents can be entrapped within the hydrophobic region of the membrane such as schematically represented in Fig. (**4**). However, the loading capacity is limited and sometimes results in unstable entities [73].

Liposomes can be tailored to deliver cargo using a diverse library of lipids that have specific biophysical behaviors [72-74]. The self-assembly can be controlled by lipid selection, providing control over liposome morphology and structure as well as biophysical characteristics. The lipids can be synthetically designed or naturally occurring compounds. Therefore, researchers can select a variety of hydrophilic head groups, specific linkers and hydrophobic moieties [75]. The development of liposomes has led to advances in the nanomedicine field. Many biomedical areas have been covered by liposomal research, including the delivery of drugs, vaccines, imaging and contrast agents [72, 73]. The control of drug-loading, liposome size, the preparation of long-circulating liposomes (PEGylated), triggered release liposomes (by light, heat, pH, ultrasound), ligand-mediated targeted liposomes and liposomes used to co-deliver drugs have been recently reviewed [72, 75].

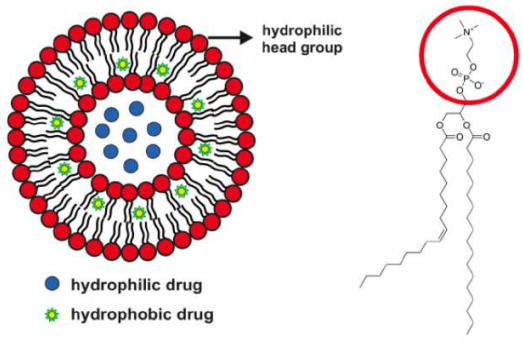

Fig. (4). Schematic representation of a drug-loaded liposome (left) and the molecular structure of a phosphatidylcholine related phospholipid (right).

Among the investigated nanomedicines, liposomes were the first to transition from concept to clinical application and they are now an established technology platform that has considerable clinical acceptance, with several FDA (Food and Drug Administration) approved formulations for cancer chemotherapy. To date, 13 clinically approved liposome agents that generate over $750 million in revenue (2011) are on the market [74].

Biodegradable Polymeric Nanoparticles

Biodegradable polymeric nanoparticles comprise primarily nanospheres and nanocapsules. They are generally employed to deliver hydrophobic active agents that can be dissolved within the oily core of nanocapsules that is surrounded by a polymeric wall or uniformly distributed in the polymeric nanosphere matrix (Fig. **5**) [76].

Biodegradable polymeric nanoparticles were initially reported a few years after liposomes [77] and they have also attracted considerable attention for improving conventional chemotherapies. The development of biodegradable polymeric nanoparticles has rapidly emerged along to establishing methods for the industrial production of polyalkylcyanoacrylate (PACA) [78], poly(lactic acid) (PLA) [79], poly-ε-caprolactone (PCL) [80], poly(lactic-*co*-glycolic acid) (PLGA) [81] and chitosan [82]. Currently, the most investigated systems are manufactured from FDA approved biodegradable polymers, including PLA, PCL and PLGA. The advantage of these polymers is that they are degraded into smaller, biocompatible molecules that are easily cleared *via* conventional paths, such as renal and hepatic filtration [83]. Nanoparticles made by PLGA and PLA are frequently employed to encapsulate anticancer drugs. The biodegradable polyester nanoparticles are generally produced using nanoprecipitation (solvent-shifting) [84] or emulsion-evaporation [85] methods. Recently, more refined techniques have also been used for biodegradable nanoparticle production, such as continuous-flow microfluidics [86] or PRINT (particle replication in nonwetting templates) [87]. Notably, the PRINT process appears to circumvent two of the major remaining

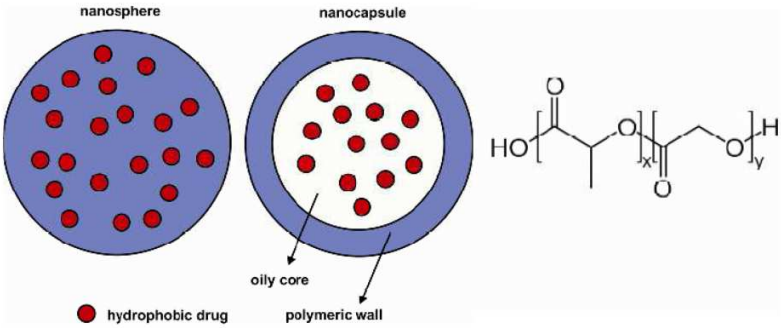

Fig. (5). Schematic representation of a drug-loaded nanosphere (left) and nanocapsule (middle). The molecular structure of PLGA, one widely used biodegradable polymer for biodegradable polymeric nanoparticle production, is also portrayed (right).

difficulties in the polymeric nanoparticles field: low encapsulation efficiency of active agents and control over particle size and dispersity. Studies have demonstrated that PLGA nanoparticles manufactured using the PRINT approach are uniformly distributed with high and efficient loadings of docetaxel (40% *w*/*w* with encapsulation efficiency higher than 90%) [88] and have proven beneficial *in vivo*.[89] Currently, there are reports of PLA and PLGA nanoparticles loaded with several antitumor agents, including paclitaxel, docetaxel and cisplatin [90, 91].

Furthermore, the development of new biodegradable polymers, as alternatives to the aforementioned FDA approved polyesters, has also attracted considerable attention. Recently, there have been reports that the acylation of poly(glycerol adipate) with fatty acids (laurate, stearate and behenate) generates new amphiphilic biodegradable polymers with promising properties for nanoparticulate drug carrier systems [92]. We have recently reported the synthesis and characterization of a new aliphatic biodegradable-based fatty acid copolyester named poly(butylene succinate-*co*-butylene dilinoleate) (PBS:PBDL). Surfactant-free 6-7% $w_{drug}/w_{polymer}$ paclitaxel-loaded nanoparticles (~ 120 nm) that had pronounced stability and relatively rapid degradation were obtained. Cell viability experiments demonstrated that the nanoparticles are fully biocompatible and non-toxic, making them potentially useful for biomedical applications [93].

Nevertheless, despite the favorable biocompatibility of polyester nanoparticles, their largest issue is rapid uptake and clearance immediately after injection unless a stabilizer is used. To circumvent this difficulty, NPs are generally produced with a stabilizing outer shell, generally achieved by grafting, conjugating or adsorbing highly hydrophilic polymers, such as poly(ethylene glycol) (PEG), polysaccharides (usually dextran or chitosan), polyvinyl alcohol (PVA) or poly(N-vinyl-2-pyrrolidone) (PVP). However, although they display excellent non-bioadhesive properties, the aforementioned hydrophilic polymers have specific weaknesses and limitations when used for long-term applications: the polysaccharides are strong activators of the complement system [94], PVA can reduce uptake and sometimes must be avoided due to associated toxicity [95, 96], while PEG and PVP may undergo oxidative degradation [97, 98]. Considerable efforts have been directed towards the development of alternative bioinert polymers to improve the blood circulation time of nanomedicines [99]. Accordingly, PLGA nanoparticles comprising D-α-tocopheryl polyethylene glycol succinate (TPGS) as an emulsifier/surfactant to deliver paclitaxel to cancer cells have been reported [100, 101]. This report detailed considerable improvements to several properties, such as sustained release, maximum tolerated dose [102] and increased bioavailability [103].

Along these same lines, we recently developed stealth polymeric nanoparticles stabilized by a non-immunogenic and non-toxic hydrophilic *N*-(2-hydroxypropyl)methacrylamide (PHPMA) copolymer. Stealth doxorubicin-loaded PBS:PBDL-PHPMA NPs that had pH-dependent doxorubicin (DOX) release were produced and *in-vitro* cytostatic efficacy in EL4 T cell lymphoma was proven [104]. This approach enabled additional combination chemotherapy using simultaneous DOX and docetaxel (DTXL) loading. Supramolecular assemblies comprising a DTXL-loaded PBS:PBDL core and a DOX-conjugated HPMA-based copolymer shell were also produced. The use of nanoparticles simultaneously loaded with DTXL and DOX more efficiently suppressed tumor cell growth in mice with EL-4 T cell lymphoma when compared with the effect of nanoparticles loaded either with DTXL or DOX separately [105].

Finally, the production of PLGA-based block copolymer micelles from PLGA-*b*-PEG and PLA-*b*-PEG has also been reported as a clever strategy to avoid rapid renal clearance of drug-loaded biodegradable polymeric nanoparticles. This category of nanomedicines is discussed in the next section.

Block Copolymer Micelles

Polymeric micelles are generally produced in aqueous solution through the spontaneous self-assembly of amphiphilic block copolymers [106]. Amphiphilic block copolymers are polymers derived from two or more blocks of monomeric species with different chemical properties that are covalently bound. Upon water contact, the hydrophobic blocks tend to reduce their contact with the hydrophilic media leading to the formation of generally spherical structures comprising a hydrophobic core stabilized by a hydrophilic shell. The size of block copolymer micelles is dependent on the polymer characteristics ranging usually from 10 to 100 nm [68, 107]. Therefore, lipophilic agents,

such as hydrophobic drugs, can by solubilized in the micellar core, significantly affecting its concentration in aqueous media. The encapsulation efficiency is dependent on several parameters, including drug and polymer solubility parameters, size, shape and physical state of the hydrophobic guest molecule, as well as block copolymer length and volume ratio [68, 108]. Additionally, the active agents can also be attached to the hydrophobic segment of block copolymers *via* an environmentally responsive chemical bond. Therefore, controlled drug release can be achieved by triggering the chemical bond or by using polymers susceptible to environmental conditions, such as biological stimuli (pH-responsive, redox-responsive, enzyme-responsive polymers) or external stimuli (thermo-responsive, photo-responsive polymers) [68, 109-111].

Currently, most investigations are centered on biodegradable polymeric micelles because their degradability property circumvents micelle accumulation, which may lead to long-term toxicity. The employment of pH-responsive micelles is another clever approach because the polymers may be triggered and destabilized in response to the slightly acidic tumor microenvironment, enabling rapid release of active agents upon arrival at the desired site and simplifying renal clearance. In such way, we recently devised block copolymers to produce nanoparticles comprising a PDPA (poly[2-(diisopropylamino)-ethyl methacrylate]) core (Fig. **6**). PDPA is a promising smart material for the construction of tumor-targeting drug delivery polymeric nanocarriers because it is able to encapsulate hydrophobic anticancer drugs and it undergoes a sharp hydrophobic-hydrophilic pH-induced transition within a pH range that is desirable for tumor-targeting drug delivery [112]. PDPA is one of the few polymers that can be loaded and quickly release hydrophobic guest molecules at specific tumor sites *via* a pH-triggered pathway at slightly acidic conditions [113, 114].

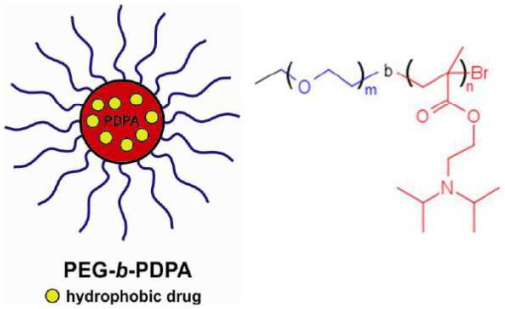

Fig. (6). Schematic representation of a pH-responsive PEG-*b*-PDPA drug-loaded block copolymer micelle (left) and the molecular structure of the block copolymer PEG-*b*-PDPA (right).

Recent advances have been promoted by using other pH-responsive block copolymers. Supramolecular assemblies based on poly(lysine) and poly(histidine) may also have potential success because their pKa is reportedly approximately 6.0-7.0 [115, 116]. To our knowledge, there are no market products based on these special polymers; however, polymeric micelles based on poly(lysine) are already being examined in clinical trials.

Polymer-Drug Conjugates

The conjugation of drugs to synthetic and natural macromolecules (Fig. **7**) has been a long-term issue [73, 117-119]. The early conjugates reported were based on polyvinylpyrrolidone (PVP) conjugated to mescaline *via* a dipeptide (GL) spacer and based on poly(N-vinylpyrrolidone) conjugated to various antibiotics [118-119]. Nevertheless, only in the mid-seventies were polymer-drug conjugates envisaged as nanomedicines [73 , 117, 120]. Ideally, polymer-drug conjugates should comprise a biocompatible polymer backbone as a vehicle and the active agent, which is bound to the polymer chain *via* a biologically responsive linker. Investigations into polymer-drug conjugates have become a fast and growing field with many conjugates being developed using a variety of responsive linkers. Undeniably, the optimization of polymer-drug linkers remains a main issue in the field. Polymer-drug linkers must be stable during bloodstream circulation and simultaneously should be able to release the conjugated drug at optimal rates upon arrival at the target site [117, 121]. The linkers are usually selected from the classes of cis-aconityl [122], hydrazone [123] (Fig. **7**), acetal [124], peptidyl [125], among other organic linkers [126].

Currently, the most intensely investigated polymer-drug conjugates are based upon highly hydrophilic polymers, such as PEG, PHPMA, poly(vinyl-pyrrolidone), poly(amino acids) and dextrans. The main advantages of these polymer-drug conjugates compared with the administration of the related free drug rely on the higher aqueous solubility of the attached hydrophobic drugs, the potential triggered release (pH, enzymes), enhanced drug bioavailability, prolonged plasma half-life, protection of the active agents against degradation and modified biodistribution (pharmacokinetics and pharmacodynamics). Linear, branched, star-like and multi-armed PEG-drug [127, 128] and HPMA-drug [119, 129, 130] conjugates have been previously investigated. Actually, linear PEG-drug conjugates are the simplest and most investigated systems. The active small molecules are usually conjugated to the distal end of the PEG chain. However, the primary limitation to this approach is the number of available conjugation sites. Consequently, branched and forked PEG-drug conjugates have been synthesized for the same purpose [127, 128, 131]. Similarly, multi-armed PEG has been widely investigated due to the presence of multi-hydroxyl or functional groups, increasing the number of available conjugation sites. Several multi-armed PEG-drug conjugates, such as NKTR-102 (PEG-irinotecan), EZN-2208 (PEG-SN38) and NKTR-105 (PEG-docetaxel), have entered into clinical trials for solid tumor treatment [127, 132].

PHPMA-drug conjugates are also frequently investigated. HPMA-DOX was the first synthetic polymer-drug conjugate to progress into clinical trials. The anticancer drug doxorubicin was attached to the HPMA copolymer *via* a biodegradable tetrapeptide spacer (GFLG). Clinical trials examining this polymer-drug conjugate initiated in the early 1990s [117,120]. In the past few years, the selection of polymeric macromolecular carriers, desired target (intracellular, endothelium, etc.) [133, 134], type of conjugation (direct or indirect) [121,135], linker chemistry [135, 136] and molecular weight [129] of PHPMA-drug conjugates has been

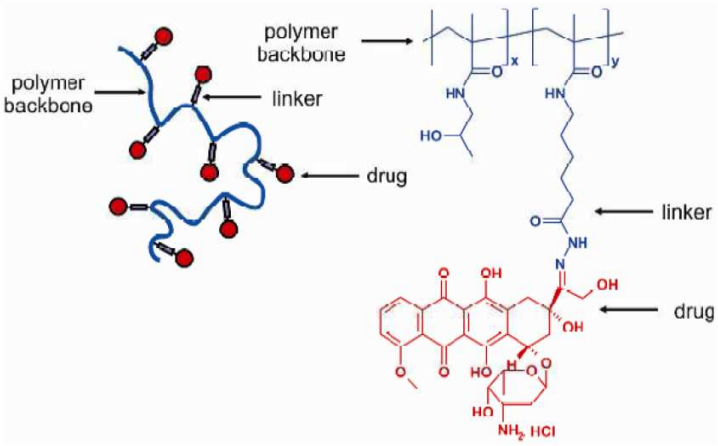

Fig. (7). Schematic representation of a polymer-drug conjugate (left) and the molecular structure of the polymer-drug conjugate PHPMA-DOX, (right) where the active agent doxorubicin is covalently bound to poly[N-(2-Hydroxypropyl) methacrylamide] (PHPMA) *via* a pH-responsive hydrazone bond (R_1R_2C=NNH-).

extensively investigated to improve antitumor efficacy. Furthermore, the drug combination approach, where different agents are bound to the same macromolecular therapeutic, has been successfully reported, *i.e.*, PHPMA-doxorubicin-aminoglutethimide [137], PHPMA-DOX-dexamethasone [138], PHPMA-DOX-gemcitabine [139], and PHPMA-DOX-Mitomycin C [140]. Subsequent investigations resulted in second-generation anticancer nanomedicines based on higher molecular weight HPMA-drug carriers containing enzymatically degradable bonds in the polymer backbone [118, 119]. The enhanced activity of the second-generation conjugates has been proven *in vivo* [130, 141].

Lastly, poly(amino acids)-drug conjugates based on poly(L-lysine) (PLL), poly(-aspartic acid) (PAA) and poly(L-glutamic acid) (PGA) have also been considered. PGA is the most accepted polymer in this class [142]. The pendant free γ-carboxyl group on each repeating unit of L-glutamic acid offers functional sites for drug attachment. Drug release is simplified because PGA itself biodegrades. PGA-paclitaxel (Opaxio™) and PGA-camptothecin have advanced to clinical trials.

PRE-CLINICAL AND CLINICAL PROGRESS OF SOFT MATTER BASED NANOMEDICINES FOR CANCER THERAPY

Considering clinical progress, although liposomes are the category with the highest number of marketed products and several more in clinical trials, there are a number of block copolymer micelles, polymer-drug conjugates and biodegradable polymeric nanoparticles currently in phase I/II, III and IV clinical trials to gain market approval. Some of these compounds have already received clinical status in specific countries. In this section, we will highlight the current status of each category of soft matter based nanomedicines designed for cancer chemotherapy described above, with regard to clinical trials as well as formulations already in clinical use.

Liposomes

The liposome class has 5 marketed products and several more in clinical trials [71]. Doxil®/Caelyx™ (doxorubicin-loaded PEGylated liposome) was approved for the treatment of Kaposi's sarcoma (1995), ovarian cancer (1999), metastatic breast cancer (2003) and multiple myeloma (2007) [143]. The greatest advantage of Doxil® compared with free drug administration is reduced cardiotoxicity [144, 145], although its efficacy in breast cancer treatment is comparable to conventional doxorubicin chemotherapy [146]. Considering AIDS-associated Kaposi's sarcoma, Doxil® increased effectiveness from 25 to 46% compared with conventional chemotherapy, where adriamycin, bleomycin and vincristine (ABV) are employed [147]. However, when compared with paclitaxel for the treatment of AIDS-associated Kaposi's sarcoma [148] and topotecan for the treatment of recurrent or non-responsive ovarian cancer [149], Doxil® demonstrated only modest improvements in survival rates [150].

Myocet® is a non-PEGylated liposomal doxorubicin formulation approved in Europe and Canada for the treatment of metastatic breast cancer. The formulation has demonstrated similar benefits as Doxil®/Caelyx™ [151]. Daunoxome® is a non-PEGylated liposomal daunorubicin formulation approved for the treatment of AIDS-associated Kaposi's sarcoma (1996) with similar efficacy compared with the ABV treatment [152]. Depocyt® is a liposomal cytarabine formulation indicated for intrathecal treatment of lymphomatous meningitis. Depocyt® investigations noted equivalent response rates compared with methotrexate treatment with a significantly less demanding dosing schedule [153]. The most recent liposomal drug approved by the FDA (Marqibo®) is a liposomal formulation of vincristine sulfate (VCR) that was designed to overcome the dosing and pharmacokinetic limitations of VCR. Marqibo® was approved in 2012 for acute lymphoblastic leukemia treatment [154].

Concerning formulations undergoing Phase III clinical trials, Lipoplatin® is a PEGylated cisplatin liposomal formu-

lation [155] that substantially reduces side effects compared with free-drug administration during the treatment of advanced squamous cell carcinoma of the head and neck [156] or when administered in combination (Lipoplatin®/gemcitabine [157] or Lipoplatin®/paclitaxel [158]) for the treatment of non-small cell lung cancer (NSCLC). Thermodox® is a temperature-sensitive PEGylated liposomal doxorubicin formulation designed to treat recurrent breast cancer (Phase II) that has yielded significant efficacy improvements [159]. However, ThermoDox® failed to meet its primary endpoint in a Phase III clinical trial in patients with hepatocellular carcinoma (HCC) [160].

Ligand-mediated targeted liposome formulations have also entered clinic trials [33]. A few examples are an oxaliplatin-loaded transferrin-targeted liposome (MBP 426) in a Phase Ib/II trial for the treatment of second line gastric, gastroesophageal or esophageal adenocarcinomas in combination with leucovorin and fluorouracil [161]. The liposomal doxorubicin targeted *via* anti-Her2-scFv antibody fragments (MM-302) [162] has progressed to Phase I, and the doxorubicin-loaded anti-EGFR immunoliposome (anti-EGFR ILs-Dox) recently underwent a Phase I clinical trial in patients with advanced solid tumors [45], which demonstrated one complete response, one partial response and ten stable diseases over a period of 2-12 months in 26 patients.

Biodegradable Polymeric Nanoparticles

Concerning biodegradable polymeric nanoparticles, doxorubicin loaded polyalkylcyanoacrylate (PIHCA) nanoparticles (Transdrug™/Livatag®) used to treat multidrug resistant hepatocarcinoma is one example that has progressed to clinical trials (currently in phase III) [163]. Transdrug™ allows doxorubicin to overcome MDR pumps [164], and its antitumour efficacy in patients with advanced HCC has been confirmed [165]. In Phase II/III, Transdrug™ significantly increased survival rates in patients with advanced HCC (32 months compared with 15 months in patients receiving standard-of-care-treatment) [166]. Despite the significant 17 months difference, the clinical trial was interrupted due to frequent and severe pulmonary adverse events. Currently, the formulation is recruiting participants into Phase III clinical trials to determine whether Transdrug™ is effective treating patients suffering from advanced HCC after failure or intolerance to Sorafenib [167].

Correspondingly, promising results have been demonstrated for HCC treatment using mitoxantrone (dihydroxyanthracenedione, DHAD) loaded into polybutylcyanoacrylate (DHAD-PBCA) nanoparticles (47% of DHAD) [168]. The activity and toxicity of these NPs against HCC were evaluated in a randomized multicenter Phase II study [169]. The DHAD-PBCA NPs increased cytotoxicity in hepatic tumors and extended the mean survival time from 3.23 months (patients receiving free DHAD) to 5.46 months.

Block Copolymer Micelles

There are several drug-loaded polymeric micelles currently in Phase I/II, III and IV clinical trials, specifically for the delivery of DOX and PTX [170, 171]. To the best of our knowledge, Genexol®-PM, a PTX formulation based on monomethoxy-PEG-*b*-poly(D,L-lactide) (MPEG-PDLLA), is the only formulation approved in this category (South Korea, Bulgaria and Hungary) for the treatment of cancer (breast, lung and ovarian cancer). The Genexol®-PM efficacy has been demonstrated in a Phase II clinical trial in patients with breast cancer [172] and in patients with advanced NSCLC when combined with cisplatin [173]. Peripheral neuropathy and myalgia adverse events were observed. However, acute hypersensitivity reactions, which are common during Taxol® and Taxotere® treatment, were not observed [172]. Genexol®-PM is currently undergoing Phase IV clinical trials [174] and therapies combined with other antitumor drugs are being developed [175].

Regarding poly(amino acids)-based block copolymer micelles, NK105 is a PTX-loaded micellar system prepared from PEG-poly(aspartic acid) (PEG-*b*-Pas), where PTX is physically entrapped (~ 23% $w_{drug}/w_{polymer}$). The nanocarrier-based formulation underwent a Phase II clinical trial against advanced or recurrent gastric cancer in 2010, demonstrating modest activity and tolerability [176]. Phase III studies in patients with breast cancer are being designed to elucidate its survival benefits [177]. Cisplatin incorporation into PEG-*b*-PGlu micelles resulted in the NC-6004 formulation. The cisplatin was incorporated *via* polymer-metal complex-formation [178]. During Phase I clinical trials in patients with solid tumors it reduced toxicity and stabilized the disease (7/17 patients) [179]. A Phase I/II clinical trial of NC-6004 combined with gemcitabine for metastatic pancreatic cancer treatment was conducted in Asia; the results demonstrated the good tolerability and acceptable efficacy of the combination [171]. Phase III studies of NC-6004 in combination with gemcitabine to determine their efficacy *versus* gemcitabine alone in patients with advanced or metastatic pancreatic cancer are currently being designed [180].

Similarly, in the formulation NK012 the agent 7-ethyl-10-hydroxy-camptothecin is chemically conjugated to the PGlu segment of PEG-*b*-PGlu, and the self-assembly resulted in 20 nm sized drug-loaded block copolymer micelles. This formulation demonstrated promising antitumor activity in Phase I clinical trials in patients with advanced solid tumors [181]. The safety and efficacy of NK012 for advanced and metastatic triple negative breast cancer treatment is ongoing (Phase II) [182], as well as, for colorectal cancer treatment in combination with 5-fluorouracil (Phase I) [183]. Similarly, NK911 is a micellar nanocarrier (~ 40 nm) consisting of a PEG-poly(aspartic acid) block copolymer conjugated to doxorubicin. Phase I investigations demonstrated a partial response (1/23 patients) or stable disease (8/23) in patients with metastatic pancreatic cancer [184]. However, its plasma clearance was ~ 400-fold higher compared with Doxil® suggesting that the NK911 has lower stability in the bloodstream. The formulation NC6300 consists of epirubicin covalently bound to PEG-*b*-polyaspartate block copolymers *via* an acid-labile hydrazone bond. This conjugate produces 40-80 nm micellar structures and is intended to be indicated for breast cancer. In pre-clinical studies, prolonged blood circulation with preferential accumulation in human liver and breast cancer xenograft models was reported [185], along with extended antitumor effects with reduced epirubicin cardiotoxicity in mice bearing Hep3B liver orthotopic tumors [186]. Following preclinical evaluations, a Phase I trial is underway in Japan in patients with advanced or metastatic solid tumors [187].

The micellar doxorubicin formulation SP1049C has been produced from the well-known class of Pluronic® micelles. This nanocarrier has demonstrated higher antitumor effects compared with the free parent drug [188, 189]. SP1049C safety and efficacy was demonstrated in Phase II investigations in patients with advanced adenocarcinoma of the esophagus and gastroesophageal junction (9/19 patients had a partial response and 8/19 patients had either a minor response or stable disease) [190].

The aptamer-conjugated PLGA-PEG-docetaxel nanoparticle (BIND-014) is an example of a ligand-mediated targeting nanocarrier able to recognize PSMA (prostate-specific membrane antigen) expressed on the cancer cell surface. This formulation was well tolerated with predictable and manageable toxicities in Phase I clinical trials [30]. These promising results are currently being continued in a Phase II trial in patients with advanced or metastatic solid cancers [191] or with metastatic castration-resistant prostate cancer [192].

Polymer-Drug Conjugates

A considerable number of polymer-drug conjugates have entered clinical trials; however, few are commercially available. Oncaspar® (mPEG-L-Asparaginase), which is an antineoplastic formulation for acute lymphoblastic leukemia treatment, is among the first polymer-drug conjugates to be clinically tested and approved by the FDA (1994). Pegfilgrastim (Neulasta®) is a PEGylated form of the recombinant human granulocyte colony-stimulating factor (GCSF) analog filgrastim. This conjugate was prepared by coupling the drug onto a 20 kDa PEG on the *N*-terminus of the filgrastim protein. It entered into clinical use in 2002 [127, 193]. Many PEG-drug and PEG-protein conjugates have been later approved for distinct diseases [127, 128, 194]. Regarding clinical studies, NKTR-102 (PEG-irinotecan) is a topoisomerase I inhibitor polymer-drug conjugate engineered by attaching irinotecan molecules to a multi-armed PEG using a biodegradable linker. The formulation is currently in a Phase II clinical trial for high grade gliomas [195] and under a Phase III trial in patients with recurrent or metastatic breast cancer [196]. The same polymer structure was employed to deliver docetaxel (NKTR-105) and 7-ethyl-10-hydroxy-camptothecin (EZN-2208). The EZN-2208 formulation is currently in ongoing Phase II studies in patients with metastatic breast cancer [197] and NKTR-105 is in a Phase I clinical trial in patients with different types of solid tumors [198]. Another promising PEG-drug conjugate is CRLX101. This formulation is a PEG-modified β-cyclodextrin-camptothecin conjugate (10-12 wt% CPT loading) capable of increasing solubility > 1000-fold compared with the parent drug CPT, enhancing the pharmacodynamics and efficacy of camptothecin [199]. CRLX101 was recently developed and is currently undergoing Phase II clinical studies in patients with advanced NSCLC [200].

Concerning conjugation to poly(amino acids), in paclitaxel poliglumex (PPX; Opaxio®) the active agent is linked to the biodegradable polymer poly-L-glutamic acid *via* the lysosomal triggered enzyme cathepsin B. However, this formulation has not demonstrated higher efficacy in NSCLC patients compared with the single parent drugs (gemcitabine or vinorelbine) [201]. PPX demonstrated similar overall survival rates compared with docetaxel and demonstrates favorable medication elimination properties to prevent the hypersensitivity reactions associated with their routine use. However, neurotoxicity (210 $mg.m^2$ dose) was common in NSCLC patients treated with PPX (Phase III) [202]. Additionally, a Phase III study in patients with advanced solid tumors is currently ongoing [203]. Camptothecin has also been conjugated to poly(L-glutamic acid) *via* a glycine linker (CT-2106) [204] with promising Phase I clinical study results for the treatment of advanced solid tumors (pancreatic, colorectal and NSCLC). This polymer-drug conjugate is in a Phase II clinical trial in advanced ovarian cancer patients (as a single agent) [205] and Phase I/II in colorectal cancer patients (in combination with 5-FU and folic acid) [206].

Regarding PHPMA-based polymer-drug conjugates, HPMA-*co*-MA-GFLG-doxorubicin was the first in this category to undergo clinical trials (1994) [117]. The poly(HPMA-*co*-MA-GFLG-doxorubicin) (PK1) were demonstrated to be equally effective and less toxic compared with free DOX in Phase I clinical trials in patients with refractory or resistant cancers [207]. This formulation also underwent a Phase II trial in patients with breast, NSCLC and colon cancers, demonstrating positive responses in 6/62 patients and limited side effects [208]. The PHPMA copolymer-Gly-Phe-Leu-Gly-doxorubicin containing galactosamine (PK2) became the first targeted polymer-drug conjugate to enter clinical studies [117]. The hepatic targeting was confirmed using ^{123}I-labeled PK2 co-injected with unlabeled PK2; however, there was major accumulation in the healthy liver rather than the hepatic tumor [62]. In a Phase I/II clinical trial in primary hepatocellular carcinoma patients, a partial response (2/23 patients), reduced tumor volume (1/23 patients) and stable disease (11/23 patients) was reported. Finally, PHMPA copolymer-platinate (AP5346, ProLindac™) is a diaminocyclohexane (DACH) platinum polymer prodrug that has demonstrated reduced toxicity and similar or, likely, superior efficacy than oxaliplatin for the treatment of solid tumors. This drug is currently in Phase II studies [62].

MAIN CHALLENGES TO MOVE FORWARD

Although the convergence of fundamental and applied research has contributed to the development of novel nanotechnology-based medical technologies that are commercially marketed products, numerous soft matter-based formulations have disappointed in clinical trials. This highlights the necessity of careful optimization and control over polymer chemistry and supramolecular assemblies to improve the stability and efficacy of cancer therapies. Furthermore, in addition to the vehicle-related challenges, the specific features of each tumor and each patient appears to be the most difficult barrier to further progress. The current primary developmental challenges are summarized in this section as vehicle-related and physiological-related barriers.

Vehicle-Related Barriers

The practical challenges related specifically to polymeric micelles depend on poor *in vivo* stability due to extensive

dilution upon injection, resulting in vehicle dissociation [184, 210]. To date, approaches to overcome this issue are based on crosslinking strategies [211]. Another issue is inefficient cellular uptake of polymeric micelles by the target cancer cells. This is caused by the presence of dense layers of stealth polymers, such as PEG, in the outer shell of the assemblies, which is required to promote long circulation of the entities in the bloodstream [212]. To achieve high drug accumulation using stealth nanocarriers, one clever strategy is the use of pH-responsive polymers that promote pH dependent dissociation of the nanocarriers upon arrival at the tumor site. This phenomenon occurs in response to the slightly acidic tumor microenvironment compared with physiological pH. Small molecular weight anticancer drugs are then able to be internalized by a simple diffusion process rather than endocytosis. Regarding polymer-drug conjugates, polymer-drug linker optimization to ensure stability during circulation is extremely important because rapid hydrolysis and drug elimination may explain many of the disappointing results obtained during clinical trials. Furthermore, high drug-loading (physically entrapped or covalently bounded) is also required. Considering the class of liposomes, drug leakage and stability during bloodstream circulation limits the higher efficacy. However, cholesterol incorporation into the bilayer, thereby increasing cohesiveness and reducing leakage, has been employed to circumvent these difficulties [150, 213].

Generally, structural parameters, such as size, shape and surface charge, have been shown to influence cellular uptake. The tumor pore size depends on tumor permeability, type, heterogeneity and tumor progression [11]. The tumor pore size usually ranges from ~10 nm to 2 μm [11, 15, 18, 19]. However, nanoparticles ranging from 10 nm to 200 nm have been shown to be preferentially accumulated *via* the EPR effect [20]. Liposomes accumulate more when their dimensions are approximately 100 nm [214], whereas only micelles ~ 30 nm can penetrate into hypovascular tumors [215]. Polymer-drug conjugates should be less than ~40 kDa and small enough to be renally filtered as a "rule of thumb" [216]. Regarding surface charge (zeta potential), opsonins tend to bind to charged or hydrophobic polymers accelerating hepatic clearance [217, 218]. The effect of soft colloid surface charge and its influence on body clearance remains controversial [219-223]. The shape of nanomedicines significantly impacts pharmacokinetics and tumor accumulation. Water soluble polymers are usually flexible and are therefore able to deform to easily pass through pores, whereas rigid structures, such as star-like and hyperbranched polymers, may encounter more difficulty [216]. For example, filomicelles persist in circulation ten times longer than their spherical counterparts [224]. The *in-vitro* cell internalization of differently shaped cationic cross-linked PEG hydrogels demonstrates that the internalization of rod-like structures occurs more rapidly and efficiently compared with other shapes with the same volume and size [219].

Therefore, considering the above-mentioned issues, the precise control and optimization these parameters will lead to improved nanomedicine design for use in various biomedical applications. To this end, the Table **1** summarizes the main advantages and the drawbacks of the above-mentioned soft matter based nanomedicines.

Table 1. Advantages and drawbacks of different soft matter based nanomedicines.

System	Main Advantage	Main Drawback
Liposomes	Encapsulation of hydrophilic and/or hydrophobic agents	Usually large structures which may reduce extravasation efficiency
Biodegradable polymeric nanoparticles	Simple manufacturing	Limited loading capacity
Block copolymer micelles	Small size enabling effective EPR accumulation	Poor *in vivo* stability and possible dissociation upon injection
Polymer-drug conjugates	Higher aqueous solubility of attached hydrophobic drugs	Instability of polymer-drug linkers

Physiological-Related Barriers

In addition to vehicle-related issues, tumor concerns must also be addressed to realize the desired expectations of nanomedicines in cancer chemotherapy. Physiological barriers are undoubtedly the most important limiting factor against enhancing the efficacy of nanotechnology-based therapies. Firstly, blood vessel fenestrations in tumor sites vary substantially. However, the pore size of brain tumor tissues usually does not exceed 10-12 nm [15]. This particular feature challenges nanoparticle design for brain tumor treatment because the assemblies are rapidly cleared *via* renal filtration when the sizes are less than 10 nm [225, 226]. Tumor pore size is dependent on physiological conditions, which vary substantially from tumor to tumor and from patient to patient [11, 25, 26, 30]. Furthermore, differences in tumor treatments have been observed in pre-clinical models (animals) to further clinical trials (humans). This is thought to be related to tumor-related physiological differences between species and studies, *i.e.*, tumor biology and clearance differ between animals and humans and pre-clinical models usually are focused on primary tumors, whereas clinical trials are conducted in metastatic patients [30]. Although there has been significant progress controlling the physical parameters of nanomaterials, this issue restricts the optimization of colloidal system requirements because differences in tumor treatments and tumor models hinder efficient accumulation. Ideally, this issue will be resolved by the personal design of nanomaterials.

Additionally, as nanomaterials reach tumor sites, passively or actively, permeation efficacy depends on tumor type, status and location [11, 20, 21, 30]. Another major challenge is the tumor negative pressure gradient because the interstitial pressure is higher in the tumor core, and therefore, the nanoparticles will always have the tendency to flow towards the periphery. A clever strategy for this issue is to increase blood pressure, reducing the pressure difference and ideally improving passive nanomaterial accumulation [227]. Furthermore, the EPR effect itself is highly heterogeneous and usually accumulation is not even, particularly in the central regions of the malignancy.

Finally, tumor resistance and MDR resistance are issues that must be considered. The strategy to circumvent these factors may lie in the field of ligand-mediated active targeting through the development of systems to target the endothelium of the tumor vasculature [25, 48] because endothelial cells have higher circulation accessibility and the tissue is genetically stable limiting the development of tumor resistance [228]. Combined therapy may be a promising strategy to suppress cancer-drug resistance because different drugs may damage or kill cancer cells during different stages of their growth cycles [105]. The co-delivery of multiple drugs through a single administration has advantages, such as possible synergistic therapeutic effects, suppression of drug resistance and the ability to control drug exposure [105, 137, 139].

FINAL REMARKS

It has focused on the application of nanotechnology in medicine and the rapid development of the emerging area of nanomedicine. This review has emphasized the potential and current uses of soft matter based nanomedicines in cancer therapies. This journey examined polymeric systems that are marketed products and in clinical trials as well as current research focused on potential novel polymeric systems intended to overcome the remaining challenges in this field. Nanomedicine is interdisciplinary and further progress cannot occur without the convergence of chemistry, biology, materials science and medicine. Recent advances in polymer chemistry, such as controlled polymerization techniques, along with elegant particle fabrication technologies should allow the preparation of tailored nanomedicines with precise control over size, polydispersity, surface properties and shape. Ultimately, these parameters could be independently varied for each patient. Regarding the specific features of distinct tumor sites, complete success can be achieved and further improvements can be accomplished by carefully examining the specific properties of each tumor. Additionally, the advance of specific developments may be achieved by considering tumor anomalies and patient-to-patient variation. Therefore, a deeper knowledge of tumor features and particularities (microenvironment, stage, heterogeneity, aggressiveness and progression) is required for the preparation of more effective nanomedicines. Nevertheless, recent advances in soft matter based nanomedicines, as reported in this review, suggest a bright future for further scientific investigations innovative soft therapeutics into clinical practice.

CONFLICT OF INTEREST

The authors confirm that this article content has no conflict of interest.

ACKNOWLEDGEMENTS

The authors gratefully acknowledge financial support of FAPESP (Grant No. 2012/14087-8), CNPq (Grant No. 470608/2012-9), GACR (Grant No. P208/10/1600), the [EEA]/[Norwegian] Financial Mechanism 2009-2014 under Project contract no [ID 7F14009] and the Charles University in Prague.

REFERENCES

[1] World Health Organization (WHO). http://www.who.int/mediacentre/news/releases/2006/pr06/en/ (July, 2014).

[2] Griffioen, A.W.; Molema, G. Angiogenesis: potentials for pharmacologic intervention in the treatment of cancer, cardiovascular diseases, and chronic inflammation. *Pharmacol. Rev.*, **2000**, *52*, 237-268.

[3] Fang, J.; Nakamura, H.; Maeda, H. The EPR effect: Unique features of tumor blood vessels for drug delivery, factors involved, and limitations and augmentation of the effect. *Adv. Drug Del. Rev.*, **2011**, *63*, 136-151.

[4] Chiche, J.; Brahimi-Horn, M.C.; Pouysségur, J. Tumour hypoxia induces a metabolic shift causing acidosis: a common feature in cancer. *J. Cell Mol. Med.*, **2010**, *14*, 771-794.

[5] van Sluis, R.; Bhujwalla, Z.M.; Raghunand, N.; Ballesteros, P.; Alvarez, J.; Cerdan, S.; Galons, R.J.; Gillies, R.J. *In vivo* imaging of extracellular pH using ^{1}H MRSI. *Magn. Reson. Med.*, **1999**, *41*, 743-750.

[6] Cardone, R.A.; Casavola, V.; Reshkin, S.J. The role of disturbed pH dynamics and the Na+/H+ exchanger in metastasis. *Nat. Rev. Cancer*, **2005**, *5*, 786-795.

[7] Binauld, S.; Stenzel, M.H. Acid-degradable polymers for drug delivery: a decade of innovation. *Chem. Commun.*, **2013**, *49*, 2082-2102.

[8] Ko, J.; Park, K.; Kim, Y.-S.; Kim, M.S.; Han, J.K.; Kim, K.; Park, R-W.; Kim, I.-S.; Song, H.K.; Lee, D.S., Kwon, I.C. Tumoral acidic extracellular pH targeting of pH-Responsive Mpeg-Poly([Beta]-Amino Ester) block copolymer micelles for cancer therapy. *J. Control. Release*, **2007**, *123*, 109-115.

[9] Chen, W.; Meng, F.; Li, F.; Ji, S.-J.; Zhong, Z. pH-responsive biodegradable micelles based on acid-labile polycarbonate hydrophobe: synthesis and triggered drug release. *Biomacromolecules*, **2009**, *10*, 1727-1735.

[10] Petrova, S.; Jäger, E.; Konefał, R.; Venturini, C.G.; Spěváček, J.; Pavlova, E.; Štěpánek, P. Novel poly(ethylene oxide monomethyl ether)-**b**-poly(ε-caprolactone) diblock copolymers containing a pH-acid labile ketal group as a block linkage. *Polym. Chem.*, **2014**, *5*, 3884-3893.

[11] Jain, R.K.; Stylianopoulos, T. Delivering nanomedicine to solid tumors. *Nat. Rev. Clin. Oncol.*, **2010**, *7*, 653-664.

[12] Ruenraroengsak, P.; Cook, J.M.; Florence, A.T. Nanosystem drug targeting: Facing up to complex realities. *J. Control. Release*, **2010**, *141*, 265-276.

[13] Cho, K.; Wang, X.; Nie, S.; Chen, Z.; Shin, D.M. Therapeutic nanoparticles for drug delivery in cancer. *Clin. Cancer Res.*, **2008**, *14*, 1310-1316.

[14] Brown J.M.; Giaccia, A.J. The unique physiology of solid tumors: opportunities (and problems) for cancer therapy. *Cancer Res.*, **1998**, *58*, 1408-1416.

[15] Chauhan, V.P.; Jain, R.K. Strategies for advancing cancer nanomedicine. *Nat. Mater.*, **2014**, *12*, 958-962.

[16] Gerlowski, L.E.; Jain, R.K. Microvascular permeability of normal and neoplastic tissues. *Microvasc. Res.*, **1986**, *31*, 288-305.

[17] Matsumura, Y.; Maeda, H. A new concept for macromolecular therapeutics in cancer chemotherapy: mechanism of tumoritropic accumulation of proteins and the antitumor agent smancs. *Cancer Res.*, **1986**, *46*, 6387-6392.

[18] Hobbs, S.K.; Monsky, W.L.; Yuan, F.; Roberts, W.G.; Griffith, L.; Torchilin, V.P.; Jain, R.K. Regulation of transport pathways in tumor vessels: role of tumor type and microenvironment. *Proc. Natl. Acad. Sci. U.S.A*, **1998**, *95*, 4607-4612.

[19] Yuan, F.; Dellian, M.; Fukumura, D.; Leunig, M.; Berk, D.A.; Torchilin. V.P.; Jain, R.K. Vascular permeability in a human tumor xenograft: molecular size dependence and cutoff size. *Cancer Res.*, **1995**, *55*, 3752-3756.

[20] Danhier, F.; Feron, O.; Préat, V. To exploit the tumor microenvironment: Passive and active tumor targeting of nanocarriers for anti-cancer drug delivery. *J. Control. Release*, **2010**, *148*, 135-146.

[21] Fang, J.; Nakamura, H.; Maeda, H. The EPR effect: Unique features of tumor blood vessels for drug delivery, factors involved, and limitations and augmentation of the effect. *Adv. Drug Del. Rev.*, **2011**, *63*, 136-151.

[22] Maeda, H.; Matsumura, Y. Tumoritropic and lymphotropic principles of macromolecular drugs. *Crit. Rev. Ther. Drug Carrier Syst.*, **1989**, *6*, 193-210.

[23] Maeda, H.; Wu, J.; Sawa, T.; Matsumura, Y.; Hori, K.Tumor vascular permeability and the EPR effect in macromolecular therapeutics: a review. *J. Control. Release*, **2000**, *65*, 271-284.

[24] Torchilin, V. Tumor delivery of macromolecular drugs based on the EPR effect. *Adv. Drug. Deliv. Rev.*, **2011**, *63*, 131-135.

[25] Lammers, T.; Kiessling, F.; Hennink, W.E.; Storm, G. Drug targeting to tumors: principles, pitfalls and (pre-) clinical progress. *J. Control. Release*, **2012**, *161*, 175-187.

[26] Bae, Y.H.; Park, K. Targeted drug delivery to tumors: myths, reality and possibility. *J. Control. Release*, **2011**, *153*, 198-205.

[27] Fukumura, D.; Yuan, F.; Monsky, W.L.; Chen, Y.; Jain, R.K. Effect of host microenvironment on the microcirculation of human colon adenocarcinoma. *Am. J. Pathol.*, **1997**, *151*, 679-688.

[28] Monsky, W.L.; Mouta Carreira, C.; Tsuzuki, Y.; Gohongi, T.; Fukumura, D.; Jain, R.K. Role of host microenvironment in angiogenesis and microvascular functions in human breast cancer xenografts: mammary fat pad versus cranial tumors. *Clin. Cancer Res.*, **2002**, *8*, 1008-1013.

[29] Prabhakar, U.; Maeda. H.; Jain. R.K.; Sevick-Muraca, E.M.; Zamboni, W.; Farokhzad, O.C.; Barry, S.T.; Gabizon, A.; Grodzinski, P.; Blakey, D.C. Challenges and key considerations of the enhanced permeability and retention effect for nanomedicine drug delivery in oncology. *Cancer Res.*, **2013**, *73*, 2412-2417.

[30] Bertrand, N.; Wu, J.; Xu, X.; Kamaly, N.; Farokhzad, O.C. Cancer nanotechnology: the impact of passive and active targeting in the era of modern cancer biology. *Adv. Drug Del. Rev.*, **2014**, *66*, 2-25.

[31] Kirpotin D.B, Drummond D.C, Shao Y, Shalaby M.R., Hong K, Nielsen U.B., Marks J.D., Benz C.C., Park J.W. Antibody targeting of long-circulating lipidic nanoparticles does not increase tumor localization but does increase internalization in animal models. *Cancer Res.*, **2006**, *66*, 6732-6740.

[32] Choi C.H.J., Alabi C.A., Webster P., Davis M.E. Mechanism of active targeting in solid tumors with transferrin-containing gold nanoparticles. *Proc. Natl. Acad. Sci U.S.A*, **2010**, *107*, 1235-1240.

[33] van der Meel, R.; Vehmeijer L.J.C.; Kok R.J.; Storm, G.; van Gaal E.V.B. Ligand-targeted particulate nanomedicines undergoing clinical evaluation: current status. *Adv. Drug Del. Rev.*, **2013**, *65*, 1284-1298.

[34] Ruoslahti, E.; Bhatia, S.N.; Sailor M.J. Targeting of drugs and nanoparticles to tumors. *J. Cell Biol.* **2010**, *188*, 759-768.

[35] Dominska, M.; Dykxhoorn, D.M. Breaking down the barriers: siRNA delivery and endosome escape. *J. Cell Sci.*, **2010**, *123*, 1183-1189.

[36] Hatakeyama, H.; Akita, H.; Ishida, E.; Hashimoto, K.; Kobayashi, H.; Aoki, T.; Yasuda, J.; Obata, K.; Kikuchi, H.; Ishida, T.; Kiwada, H.; Harashima, H. Tumor targeting of doxorubicin by anti-MT1-MMP antibody-modified PEG liposomes. *Int. J. Pharm.*, **2007**, *342*, 194-200.

[37] Morachis, J.M.; Mahmoud, E.A.; Almutairi, A. Physical and chemical strategies for therapeutic delivery by using polymeric nanoparticles. *Pharmacol. Rev.*, **2012**, *64*, 505-519.

[38] Elias, D.R.; Poloukhtine, A.; Popik, V.; Tsourkas, A. Effect of ligand density, receptor density, and nanoparticle size on cell targeting. *Nanomedicine*, **2013**, *9*, 194-201.

[39] Gao, H.; Yang, Z.; Zhang, S.; Cao, S.; Shen, S.; Pang, Z.; Jiang, X. Ligand modified nanoparticles increases cell uptake, alters endocytosis and elevates glioma distribution and internalization. *Sci. Rep.*, **2013**, *3*, 2534.

[40] Ke, W.; Shao, K.; Huang, R.; Han, L.; Liu, Y.; Li, J.; Kuang, Y.; Ye, L.; Lou, J.; Jiang, C. Gene delivery targeted to the brain using an Angiopep-conjugated polyethyleneglycol-modified polyamidoamine dendrimer. *Biomaterials*, **2009**, *30*, 6976-6985.

[41] Tada, H.; Higuchi, H.; Wanatabe, T.M.; Ohuchi, N. *In vivo* real-time tracking of single quantum dots conjugated with monoclonal anti-HER2 antibody in tumors of mice**.** *Cancer Res.*, **2007**, *67*, 1138-1144.

[42] Leserman, L.D.; Barbet, J.; Kourilsky, F.; Weinstein, J.N. Targeting to cells of fluorescent liposomes covalently coupled with monoclonal antibody or protein A. *Nature*, **1980**, *288*, 602-604.

[43] Heath, T.D.; Fraley, R.T.; Papahadjopoulos, D. Antibody targeting of liposomes: cell specificity obtained by conjugation of F(ab')2 to vesicle surface. *Science*, **1980**, *210*, 539-541.

[44] Kamaly, N.; Xiao. Z.; Valencia, P.M.; Radovic-Moreno, A.F.; Farokhzad, O.C. Targeted polymeric therapeutic nanoparticles: design, development and clinical translation. *Chem. Soc. Rev.*, **2012**, *41*, 2971-3010.

[45] Mamot, C.; Ritschard, R.; Wicki, A.; Stehle, G.; Dieterle, T.; Bubendorf, L.; Hilker, C.; Deuster, S.; Herrmann, R.; Rochlitz, C. Tolerability, safety, pharmacokinetics, and efficacy of doxorubicin-loaded anti-EGFR immunoliposomes in advanced solid tumours: A Phase 1 dose-escalation study. *Lancet Oncol.*, **2012**, *13*, 1234-1241.

[46] Senzer, N.; Nemunaitis, J.; Nemunaitis, D.; Bedell, C.; Edelman, G.; Barve, M.; Nunan, R.; Pirollo, K.F.; Rait, A.; Chang, E.H. Phase I study of a systemically delivered p53 nanoparticle in advanced solid tumors. *Mol. Ther.*, **2013**, *21*, 1096-1103.

[47] Corti, A.; Pastorino, F.; Curnis, F.; Arap, W.; Ponzoni, M.; Pasqualini, R. Targeted drug delivery and penetration into solid tumors. *Medicinal Res. Rev.*, **2012**, *32*, 1078-1091.

[48] Kunjachan, S.; Pola, R.; Gremse, F.; Theek, B.; Ehling, J.; Moeckel, D.; Hermanns-Sachweh, B.; Pechar, M.; Ulbrich, K.; Hennink, W.E.; Storm, G.; Lederle, W.; Kiessling, F.; Lammers, T. Passive versus active tumor targeting using RGD- and NGR-modified polymeric nanomedicines. *Nano Lett.*, **2014**, *14*, 972-981.

[49] Cheng, Z.; Al Zaki, A.; Hui, J.Z.; Muzykantov, V.R.; Tsourkas, A. Multifunctional nanoparticles: Cost versus benefit of adding targeting and imaging capabilities. *Science*, **2012**, *338*, 903-910.

[50] Lu, Y.; Low, P.S. Folate-mediated delivery of macromolecular anticancer therapeutic agents. *Adv. Drug Del. Rev.*, **2002**, *54*, 675-693.

[51] Zhao, X.; Li, H.; Lee, R.J. Targeted drug delivery via folate receptors. *Expert Opin. Drug Deliv.*, **2008**, *5*, 309-319.

[52] Gabizon, A.; Shmeeda, H.; Horowitz, A.T.; Zalipsky, S. Tumor cell targeting of liposome-entrapped drugs with phospholipid-anchored folic acid-PEG conjugates. *Adv. Drug Del. Rev.*, **2004**, *56*, 1177-1192.

[53] Ward, C.M.; Pechar, M.; Oupicky, D.; Ulbrich, K.; Seymour, L.W. Modification of pLL/DNA complexes with a multivalent hydrophilic polymer permits folate-mediated targeting *in vitro* and prolonged plasma circulation *in vivo*. *Journal Gene Med.*, **2002**, *4*, 536-547.

[54] Riviere, K.; Huang, Z.; Jerger, K.; Macaraeg, N.; Szoka, F.C.Jr. Antitumor effect of folate-targeted liposomal doxorubicin in KB tumor-bearing mice after intravenous administration. *J. Drug Target*, **2011**, *19*, 14-24.

[55] Bae, Y.; Jang, W.-D.; Nishiyama, N.; Fukushima, S.; Kataoka, K. Multifunctional polymeric micelles with folate-mediated cancer cell targeting and pH-triggered drug releasing properties for active intracellular drug delivery. *Mol. Biosyst.*, **2005**, *3*, 242-250.

[56] Chandrasekar, D.; Sistla, R.; Ahmad, F.J.; Khar, R.K.; Diwan, P.V. The development of folate-PAMAM dendrimer conjugates for targeted delivery of anti-arthritic drugs and their pharmacokinetics and biodistribution in arthritic rats. *Biomaterials*, **2007**, *3*, 504-12.

[57] Parker, N.; Turk, M.J.; Westrick, E.; Lewis, J.D.; Low, P.S.; Leamon, C.P. Folate receptor expression in carcinomas and normal tissues determined by a quantitative radioligand binding assay. *Analytical Biochem.*, **2005**, *338*, 284-293.

[58] Das, M.; Mohanty, C.; Sahoo S.K. Ligand-based targeted therapy for cancer tissue. *Expert Opin. Drug Deliv.*, **2009**, *6*, 285-304.

[59] Davis, B.G.; Robinson, M.A. Drug delivery systems based on sugar-macromolecule conjugates. *Curr. Opin. Drug Discovery Dev.*, **2002**, *5*, 279-288.

[60] Qin, Y.; Fan, W.; Chen, H.; Yao, N.; Tang, W.; Tang, J.; Yuan, W.; Kuai, R.; Zhang, Z.; Wu, Y.; He, Q. *In vitro* and *in vivo* investigation of glucose-mediated brain-targeting liposomes. *J. Drug Target*, **2010**, *18*, 536-49.

[61] Bergen, J.M.; Von Recum, H.A.; Goodman, T.T.; Massey, A.P.; Pun, S.H. Gold nanoparticles as a versatile platform for optimizing physicochemical parameters for targeted drug delivery. *Macromol. Biosci.*, **2006**, *6*, 506-516.

[62] Seymour, L.W.; Ferry, D.R.; Anderson, D.; Hesslewood, S.; Julyan, P.J.; Poyner, R.; Doran, J.; Young, A.M.; Burtles, S.; Kerr, D.J. Hepatic drug targeting: Phase I evaluation of polymer-bound doxorubicin *J. Clin. Oncol.*, **2002**, *20*, 1668-1676.

[63] Shi, J.; Xiao, Z.; Kamaly, N.; Farokhzad, O.C. Self-assembled targeted nanoparticles: Evolution of technologies and bench to bedside translation *Acc. Chem. Res.*, **2011**, *44*, 1123-1134.

[64] Hillier, S.M.; Maresca, K.P.; Femia, F.J.; Marquis, J.C.; Foss, C.A.; Nguyen, N.; Zimmerman, C.N.; Barrett, J.A.; Eckelman, W.C.; Pomper, M.G.; Joyal, J.L.; Babich, J.W. Preclinical evaluation of novel glutamate-urea-lysine analogues that target prostate-specific membrane antigen as molecular imaging pharmaceuticals for prostate cancer. *Cancer Res.*, **2009**, *69*, 6932-6940.

[65] Hrkach, J.; Von Hoff, D.; Ali, M.M.; Andrianova, E.; Auer, J.; Campbell, T.; DeWitt, D.; Figa, M.; Figueiredo, M.; Horhota, A.; Low, S.; McDonnell, K.; Peeke, E.; Retnajaran, B.; Sabnis, A.; Schnipper, E.;, Song, J.J.; Song, Y.H.; Summa, J.; Tompsett, D.; Troiano, G.; Van Geen Hoven, T.; Wright, J.; LoRusso, P.; Kantoff, P.W.; Bander, N.H.; Sweeney, C.; Farokhzad, O.C.; Langer, R.; Zale, S. Preclinical development and clinical translation of a PSMA-targeted docetaxel nanoparticle with a differentiated pharmacological profile. *Sci. Transl. Med*., **2012**, *4*, 128-139.

[66] Mura, S.; Nicolas, J.; Couvreur, P. Stimuli-responsive nanocarriers for drug delivery. *Nat. Mater*., **2013**, *12*, 991-1003.

[67] Sahay, G.; Alakhova, D.Y.; Kabanov, A.V. Endocytosis of nanomedicines. *J. Control. Release*, **2010**, *145*, 182-195.

[68] Wei, H.; Zhuo, R.-X.; Zhang, X.-Z. Design and development of polymeric micelles with cleavable links for intracellular drug delivery. *Prog. Pol. Sci*., **2013**, *38*, 503-535.

[69] Bangham, A.D.; Standish, M.M.; Watkins, J.C. Diffusion of univalent ions across the lamellae of swollen phospholipids. *J. Mol. Biol*., **1965**, *13*, 238-252.

[70] Deamer, D.W. From "Banghasomes" to liposomes: A memoir of Alec Bangham, 1921-2010. *FASEB J*., **2010**, *24*, 1308-1310.

[71] Allen, T.M.; Cullis, P.R. Liposomal drug delivery systems: From concept to clinical applications. *Adv. Drug Del. Rev*., **2013**, *65*, 36-48.

[72] Torchilin, V.P. Recent advances with liposomes as pharmaceutical carriers. *Nat. Rev. Drug Discov*., **2005**, *4*, 145-160.

[73] Duncan, R. The dawning era of polymer therapeutics. *Nat. Rev. Drug. Discov*., **2003**, *2*, 347-360.

[74] Kohli, A.G.; Kierstead, P.H.; Venditto, V.J.; Walsh, C.L.; Szoka, F.C. Designer lipids for drug delivery: From heads to tails. *J. Control. Release*, **2014**, DOI: 10.1016/j.jconrel.2014.04.047.

[75] Ozpolat, B.; Sood, A.K.; Lopez-Berestein, G. Liposomal siRNA nanocarriers for cancer therapy. *Adv. Drug Del. Rev*., **2014**, *66*, 110-116.

[76] Couvreur, P. Nanoparticles in drug delivery: Past, present and future. *Adv. Drug Del. Rev*., **2013**, *65*, 21-23.

[77] Marty, J.J.; Oppenheim, R.C.; Speiser, P. Nanoparticles - a new colloidal drug delivery system. *Pharm. Acta Helv*., **1978**, *53*, 17-23.

[78] Illum, L.; Jones, P.D.; Baldwin, R.W.; Davis, S.S. Tissue distribution of polyhexyl-2-cyanoacrylate nanoparticles coated with monoclonal antibodies in mice bearing human tumor xenografts. *J. Pharmacol. Exp. Ther*., **1984**, *230*, 733-736.

[79] Jalil, R.-U. Biodegradable poly(lactic acid) and poly(lactide-*co*-glycolide) polymers in sustained drug delivery. *Drug Dev. Ind. Pharm*., **1990**, *16*, 2353-2367.

[80] Heller, J. Biodegradable polymers in controlled drug delivery. *Crit. Rev. Ther. Drug*., **1984**, *1*, 39-90.

[81] Gurny, R.; Peppas, N.A.; Harrington, D.D.; Banker, G.S. Development of biodegradable and injectable latices for controlled release of potent drugs. *Drug Dev. Ind. Pharm*., **1981**, *7*, 1-25.

[82] Calvo, P.; Remuñán-López, C.; Vila-Jato, J.L.; Alonso, M.J. Novel hydrophilic chitosan-polyethylene oxide nanoparticles as protein carriers. *J. Appl. Polym. Sci*., **1997**, *63*, 125-132.

[83] Soppimath, K.S.; Aminabhavi, T.M.; Kulkarni, A.R.; Rudzinski, W.E. Biodegradable polymeric nanoparticles as drug delivery devices. *J. Control. Release*, **2001**, *70*, 1-20.

[84] Fessi, H.; Puisieux, F.; Devissaguet, J.-Ph.; Ammoury, N.; Benita, S. Nanocapsule formation by interfacial polymer deposition following solvent displacement. *Int. J. Pharm*., **1984**, *55*, R1-R4.

[85] Quintanar-Guerrero, D.; Allémann, E.; Fessi, H.; Doelker, E. Preparation techniques and mechanisms of formation of biodegradable nanoparticles from preformed polymers. *Drug Dev. Ind. Pharm*., **1998**, *24*, 1113-1128.

[86] Karnik R.; Gu F.; Basto, P.; Cannizzaro, C.; Dean, L.; Kyei-Manu, W.; Langer, R.; Farokhzad, O.C. Microfluidic platform for controlled synthesis of polymeric nanoparticles. *Nano Lett*., **2008**, *8*, 2906-2912.

[87] Rolland, J.P. Maynor, B.W.; Euliss, L.E.; Exner, A.E.; Denison, G.M.; DeSimone, J.M. Direct fabrication and harvesting of monodisperse, shape-specific nanobiomaterials. *J. Am. Chem. Soc*., **2005**, *127*, 10096-10100.

[88] Enlow, E.M.; Luft, J.C.; Napier, M.E.; Desimone, J.M. Potent engineered PLGA nanoparticles by virtue of exceptionally high chemotherapeutic loadings. *Nano Lett*., **2011**, *11*, 808-813.

[89] Chu, K.S.; Hasan, W.; Rawal, S.; Walsh, M.D.; Enlow, E.M.; Luft, J.C.; Bridges, A.S.; Kuijer, J.L.; Napier, M.E.; Zamboni, W.C.; DeSimone, J.M. Plasma, tumor and tissue pharmacokinetics of docetaxel delivered via nanoparticles of different sizes and shapes in mice bearing SKOV-3 human ovarian carcinoma xenograft. *Nanomedicine*, **2013**, *9*, 686-693.

[90] Gaucher, G.; Robert H. Marchessault, R.H.; Leroux, J.-C. Polyester-based micelles and nanoparticles for the parenteral delivery of taxanes. *J. Control. Release*, **2010**, *143*, 2-12.

[91] Tong, R.; Gabrielson N.P.; Fan, T.M.; Cheng, J. Polymeric nanomedicines based on poly(lactide) and poly(lactide-*co*-glycolide). *Curr. Opin. Solid State Mater. Sci*., **2012**, *16*, 323-332.

[92] Weiss, V.M.; Naolou, T.; Hause, G.; Kuntsche, J.; Kressler, J.; Mäder, K. Poly(glycerol adipate)-fatty acid esters as versatile nanocarriers: From nanocubes over ellipsoids to nanospheres. *J. Control. Release*, **2012**, *158*, 156-164.

[93] Jäger, A.; Gromadzki, D.; Jäger, E.; Giacomelli, F.C.; Kozlowska, A.; Kobera, L.; Brus, J.; Říhová, B.; El Fray, M.; Ulbrich, K.; Štěpánek, P. Novel "soft" biodegradable nanoparticles prepared from aliphatic based monomers as a potential drug delivery system. *Soft Matter*, **2012**, *8*, 4343-4354.

[94] Lemarchand, C.; Gref, R.; Passirani, C.; Garcion, E.; Petri, B.; Müller, R.; Costantini, D.; Couvreur, P. Influence of polysaccharide coating on the interactions of nanoparticles with biological systems. *Biomaterials*, **2006**, *27*, 101-118.

[95] Rudt, S.; Müller, R.H. *In vitro* phagocytosis assay of nano- and microparticles by chemiluminescence. II. Effect of surface modification by coating of particles with poloxamer on the phagocytic uptake. *J. Control. Release*, **1993**, *25*, 51-59.

[96] Sahho, S.K.; Panyam, J.; Prabha, S.; Labhasetwar, V. Residual polyvinyl alcohol associated with poly (D,L-lactide-*co*-glycolide) nanoparticles affects their physical properties and cellular uptake. *J. Control. Release*, **2002**, *82*, 105-114.

[97] Roosjen, A.; de Vries, J.; van der Mei, H.C.; Norde, W.; Busscher, H. Stability and effectiveness against bacterial adhesion of poly(ethylene oxide) coatings in biological fluids. *J. Biomed. Mater. Res. Part B*, **2005**, *73B*, 347-354.

[98] Branch, D.W.; Wheeler, B.C.; Brewer, G.J.; Leckband, D.E. Long-term stability of grafted polyethylene glycol surfaces for use with microstamped substrates in neuronal cell culture. *Biomaterials*, **2001**, *22*, 1035-1047.

[99] Rodriguez-Emmeneger, C.; Jäger, A.; Jäger, E.; Štěpánek, P. Bollogna-Alles, A.; Guterres, S.S.; Pohlmann, A.R.; Brynda, E. Polymeric nanocapsules ultra stable in complex biological media. *Colloids Surf. B*, **2011**, *83*, 376-381.

[100] Feng, S.-S.; Mu, L.; Win, K.Y.; Huang, G. Nanoparticles of biodegradable polymers for clinical administration of paclitaxel. *Curr. Med. Chem*., **2004**, *11*, 413-424.

[101] Win, K.Y.; Feng, S.-S. Effects of particle size and surface coating on cellular uptake of polymeric nanoparticles for oral delivery of anticancer drugs. *Biomaterials*, **2005**, *26*, 2713-2722.

[102] Feng, S.-S.; Zhao, L.; Zhang, Z.; Bhakta, G.; Win, K.Y.; Dong, Y.; Chien, S. Chemotherapeutic engineering: Vitamin E TPGS-emulsified nanoparticles of biodegradable polymers realized sustainable paclitaxel chemotherapy for 168 h *in vivo*. *Chem. Eng. Sci*., **2007**, *62*, 6641-6648.

[103] Zhao, L.; Feng, S.-S. Enhanced oral bioavailability of paclitaxel formulated in vitamin E-TPGS emulsified nanoparticles of biodegradable polymers: *In vitro* and *in vivo* studies. *J. Pharm. Sci*., **2010**, *99*, 3552-3560.

[104] Jäger, E.; Jäger, A.; Etrych, T.; Giacomelli, F.C.; Chytil, P.; Jigounov, A.; Putaux, J.-L.; Říhová, B.; Ulbrich, K.; Štěpánek, P. Self-assembly of biodegradable copolyester and reactive HPMA-based polymers into nanoparticles as an alternative stealth drug delivery system. *Soft Matter*, **2012**, *8*, 9563-9575.

[105] Jäger, E.; Jäger, A.; Chytil, P.; Etrych, T.; Říhová, B.; Giacomelli, F.C.; Štěpánek, P.; Ulbrich, K. Combination chemotherapy using core-shell nanoparticles through the self-assembly of HPMA-based copolymers and degradable polyester. *J. Control. Release*, **2013**, *165*, 153-161.

[106] Tuzar, Z.; Kratochvil, P. Block and graft copolymer micelles in solution. *Adv. Colloid Interface Sci*., **1976**, *6*, 201-232.

[107] Kataoka, K.; Harada, A.; Nagasaki, Y. Block copolymer micelles for drug delivery: design, characterization and biological significance. *Adv. Drug Del. Rev*., **2001**, *47*, 113-131.

[108] Torchilin, V.P. Micellar nanocarriers: pharmaceutical perspectives. *Pharm. Res*., **2007**, *24*, 1-16.

[109] Nishiyyama, N.; Kataoka, K. Current state, achievements and future prospects of polymeric micelles as nanocarriers for drug and gene delivery. *Pharmacol. Ther.*, **2006**, *112*, 630-648.

[110] Rapoport, N.; Physical stimuli-responsive polymeric micelles for anti-cancer drug delivery. *Prog. Pol. Sci.*, **2007**, *32*, 962-990.

[111] Schmaljohann, D. Thermo- and pH-responsive polymers in drug delivery. *Adv. Drug. Del. Rev.*, **2006**, *58*, 1655-1670.

[112] Giacomelli, F.C.; Štěpánek, P.; Giacomelli, C.; Schmidt, V.; Jäger, E.; Jäger, A.; Ulbrich, K. pH-triggered block copolymer micelles based on a pH-responsive PDPA (poly[*2*-(diisopropylamino)ethyl methacrylate])inner core and a PEO (poly(ethylene oxide)) outer shell as a potential tool for the cancer therapy. *Soft Matter*, **2011**, *7*, 9316-9325.

[113] Pegoraro, C.; Cecchin, D.; Gracia, L.S.; Warren, N.; Madsen, J.; Armes, S.P.; Lewis, A.; MacNeil, S.; Battaglia, G. Enhanced drug delivery to melanoma cells using PMPC-PDPA polymersomes. *Cancer Lett.*, **2013**, *334*, 328-337.

[114] Wang, Y.; Zhou, K.; Huang, G.; Hensley, C.; Huang, X.; Ma, X.; Zhao, T.; Sumer, B.D.; DeBerardinis, R.J.; Gao, J. A nanoparticle-based strategy for the imaging of a broad range of tumours by non-linear amplification of microenvironment signals. *Nat. Mater.*, **2014**, *13*, 204-212.

[115] Lavasanifar, A.; Samuel, J.; Kown, G.S. Poly(ethylene oxide)-block-poly(L-amino acid) micelles for drug delivery. *Adv. Drug Del. Rev.*, **2002**, *54*, 169-190.

[116] Osada, K.; Christie, R.J.; Kataoka, K. Polymeric micelles from poly(ethylene glycol)-poly(amino acid) block copolymer for drug and gene delivery. *J. R. Soc. Interface*, **2009**, *6*, S325-S339.

[117] Duncan, R. Polymer conjugates as anticancer nanomedicines. *Nat. Rev. Cancer*, **2006**, *6*, 688-701.

[118] Kopeček, J. Polymer-drug conjugates: Origins, progress to date and future directions. *Adv. Drug Del. Rev.*, **2013**, *65*, 49-59.

[119] Yang, J.; Kopeček, J. Macromolecular therapeutics. *J. Control. Release*, **2014**, DOI: 10.1016/j.jconrel.2014.04.013.

[120] Duncan, R.; Vicent, M.J. Polymer therapeutics-prospects for 21st century: The end of the beginning. *Adv. Drug Del. Rev.*, **2013**, *65*, 60-70.

[121] Ulbrich, K.; Subr, V. Polymeric anticancer drugs with pH-controlled activation. *Adv. Drug Del. Rev.*, **2004**, *56*, 1023-1050.

[122] Choi, W.M.; Kopečekova, P.; Minko, T.; Kopeček, J. Synthesis of HPMA copolymer containing adriamycin bound via an acid-labile spacer and its activity toward human ovarian carcinoma cells *J. Bioact. Compat. Polym.*, **1999**, *14*, 447-456.

[123] Etrych, T. Jelínkova, M.; Říhová, B.; Ulbrich, K. New HPMA copolymers containing doxorubicin bound via pH-sensitive linkage: synthesis and preliminary *in vitro* and *in vivo* biological properties. *J. Control. Release*, **2001**, *73*, 89-102.

[124] Murthy, N.; Campbell, J.; Fausto, N.; Hoffman, A.S.; Stayton, P.S. Design and synthesis of pH-responsive polymeric carriers that target uptake and enhance the intracellular delivery of oligonucleotides. *J. Control. Release*, **2003**, *89*, 365-374.

[125] Veronese, F.M.; Schiavon, O.; Pasut, G.; Mendichi, R.; Andersson, L.; Tsirk, A.; Ford, J.; Wu, G.; Kneller, S.; Davies, J.; Duncan, R. PEG-Doxorubicin conjugates: Influence of polymer structure on drug release, *in vitro* cytotoxicity, biodistribution, and antitumor activity. *Bioconjugate Chem.*, **2005**, *16*, 775-784.

[126] Blencowe, C.A.; Russel, A.T.; Greco, F.; Hayes, W.; Thornthwaite, D.W. Self-immolative linkers in polymeric delivery systems. *Polym. Chem.*, **2011**, *2*, 773-790.

[127] Li, W.; Zhan, P.; De Clerq, E.; Lou, H.; Liu, X. Current drug research on PEGylation with small molecular agents. *Prog. Pol. Sci.*, **2013**, *38*, 421-444.

[128] Veronese, F.M.; Pasut, G. PEGylation, successful approach to drug delivery. *Drug Discov. Today*, **2005**, *10*, 1451-1458.

[129] Etrych, T.; Šubr, V.; Strohalm, J.; Širová, M.; Říhová, B.; Ulbrich, K. HPMA copolymer-doxorubicin conjugates: The effects of molecular weight and architecture on biodistribution and *in vivo* activity. *J. Control. Release*, **2012**, *164*, 346-354.

[130] Pan, H.; Sima, M.; Yang, J.; Kopeček, J. Synthesis of long-circulating, backbone degradable HPMA copolymer-doxorubicin conjugates and evaluation of molecular-weight-dependent antitumor efficacy. *Macromol. Biosci.*, **2013**, *13*, 155-160.

[131] Roberts, M.J.; Bentley, M.D.; Harris, J.M. Chemistry for peptide and protein PEGylation. *Adv. Drug Del. Rev.*, **2002**, *54*, 459-476.

[132] Pang, X.; Du, H.-L.; Zhang, H.-Q.; Zhai, Y.-J.; Zhai, G.-X. Polymer-drug conjugates: present state of play and future perspectives. *Drug Discov. Today*, **2013**, *18*, 1316-1322.

[133] Pola, R.; Studenovský, M.; Pechar, M.; Ulbrich, K.; Hovorka, O.; Větvička, D.; Říhová, B. HPMA-copolymer conjugates targeted to tumor endothelium using synthetic oligopeptides. *J. Drug Target.*, **2009**, *17*, 763-776.

[134] Etrych, T.; Strohalm, J.; Kovář, L.; Kabešová, M.; Říhová, B.; Ulbrich, K. HPMA copolymer conjugates with reduced anti-CD20 antibody for cell-specific drug targeting. I. Synthesis and *in vitro* evaluation of binding efficacy and cytostatic activity. *J. Control. Release*, **2009**, *140*, 18-26.

[135] Ulbrich, K.; Šubr, V. Structural and chemical aspects of HPMA copolymers as drug carriers. *Adv. Drug Del. Rev.*, **2010**, *62*, 150-166.

[136] Etrych, T.; Šubr, V.; Laga, R.; Říhová, B.; Ulbrich, K. Polymer conjugates of doxorubicin bound through an amide and hydrazone bond: Impact of the carrier structure onto synergistic action in the treatment of solid tumours. *Eur. J. Pharm. Sci.*, **2014**, *58*, 1-12.

[137] Vicent, M.J.; Greco, F.; Nicholson, R.I.; Paul, A.; Griffiths, P.C.; Duncan, R. Polymer therapeutics designed for a combination therapy of hormone-dependent cancer. *Angew. Chem. Int. Ed.*, **2005**, *44*, 4061-4066.

[138] Kostkova, H.; Etrych, T.; Říhova, B.; Ulbrich, K. Synergistic effect of HPMA copolymer-bound doxorubicin and dexamethasone *in vivo* on mouse lymphomas. *J. Biocom. Bioconj. Pol.*, **2011**, *26*, 270-286.

[139] Lammers, T.; Šubr, V.; Ulbrich, K.; Peschke, P.; Huber, P.E.; Hennink, W.E.; Storm, G. Simultaneous delivery of doxorubicin and gemcitabine to tumors *in vivo* using prototypic polymeric drug carriers. *Biomaterials*, **2009**, *30*, 3466-3475.

[140] Kostkova, H.; Etrych, T.; Říhova, B.; Koskta, L.; Starovoytova, L.; Kovar, M.; Ulbrich, K. HPMA copolymer conjugates of dox and mitomycin C for combination therapy: physicochemical characterization, cytotoxic effects, combination index analysis, and anti-tumor efficacy. *Macromol. Biosci.*, **2013**, *13*, 1648-1660.

[141] Zhang, R.; Luo, K.; Yang, J.; Sima, M.; Sun, Y.; Janát-Amsbury, M.M.; Kopeček, J. Synthesis and evaluation of a backbone biodegradable multiblock HPMA copolymer nanocarrier for the systemic delivery of paclitaxel. *J. Control. Release*, **2013**, *166*, 66-74.

[142] Li, C.; Wallace, S. Polymer-drug conjugates: Recent development in clinical oncology. *Adv. Drug Del. Rev.*, **2008**, *60*, 886-898.

[143] Barenholz, Y. Doxil® - The first FDA-approved nano-drug: Lessons learned. *J. Control. Release*, **2012**, *160*, 117-134.

[144] Batist, G. Cardiac safety of liposomal anthracyclines. *Cardiovasc. Toxicol.*, **2007**, *7*, 72-74.

[145] Rahman, A.M.; Yusuf, S.W.; Ewer, M.S. Anthracycline-induced cardiotoxicity and the cardiac-sparing effect of liposomal formulation. *Int. J. Nanomedicine*, **2007**, *2*, 567-583.

[146] O'Brien, M.E.R.; Wigler, N.; Inbar, M.; Rosso, R.; Grischke, E.; Santoro, A.; Catane, R.; Kieback, D.G.; Tomczak, P.; Ackland, S.P.; Orlandi, F.; Mellars, L.; Alland, L.; Tendler, C. Reduced cardiotoxicity and comparable efficacy in a phase III trial of pegylated liposomal doxorubicin HCl (CAELYX™/Doxil®) versus conventional doxorubicin for first-line treatment of metastatic breast cancer. *Ann. Oncol.*, **2004**, *15*, 440-449.

[147] Northfelt, D.W.; Dezube, B.J.; Thommes, J.A.; Miller, B.J.; Fischl, M.A.; Friedman-Kien, A.; Kaplan, L.D.; Du Mond, C.; Mamelok, R.D.; Henry, D.H. Pegylated-liposomal doxorubicin versus doxorubicin, bleomycin, and vincristine in the treatment of AIDS-related Kaposi's sarcoma: results of a randomized phase III clinical trial. *Clin. Oncol.*, **1998**, *16*, 2445-2451.

[148] Cianfrocca, M.; Lee, S.; Roenn, J.V., Tulpule, A.; Dezube, B.J.; Aboulafia, D.M.; Ambinder, R.F.; Lee, J.Y.; Krown, S.E.; Sparano, J.A. Randomized trial of paclitaxel versus pegylated liposomal doxorubicin for advanced human immunodeficiency virus-associated Kaposi sarcoma. *Cancer*, **2010**, *116*, 3969-3977.

[149] Gordon, A.N.; Fleagle, J.T.; Guthrie, D.; Parkin, D.E.; Gore, M.E.; Lacave, A.J. Recurrent epithelial ovarian carcinoma: A randomized Phase III study of pegylated liposomal doxorubicin versus topotecan. *J. Clin. Oncol.*, **2001**, *19*, 3312-3322.

[150] Dawidczyk, C.M.; Kim, C.; Park, J.H.; Russel, L.M.; Lee, K.H.; Pomper, M.G.; Searson, P.C. State-of-the-art in design rules for drug delivery platforms: Lessons learned from FDA-approved nanomedicines. *J. Control. Release*, **2014**, *187*, 133-144.

[151] Harris, L.; Batist, G.; Belt, R.; Rovira, D.; Navari, R.; Azarnia, N.; Welles, L.; Winer, E. Liposome-encapsulated doxorubicin compared with conventional doxorubicin in a randomized multicenter trial as first-line therapy of metastatic breast carcinoma. *Cancer*, **2002**, *94*, 25-36.

[152] Gill, P.S.; Wernz, J.; Scadden, D.T.; Cohen, P.; Mukwaya, G.M.; von Roenn, J.H.; Jacobs, M.; Kempin, S.; Silverberg, I.; Gonzales, G.; Rarick, M.U.; Myers, A.M.; Shepherd, F.; Sawka, C.; Pike, M.C.; Ross, M.E. Randomized phase III trial of liposomal daunorubicin versus doxorubicin, bleomycin, and vincristine in AIDS-related Kaposi's sarcoma. *J. Clin. Oncol.*, **1996**, *14*, 2353-2364.

[153] Glantz, M.J.; Jaeckle, K.A.; Chamberlain, M.C.; Phuphanich, S.; Recht, L.; Swinnen, L.J.; Maria, B.; LaFollette, S.; Schmann, G.B.; Cole, BF.; Howell, S.B. A randomized controlled trial comparing intrathecal sustained-release cytarabine (DepoCyt) to intrathecal methotrexate in patients with neoplastic meningitis from solid tumors. *Clin. Cancer Res.*, **1999**, *11*, 3394-3402.

[154] Silverman, J.A.; Deitcher, S.R. Marqibo® (vincristine sulfate liposome injection) improves the pharmacokinetics and pharmacodynamics of vincristine. *Cancer Chemother. Pharmacol.*, **2013**, *71*, 555-564.

[155] Stathopoulos, G.P.; Boulikas, T. J. Lipoplatin formulation review article. *Drug Deliv.*, **2012**, 2012:581363.

[156] Jehn, C.F.; Boulikas, T.; Kourvetaris, A.; Kofla, G.; Possinger, K.; Lüftner, D. First safety and response results of a randomized Phase III study with liposomal Platin in the treatment of advanced squamous cell carcinoma of the head and neck (SCCHN). *Anticancer Res.*, **2008**, *28*, 3961-3964.

[157] Mylonakis, N.; Athanasiou, A.; Ziras, N.; Angel, J.; Rapti, A.; Lampaki, S.; Politis, N.; Karanikas, C. Kosmas, C. Phase II study of liposomal cisplatin (Lipoplatin™) plus gemcitabine versus cisplatin plus gemcitabine as first line treatment in inoperable (stage IIIB/IV) non-small cell lung cancer. *Lung Cancer*, **2010**, *68*, 240-247.

[158] Stathopoulos, G.P.; Antoniou, D.; Dimitroulis, J.; Michalopoulou, P.; Bastas. A.; Marosis, K.; Stathopoulous, J.; Provata, A.; Yiamboudakis, P.; Veldekis, D.; Lolis, N.; Georgatou, N.; Toubis, M.; Pappas, Ch.; Tsoukalas, G. Liposomal cisplatin combined with paclitaxel versus cisplatin and paclitaxel in non-small-cell lung cancer: A randomized phase III multicenter trial. *Ann. Oncol.*, **2010**, *21*, 2227-2232.

[159] http://clinicaltrials.gov/ct2/results?term=thermodox (July, 2014).

[160] http://celsion.com/docs/pipeline_overview (July, 2014).

[161] http://clinicaltrials.gov/ct2/show/NCT00964080 (July, 2014).

[162] Wickham, T.; Futch, K. *Cancer Res.*, **2012**, *72*, P5-18-09.

[163] http://clinicaltrials.gov/show/NCT01655693 (June, 2014)

[164] Barraud, L.; Merle, P.; Soma, E.; Lefrançois, L.; Guerret, S.; Chevallier, M.; Dubernet, C.; Couvreur, P.; Trépo, C.; Vitvitski, L. Increase of doxorubicin sensitivity by doxorubicin-loading into nanoparticles for hepatocellular carcinoma cells *in vitro* and *in vivo*. *J. Hepatol.*, **2005**, *42*, 736-743.

[165] Merle, P.; Ahmed, S.Si.; Habersetzer, F.; Abergel, A.; Taieb, J.; Bonyhay, L.; Costantini, D.; Dufour-Lamartinie, J.; Trepo, C. Phase 1 study of intra-arterial hepatic (IAH) delivery of doxorubicin-transdrug (DT) for patients with advanced hepatocellular carcinoma (HCC). *J. Clin. Oncol.*, **2006**, *24*, 14094.

[166] www.BioAlliancePharma.com (July 2014)

[167] http://clinicaltrials.gov/show/NCT01655693 (June 2014).

[168] Zhang, Z.; Liao, G.; Nagai, T.; Hou, S. Mitoxantrone polybutyl cyanoacrylate nanoparticles as an anti-neoplastic targeting drug delivery system. *Int. J. Pharm.*, **1996**, *139*, 1-8.

[169] Zhou, Q.; Sun, X.; Zeng, L.; Liu, J.; Zhang, Z. A randomized multicenter phase II clinical trial of mitoxantrone-loaded nanoparticles in the treatment of 108 patients with unresected hepatocellular carcinoma. *Nanomedicine*, **2009**, *5*, 419-426.

[170] Lu, Y.; Park, K. Polymeric micelles and alternative nanonized delivery vehicles for poorly soluble drugs. *Int. J. Pharm.*, **2013**, *453*, 198-214.

[171] Cabral, H.; Kataoka, K. Progress of drug-loaded polymeric micelles into clinical studies. *J. Control. Release*, **2014**, DOI: 10.1016/j.jconrel.2014.06.042.

[172] Lee, K.S.; Chung, H.C.; Im, S.A.; Park, Y.H.; Kim, C.S.; Kim, S.B.; Rha, S.Y.; Lee, M.Y.; Ro, J. Multicenter phase II trial of Genexol-PM, a Cremophor-free, polymeric micelle formulation of paclitaxel, in patients with metastatic breast cancer. *Breast Cancer Res. Treat.*, **2008**, *108*, 241-250.

[173] Kim, D.-W.; Kim, S.-Y.; Kim, H.-K.; Kim, S.-W.; Shin, S.W.; Kim, J.S.; Park, K.; Lee, M.Y.; Heo, D.S. Multicenter phase II trial of Genexol-PM, a novel Cremophor-free, polymeric micelle formulation of paclitaxel, with cisplatin in patients with advanced non-small-cell lung cancer. *Ann. Oncol.*, **2007**, *18*, 2009-2014.

[174] http://clinicaltrials.gov/ct2/show/NCT00912639 (June, 2014)

[175] http://clinicaltrials.gov/ct2/show/NCT01689194 (June, 2014)

[176] Kato, K.; Chin, K.; Yoshikawa, T.; Yamaguchi, K.; Tsuji, Y.; Esaki, T.; Sakai, K.; Kimura, M.; Hamaguchi, T.; Shimada, Y.; Matsumara, Y.; Ikeda, R. Phase II study of NK105, a paclitaxel-incorporating micellar nanoparticle, for previously treated advanced or recurrent gastric cancer. *Invest. New Drugs*, **2012**, *30*, 1621-1627.

[177] http://clinicaltrials.gov/ct2/show/NCT01644890 (June, 2014)

[178] Nishiyama, N.; Okazaki, S.; Cabral, H.; Miyamoto, M.; Kato, Y.; Sugiyama, Y.; Nishio, K.; Matsumura, Y.; Kataoka, K. Novel cisplatin-incorporated polymeric micelles can eradicate solid tumors in mice. *Cancer Res.*, **2003**, *63*, 8977-8983.

[179] Plummer, R.; Wilson, R.H.; Calvert, H.; Boddy, A.V.; Griffin, M.; Sludden, J.; Tilby, M.J.; Eatock, M.; Pearson, D.G.; Ottley, C.J.; Matsumura, Y.; Kataoka, K.; Nishiya, T. A Phase I clinical study of cisplatin-incorporated polymeric micelles (NC-6004) in patients with solid tumours. *Brit. J. Cancer*, **2011**, *104*, 593- 598.

[180] http://clinicaltrials.gov/ct2/show/NCT02043288 (June, 2014)

[181] Matsumura, Y. Preclinical and clinical studies of NK012, an SN-38-incorporating polymeric micelles, which is designed based on EPR effect. *Adv. Drug Del. Rev.*, **2011**, *63*, 184-192.

[182] http://clinicaltrials.gov/ct2/show/NCT00951054 (June, 2014)

[183] http://clinicaltrials.gov/ct2/show/NCT01238939 (June, 2014)

[184] Matsumura, Y.; Hamaguchi, T.; Ura, T.; Muro, K.; Yamada, Y.; Shimada, Y.; Shirao, K.; Okusaka, T.; Ueno, H.; Ikeda, M.; Watanabe, W. Phase I clinical trial and pharmacokinetic evaluation of NK911, a micelle-encapsulated doxorubicin. *Br. J. Cancer*, **2004**, *91*, 1775-1781.

[185] Harada, M.; Bobe, I.; Saito, H.; Shibata, N.; Tanaka, R.; Hayashi, T.; Kato, Y. Improved anti-tumor activity of stabilized anthracycline polymeric micelle formulation, NC-6300. *Cancer Sci.*, **2011**, *102*, 192-199.

[186] Takahashi, A.; Yamamoto, Y.; Yasunaga, M.; Koga, Y.; Kuroda, J.-I.; Takigahira, M.; Harada, M.; Saito, H.; Hayashi, T.; Kato, Y.; Kinishita, T.; Ohkohchi, N.; Hyodo, I.; Matsumura, Y. NC-6300, an epirubicin-incorporating micelle, extends the antitumor effect and reduces the cardiotoxicity of epirubicin. *Cancer Sci.*, **2013**, *104*, 920-925.

[187] Matsumura, Y. The drug discovery by nanomedicine and its clinical experience. *Jpn. J. Clin. Oncol.*, **2014**, *44*, 515-525.

[188] Alakhov, V.; Klinski, E.; Li, S.; Pietrzynski, G.; Venne, A.; Batrakova, E.; Bronitch, T.; Kabanov, A. Block copolymer-based formulation of doxorubicin. From cell screen to clinical trials. *Colloids Surf. B*, **1999**, *16*, 113-134.

[189] Danson, S.; Ferry, D.; Alakhov, V.; Margison, J.; Kerr, D.; Jowle, D.; Brampton, M.; Halbert, G.; Ranson, M. Phase I dose escalation and pharmacokinetic study of pluronic polymer-bound doxorubicin (SP1049C) in patients with advanced cancer. *Br. J. Cancer*, **2004**, *90*, 2085-2091.

[190] Valle, J.W.; Armstrong, A.; Newman, C.; Alakhov, V.; Pietrzynski, G.; Brewer, J.; Campbell, S.; Corrie, P.; Rowinsky, E.K.; Ranson, M. A phase 2 study of SP1049C, doxorubicin in P-glycoprotein-targeting pluronics, in patients with advanced adenocarcinoma of the esophagus and gastroesophageal junction. *Invest. New Drugs*, **2011**, *5*, 1029-1037.

[191] http://clinicaltrials.gov/ct2/show/NCT01300533 (June, 2014)

[192] http://clinicaltrials.gov/ct2/show/NCT01812746 (June, 2014)

[193] Duncan, R. Polymer therapeutics: Top 10 selling pharmaceuticals - What next? *J. Control. Release*, **2014**, DOI: 10.1016/j.jconrel.2014.05.001.

[194] Pasut, G.; Veronese, F.M. State of the art in PEGylation: The great versatility achieved after forty years of research. *J. Control. Release*, **2012**, *161*, 461-472.

[195] http://clinicaltrials.gov/ct2/show/NCT01663012 (June, 2014)

[196] http://clinicaltrials.gov/ct2/show/NCT01492101 (June, 2014)

[197] http://clinicaltrials.gov/ct2/show/NCT01036113 (July, 2014)

[198] http://www.nektar.com/product_pipeline/oncology_nktr-105.html (July, 2014)

[199] Svenson, S.; Wolfgang, M.; Hwang, J.; Ryan, J.; Eliasof, S. Preclinical to clinical development of the novel camptothecin nanopharmaceutical CRLX101. *J. Control. Release*, **2011**, *153*, 46-55.
[200] http://clinicaltrials.gov/ct2/show/NCT01380769 (July, 2014)
[201] O'Brien, M.E.; Socinski, M.A.; Popovich, A.Y.; Bondarenko, I.N.; Tomova, A.; Bilynsky, B.T.; Hotko, Y.S.; Ganul, V.L.; Kostinsky, I.Y.; Eisenfeld, A.J.; Sandalic, L.; Oldham, F.B.; Bandstra, B.; Sandler, A.B.; Singer, J.W. Randomized phase III trial comparing single-agent paclitaxel poliglumex (CT-2103, PPX) with single-agent gemcitabine or vinorelbine for the treatment of PS 2 patients with chemotherapy-naïve advanced non-small cell lung cancer. *J. Thorac. Oncol*., **2008**, *7*, 728-734.
[202] Paz-Ares, L.; Ross, H.; O'brien, M.; Riviere, A.; Gatzemeier, U.; Von Pawel, J.; Kaukel, E.; Freitag, L.; digel, W.; Bischoff, H.; Garcia-Campelo, R.; Iannotti, N.; Reiterer, P.; Bover, I.; Prendiville, J.; Eisenfeld, A.J.; Oldham, F.B.; Bandstra, B.; Singer, J.W.; Bononi, P. Phase III trial comparing paclitaxel poliglumex vs docetaxel in the second-line treatment of non-small-cell lung cancer. *Brit. J. Cancer*, **2008**, *98*, 1608-1613.
[203] http://clinicaltrials.gov/ct2/show/NCT00108745 (July, 2014).
[204] Homsi, J.; Simon, G.R.; Garrett, C.R.; Springett, G.; De Conti, R.; Chiappori, A.A.; Munster, P.N.; Burton, M.K.; Stromatt, S.; Allievi, C.; Angiuli, P.; Eisenfeld, A.; Sullivan, D.M.; Daud, A.I. Phase I trial of poly-l-glutamate camptothecin (CT-2106) administered weekly in patients with advanced solid malignancies. *Clin. Cancer Res*., **2007**, *13*, 5855-5861.
[205] http://clinicaltrials.gov/ct2/show/NCT00291837 (July, 2014)
[206] http://clinicaltrials.gov/ct2/show/NCT00291785 (July, 2014)
[207] Vasey, P.A.; Kaye, S.B.; Morrison, R.; Twelves, C.; Wilson, P.; Duncan, R.; Thomson, A.H.; Murray, L.S.; Hilditch, T.E.; Murray, T.; Burtles, S.; Fraier, D.; Frigerio, E.; Cassidy. Phase I clinical and pharmacokinetic study of PK1 [N-(2-hydroxypropyl)methacrylamide copolymer doxorubicin]: first member of a new class of chemotherapeutic agents-drug-polymer conjugates. *J. Clin. Cancer Res*., **1999**, *1*, 83-94.
[208] Seymour, L.W.; Ferry, D.R.; Kerr, D.J.; Rea, D.; Whitlock, M.; Poyner, R.; Boivin, C.; Hesslewood, S.; Twelves, C.; Blackie, R.; Schatzlein, A.; Jodrell, D.; Bissett, D.; Calvert, H.; Lind, M.; Robbins, A.; Burtles, S.; Duncan, R.; Cassidy, J. Phase II studies of polymer-doxorubicin (PK1, FCE28068) in the treatment of breast, lung and colorectal cancer. *Int. J. Oncol*., **2009**, *34*, 1629-1636.
[209] Nowotnik, D.P.; Cvitkovic, E. ProLindac™ (AP5346): A review of the development of an HPMA DACH platinum polymer therapeutic. *Adv. Drug Del. Rev*., **2009**, *61*, 1214-1219.
[210] Owen, S.C.; Cahn, D.P.Y.; Shoichet, M.S. Polymeric micelle stability. *Nano Today*, **2012**, *7*, 53-65.
[211] Talelli, M.; Iman, M.; Varkouhi, A.K.; Rijcken, C.J.F.; Schiffelers, R.M.; Etrych, T.; Ulbrich, K.; van Nostrun, C.F.; Lammers, T.; Storm, G.; Hennink, W.E. Core-crosslinked polymeric micelles with controlled release of covalently entrapped doxorubicin. *Biomaterials*, **2010**, *31*, 7797-7804.
[212] Cho, E.C.; Zhang, Q.; Xia, Y.N. The effect of sedimentation and diffusion on cellular uptake of gold nanoparticles. *Nat. Nanotechnol*., **2011**, *6*, 385-391.
[213] Gabizon, A.; Shmeeda, H.; Barenholz, Y. Pharmacokinetics of pegylated liposomal doxorubicin. *Clin. Pharmakokinetics*, **2003**, *42*, 419-436.
[214] Uchiyama, K.; Nagayasu, A.; Yamagiwa, Y.; Nishida, T.; Harashima, H.; Kiwada, H. Effects of the size and fluidity of liposomes on their accumulation in tumors: A presumption of their interaction with tumors. *Int. J. Pharm*., **1995**, *121*, 195-203.
[215] Cabral, H.; Matsumoto, Y.; Mizuno, K.; Chen, Q.; Murakami, M.; Kimura, M.; Terada, Y.; Kataoka, K. Accumulation of sub-100 nm polymeric micelles in poorly permeable tumours depends on size. *Nat. Nanotechnol*., **2011**, *6*, 815-823.
[216] Fox, M.E.; Szoka, F.C.; Fréchet, J.M.J. Soluble Polymer Carriers for the Treatment of Cancer: The importance of molecular architecture. *Acc. Chem. Res*., **2009**, *42*, 1141-1151.
[217] Owens, D.E.; Peppas, N.A. Opsonization, biodistribution, and pharmacokinetics of polymeric nanoparticles. *Int. J. Pharm*., **2006**, *307*, 93-102.
[218] Dobrovolskaia, M.A.; Aggarwal, P.; Hall, J.B.; McNeil, S.E. Preclinical studies to understand nanoparticle interaction with the immune system and its potential effects on nanoparticle biodistribution. *Mol. Pharm*., **2008**, *5*, 487-495.
[219] Gratton, S.E.A.; Ropp, P.A.; Pohlhaus, P.D.; Luft, J.C.; Madden, V.J.; Napier, M.E.; DeSimone, J.M. The effect of particle design on cellular internalization pathways. *Proc. Natl. Acad. Sci. U.S.A*., **2008**, *105*, 11613-11618.
[220] He, C.; Hu, Y.; Yin, L.; Tang, C.; Yin, C. Effects of particle size and surface charge on cellular uptake and biodistribution of polymeric nanoparticles. *Biomaterials*, **2010**, *31*, 3657-3666.
[221] Xiao, K.; Li, Y.; Luo, J.; Lee, J.C.; Xiao, W.; Gonik, A.M.; Agarwal, R.G.; Lam, K.S. The effect of surface charge on *in vivo* biodistribution of PEG-oligocholic acid based micellar nanoparticles. *Biomaterials*, **2011**, *32*, 3435-3446.
[222] Zhu, M.; Nie, G.; Meng, H.; Xia, T.; Nel, A.; Zhao, Y. Physicochemical properties determine nanomaterial cellular uptake, transport, and fate. *Acc. Chem. Res*., **2013**, *46*, 622-631.
[223] Mu, Q.; Jaing, G.; Chen, L.; Zhou, H.; Fourches, D.; Tropsha, A.; Yan, B. Chemical basis of interactions between engineered nanoparticles and biological systems. *Chem. Rev*., **2014**, DOI: 10.1021/cr400295a.
[224] Geng, Y.; Dalhaimer, P.; Cai, s.; Tsai, R.; Tewari, M.; Minko, T.; Discher, D.E. Shape effects of filaments versus spherical particles in flow and drug delivery. *Nat. Nanotech*., **2007**, *2*, 249-255.
[225] Choi, H.S.; Liu, W.; Misra, P.; Tanaka, E.; Zimmer, J.P.; Ipe, B.I.; Bawendi, M.G.; Frangioni, J.V. Renal clearance of quantum dots. *Nat. Biotechnol*., **2007**, *25*, 1165-1170.
[226] Longmire, M.; Choyke, P.L.; Kobayashi, H. Clearance properties of nano-sized particles and molecules as imaging agents: considerations and caveats. *Nanomedicine*, **2008**, *3*, 703-717.
[227] Maeda, H.; Nakamura, H.; Fang, J. The EPR effect for macromolecular drug delivery to solid tumors: Improvement of tumor uptake, lowering of systemic toxicity, and distinct tumor imaging *in vivo*. *Adv. Drug Del. Rev*., **2013**, *65*, 71-79.
[228] Koning, G.A.; Fretz, M.M.; Woroniecka, U.; Storm, G.; Krijger, G.C. Targeting liposomes to tumor endothelial cells for neutron capture therapy. *Appl. Radiat. Isot*., **2004**, *61*, 963-967.

Journal of Controlled Release 165 (2013) 153–161

Contents lists available at SciVerse ScienceDirect

Journal of Controlled Release

journal homepage: www.elsevier.com/locate/jconrel

NANOMEDICINE

Combination chemotherapy using core-shell nanoparticles through the self-assembly of HPMA-based copolymers and degradable polyester

Eliézer Jäger [a,*], Alessandro Jäger [a], Petr Chytil [a], Tomáš Etrych [a], Blanka Říhová [b], Fernando Carlos Giacomelli [c], Petr Štěpánek [a], Karel Ulbrich [a]

[a] Institute of Macromolecular Chemistry, Academy of Sciences of the Czech Republic, Heyrovsky Sq. 2, 162 06 Prague 6, Czech Republic
[b] Institute of Microbiology, Academy of Sciences of the Czech Republic, v.v.i., Vídenska 1083, 142 20 Prague 4, Czech Republic
[c] Centro de Ciências Naturais e Humanas, Universidade Federal do ABC, 09210-170 Santo André, Brazil

ARTICLE INFO

Article history:
Received 20 August 2012
Accepted 16 November 2012
Available online 23 November 2012

Keywords:
Combination therapy
Polymeric core-shell nanoparticles
Docetaxel
Doxorubicin
EL-4 T cell lymphoma in vivo

ABSTRACT

The preparation of core-shell polymeric nanoparticles simultaneously loaded with docetaxel (DTXL) and doxorubicin (DOX) is reported herein. The self-assembly of the aliphatic biodegradable copolyester PBS/PBDL (poly(butylene succinate-co-butylene dilinoleate)) and HPMA-based copolymers (*N*-(2-hydroxypropyl) methacrylamide-based copolymers) hydrophobically modified by the incorporation of cholesterol led to the formation of narrow-size-distributed (PDI<0.10) sub-200-nm polymeric nanoparticles suitable for passive tumor-targeting drug delivery based on the size-dependent EPR (enhanced permeability and retention) effect. The PHPMA provided to the self-assembled nanoparticle stability against aggregation as evaluated in vitro. The highly hydrophobic drug docetaxel (DTXL) was physically entrapped within the PBS/PBDL copolyester core and the hydrophilic drug doxorubicin hydrochloride (DOX·HCl) was chemically conjugated to the reactive PHPMA copolymer shell via hydrazone bonding that allowed its pH-sensitive release. This strategy enabled the combination chemotherapy by the simultaneous DOX and DTXL drug delivery. The structure of the nanoparticles was characterized in detail using static (SLS), dynamic (DLS) and electrophoretic (ELS) light scattering besides transmission electron microscopy (TEM). The use of nanoparticles simultaneously loaded with DTXL and DOX provided a more efficient suppression of tumor-cell growth in mice bearing EL-4 T cell lymphoma when compared to the effect of nanoparticles loaded with either DTXL or DOX separately. Additionally, the obtained self-assembled nanoparticles enable further development of targeting strategies based on the use of multiple ligands attached to an HPMA copolymer on the particle surface for simultaneous passive and active targeting and different combination therapies.

1. Introduction

Combined therapy could provide a promising strategy to suppress cancer-drug resistance because different drugs may damage or kill cancer cells at different stages of their growth cycles through distinct mechanisms of action. Clinically, it has been reported that a variety of drug combinations can induce synergisms in their activities and prevent disease recurrence [1]. Nevertheless, one major challenge of combination therapy is to unify the pharmacokinetics and cellular uptake of various drug molecules to precisely control the dosage and scheduling of multiple drugs, thereby maximizing their combined effects [2]. Load multiple therapeutic agents into a single drug-delivery vehicle for concurrent delivery to the desired sites of action provide a straightforward solution to this problem [3,4]. The systems based on reactive *N*-(2-hydroxypropyl)methacrylamide (HPMA) copolymers are successful examples. The polymer is highly hydrophilic, non-immunogenic and non-toxic and remains in the circulation for an extended period of time to enable drug combination therapy [5,6]. The HPMA copolymers (PHPMA) have recently been used as drug carriers for the combination of doxorubicin and aminoglutethimide [7], gemcitabine and doxorubicin with radiolabeled iodine-131-bound tyrosinamide [3] in addition to doxorubicin and dexamethasone [8]. Remarkable improvements have been confirmed in the therapeutic effects.

Promising advances in cancer treatment via combination therapy have also been achieved with polymeric nanoparticles (NPs). Several NP drug-delivery systems have demonstrated the ability to co-deliver multiple drugs [9–11]. The delivery of multiple drugs through a single nanoparticle has several advantages over delivery using co-administered NPs including the delivery of the drugs in the correct drug ratio, possible synergistic therapeutic effects, suppressed drug resistance and the ability to control drug exposure [12–14]. These two active research fields have recently converged to further improve the efficacy of cancer therapeutics.

This work details an alternative protocol for preparing sub-200-nm core-shell polymeric nanoparticles through the self-assembly of a

* Corresponding author. Tel.: +420 296 809 322.
E-mail address: jager@imc.cas.cz (E. Jäger).

0168-3659/$ – see front matter © 2012 Elsevier B.V. All rights reserved.
http://dx.doi.org/10.1016/j.jconrel.2012.11.009

biodegradable copolyester (PBS/PBDL) and hydrophobically modified HPMA-based copolymers. The anticancer drug doxorubicin (DOX) has been chemically conjugated to HPMA copolymer. The NPs are based on the following: (*i*) a biodegradable hydrophobic copolyester core (PBS/PBDL) that is able to carry the poorly water-soluble bioactive drug docetaxel (DTXL) with high loading and efficiency and (*ii*) a doxorubicin-conjugated HPMA copolymer hydrophilic shell that allows the NPs to escape recognition by the immune system components due to its protein-repellent properties. The use of hydrazone bonds permits the DOX, which is chemically attached to the HPMA copolymer, to be released via a pH-triggered pathway, thereby yielding nanoparticles potentially suitable for use in combination chemotherapy in vivo.

The nanoparticles were designed to enhance the accumulation and uptake of the therapeutics in solid tumors through the combination of their generally leaky microvasculature and missing or tight lymphatic capillary systems. This effect is known as the enhanced permeability and retention (EPR) effect. Such mechanisms generally guide the principles of passive tumor targeting. The EPR effect can be observed in almost all human solid tumors except in hypovascular sites (prostate or pancreatic cancer) [15]. The use of HPMA-based copolymers was encouraged by their known capability to decrease liver accumulation and prolong the circulation time of nanoparticles, as previously reported for PHPMA-modified liposomes [16] and PHPMA-modified nanospheres [17]. In polyelectrolyte complexes, extended plasma circulation, protein repellence and resistance to opsonization were successfully achieved [18].

As proof-of-principle, the current study demonstrates that the simultaneous delivery of DOX and DTXL to solid tumors is feasible in vivo through core-shell NPs using the HPMA-based copolymers and the PBS/PBDL degradable copolyester. The core-shell NPs were characterized in detail using static, dynamic and electrophoretic light-scattering techniques in addition to transmission electron microscopy, and their effectiveness was demonstrated in vivo in mice bearing EL-4 T cell lymphoma.

2. Experimental section

2.1. Materials

Dimerized fatty acid (DFA)—hydrogenated dilinoleic acid (DLA), trade name Pripol 1009, molecular weight ~570 $g \cdot mol^{-1}$, (C36) (Uniqema BV, The Netherlands); 1,4-butanediol (BD, Aldrich Chemie, CZ); succinic acid (SA, Aldrich Chemie, CZ); acetone (Merck, CZ) and THF (Merck, CZ) were used as received. Methacryloyl chloride, and 2,2′-azobis(isobutyronitrile) (AIBN) were purchased from Sigma-Aldrich. All other chemicals and solvents were of analytical grade. The solvents were dried and purified using conventional procedures and distilled prior to use. Human plasma was purchased from Sigma-Aldrich. All water was pretreated with the Milli-Q® Plus System (Millipore Corporation). Doxorubicin hydrochloride (DOX·HCl) was purchased from Meiji Seiko, Japan and docetaxel (DTXL) was purchased from Aurisco, China.

2.2. Synthesis and characterization of the copolyester

The synthesis of the aliphatic copolyester was performed following a previously described two-step melt polycondensation (esterification and polycondensation) protocol [19,20]. SA, DLA and BD were loaded into a glass reactor in a 1/2.2 molar ratio with the catalyst TBT (4×10^{-4} mol/mol diacids). The vessel was further evacuated and filled with argon. The reaction mixture was heated at 200 °C and stirred at constant speed (400 rpm). This first step (esterification) was considered complete when the theoretical H_2O yield (approximately 4 h) was removed from the reaction mixture by distillation and collected in a graduate cylinder. The polycondensation reaction was carried out at 250 °C, ~0.03 atm, under stirred at a constant speed (700 rpm) and it has been considered complete after 8 h.

The copolyester was purified via dissolution in chloroform and precipitation with methanol. The number average molecular weight (M_n) and molecular weight distribution (polydispersity, M_w/M_n) of the synthesized copolymer were determined using SEC [20]. Tetrahydrofuran (THF) was used as the mobile phase at a flow rate of 0.5 $mL \cdot min^{-1}$. The injection-loop volume was 0.1 mL. Measurements were performed using triple viscosity/concentration/light scattering detection. The apparatus was connected to a DAWN DSP-F light-scattering photometer (Wyatt Technology Corp.), a Viscotek model TDA 301 modified differential viscometer (without internal light scattering and concentration detectors) and a Shodex RI 71 differential refractometer. The data were accumulated and processed using the Astra and triSEC software packages. The ^{1}H NMR and ^{13}C NMR spectra were collected on a Bruker AMX-300 spectrometer at 25 °C operating at 300.1 MHz (^{1}H NMR) or 75.5 MHz (^{13}C NMR). The PBS/PBDL copolyester was dissolved in deuterated chloroform ($CDCl_3$) and the spectra were internally referenced to tetramethylsilane (TMS). Sixty-four scans were acquired for the ^{1}H NMR and 1000–10,000 scans for the ^{13}C NMR with 32 K and 62 K data points and delay times of 1 and 2 s, respectively. The quantitative ^{1}H NMR spectra were recorded with pulse widths of 6 ms (π/3) and a delay time of 20 s. For the ^{13}C NMR, the pulse and spectral widths were 4.3 ms (π/2) and 18 kHz, respectively.

2.3. Synthesis of both the PHPMA-chol (amphiphilic copolymer based on HPMA bearing a covalently bound cholesterol anchor) and the PHPMA-chol-DOX conjugate

2.3.1. Synthesis of the monomers

N-(2-hydroxypropyl)methacrylamide (HPMA) [21]: m.p. 69–70 °C, $(C_7H_{13}NO_2)_n$ $(143.19)_n$: calcd. C 58.72, H 9.15, N 9.78; found C 58.98, H 9.18, N 9.82; 6-methacrylamidohexanohydrazide (MA-εAhx-$NHNH_2$) [22]: m.p. 79–81 °C, $(C_{10}H_{17}N_3O_2)_n$ $(213.28)_n$: calcd. C 56.32, H 8.98, N 19.70; found C 56.49, H 8.63, N 19.83; and cholest-5en-3β-yl 6-methacrylamido hexanoate (MA-εAhx-chol) [23]: m.p. 98–100 °C, $(C_{37}H_{61}NO_3)_n$ $(567.90)_n$: calcd. C 78.25, H 10.83, N 2.47; found C 78.73, H 10.85, N 2.34, were prepared as previously described. The structure and purity of the monomers were examined using ^{1}H-NMR (Bruker spectrometer, 300 MHz) and HPLC (Shimadzu 10VP) with a C_{18} reverse-phase Chromolith Performance RP-18e (4.6×100 mm) column with diode array detection. The eluent was water–acetonitrile with gradient of 5–95 vol.% acetonitrile, 0.1 vol.% TFA and a flow-rate of 1 $mL \cdot min^{-1}$.

2.3.2. Synthesis of PHPMA-chol

The polymer precursor PHPMA-chol was prepared in solution via the free-radical polymerization of HPMA, MA-εAhx-$NHNH_2$ and MA-εAhx-chol in methanol using AIBN as an initiator: AIBN (1 wt.%), monomers (14 wt.%), molar ratio HPMA/MA-εAhx-$NHNH_2$/MA-εAhx-chol (89.6:8:2.4). The polymerization conditions and method of polymer isolation are described in the literature [22].

2.3.3. Synthesis of PHPMA-chol-DOX conjugate

The synthesis of the PHPMA-chol-DOX conjugate was performed through a reaction of the corresponding polymer precursor (PHPMA-chol) containing hydrazide groups with DOX in methanol in darkness. The polymer drug conjugate (PHPMA-chol-DOX) was purified to remove low-molecular-weight impurities (DOX or its degradation products) by gel filtration using a Sephadex LH-20 column with methanol as the eluent [23].

2.4. Characterization of HPMA-based polymers

The molecular weights of the polymers were determined with a Shimadzu HPLC system equipped with a GPC column (TSKgel G3000SWxl (300×7.8 mm; 5 μm)), an Optilab®-rEX UV/Vis refractive

index (RI) and DAWN EOS multiangle light scattering (MALS) (Wyatt Technology Co., USA) detectors using a methanol–sodium acetate buffer (0.3 M; pH 6.5) mixture (80:20 vol.%; flow rate = 0.5 mL·min^{-1}).

The cholesterol content in the PHPMA-chol was determined using ^{1}H NMR (Bruker spectrometer, 300 MHz) in $(CD_3)_2SO$, and the integral intensities of the ^{1}H NMR spectra were compared: δ 5.32 t, 1H (C = CH of cholesterol); δ 8.05 d; δ 3.68 Br, 1H (CH – O*H* of HPMA). The content of the hydrazide groups in the PHPMA-chol was determined using a modified TNBSA assay as described in the literature [22]. The total DOX content in the PHPMA-chol-DOX was measured using UV/Vis spectrophotometry in methanol [23]. The quantity of unbound DOX was determined by HPLC using a TSKgel G3000SWxl column (300 × 7.8 mm; 5 μm) equipped with a Shimadzu SPD-M10A photo-diode array detector (488 nm) and a methanol–sodium acetate buffer (0.3 M; pH 6.5; 80:20 vol.% mixture; flow-rate = 0.5 mL·min^{-1}).

2.5. Preparation of the nanoparticles

The core-shell NPs were prepared using a combination of the nanoprecipitation protocol and self-assembly. The following five NPs were prepared using the PBS/PBDL copolyester and HPMA-based polymers (Fig. 1): NP0 (PBS/PBDL uncovered and drug-free NPs), NP1 (drug-free NPs consisting of a PBS/PBDL core coated with PHPMA-chol), NPDTXL (DTXL-loaded NPs with DTXL loaded into the PBS/PBDL core coated with PHPMA-chol), NPDOX (NPs consisting of a PBS/PBDL core coated with PHPMA-chol-DOX) and NPDTXL-DOX (NPs prepared as a DTXL-loaded PBS/PBDL core coated with PHPMA-chol-DOX; DTXL/DOX in an ~2/1 mol/mol ratio).

To prepare the NPDTXL-DOX, a preheated (40 °C) acetone solution (5 mL) containing the PBS/PBDL copolyester (60 mg) and DTXL (4.25 mg) was added drop-wise (EW-74900-00, Cole-Parmer®) into a pre-heated (40 °C) 5% *v/v* ethanol Milli-Q® water solution (10 mL, pH = 7.4) containing the HPMA-chol-DOX copolymer (12.5 mg) (10.1% w_{DOX}/w_{PHPMA}). The pre-formed NPs were allowed to self-assemble over 2 h. The remaining acetone was then evaporated under reduced pressure. Possible free molecules were removed by washing the NP solution using an Amicon Ultra-4 centrifugal filter with a molecular-weight cut-off of 30 kDa (Millipore, Prague, CZ). The NPs were resuspended to yield the final desired volume (10 mL) and used immediately. The NPs, named NP0, NP1, NPDTXL and NPDOX, were prepared using essentially the same procedure.

2.6. Scattering characterization of the nanoparticles

2.6.1. Dynamic light scattering (DLS)

The DLS measurements were performed using an ALV CGE laser goniometer consisting of a 22-mW HeNe linear polarized laser operating at a wavelength (λ) of 632.8 nm, an ALV 6010 correlator, and a pair of avalanche photodiodes operating in the pseudo cross-correlation mode. The samples were loaded into 10-mm diameter glass cells and maintained at 25 ± 1 °C. The data were collected using the ALV correlator control software with a counting time of 90 s. The measured intensity correlation functions $g_2(t)$ were analyzed using the REPES algorithm [24] resulting in distributions of the relaxation times shown with equal area representation as $\tau A(\tau)$. The mean relaxation time, or relaxation frequency ($\Gamma = \tau^{-1}$), is related to the diffusion coefficient (D) of the nanoparticles as follows: $D = \frac{\Gamma}{q^2}$ in which $q = \frac{4\pi n \sin(\theta/2)}{\lambda}$ is the scattering vector with n being the refractive index of the solvent and θ the scattering angle. The hydrodynamic radius (R_H), or the distributions of R_H, were calculated using the well-known Stokes–Einstein relationship:

$$R_H = \frac{k_B T}{6\pi\eta D} \quad (1)$$

in which k_B is the Boltzmann constant, T is the absolute temperature and η is the viscosity of the solvent. At least 5 measurements were performed for each sample to check their reproducibility. The polydispersity of the nanoparticles was assessed using the cumulant analysis [24] of the correlation functions measured at 90° as follows:

$$\ln g_1(t) = \ln C - \Gamma t + \frac{\mu_2}{2} t^2 \quad (2)$$

in which C is the amplitude of the correlation function and Γ is the relaxation frequency (τ^{-1}). The parameter μ_2 is known as the second-order cumulant and was used to compute the polydispersity index of the samples (PDI = μ_2/Γ^2).

2.6.2. Static light scattering (SLS)

In the SLS mode, the samples were loaded into quartz cells (Hellma, Germany), and the scattering angle was adjusted stepwise from 30 to 150° with a 10° increase. The absolute light scattering is related to the weight-average molecular weight ($M_{w(NP)}$) and to the radius of gyration (R_G) of the NPs by the Zimm formalism:

$$\frac{Kc}{R_\theta} = \frac{1}{M_{w(NP)}}\left(1 + \frac{R_G^2 q^2}{3}\right) \quad (3)$$

in which K is the optical constant that includes the square of the refractive index increment (dn/dc), R_θ is the excess normalized scattered intensity (toluene was applied as the standard solvent) and c is the polymer concentration given in mg·mL^{-1}. The refractive index increment (dn/dc) of the PBS/PBDL NPs in pure water (0.153 mL·g^{-1}) and PHPMA-chol (0.167 mL·g^{-1}) was taken from our previous literature data [20,25]. The concentrations and refractive index increments of the core-shell NPs as a function of the molar mixing ratio were estimated on the basis of the complex formation model [26].

The average density of the nanoparticles (d) was estimated as:

$$d = \frac{3M_{w(NP)}}{4\pi N_A (R_H)^3} \quad (4)$$

in which N_A is Avogadro's number.

2.6.3. Electrophoretic light scattering (ELS)

The ELS measurements (Zetasizer NanoZS instrument, Malvern Instruments, UK) were employed to determine the average zeta potential (ζ) of the nanoparticles. The equipment measures the electrophoretic mobility (U_E) and converts that value to the ζ-potential (mV) through Henry's equation. The Henry's function was calculated using the Smoluchowski approximation. The measurements were performed

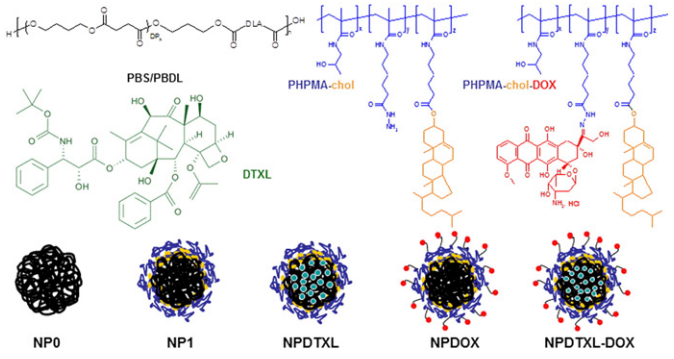

Fig. 1. Molecular structure of the PBS/PBDL copolyester — *left*, PHPMA-chol — *middle* and PHPMA-chol-DOX — *right* (top) and schematic representation of the prepared NPs (bottom) (PBS/PBDL — black, PHPMA — blue, cholesterol anchor — yellow, DTXL — green, and DOX — red).

in double distilled water at 25 °C and the reported ζ-potential values are the average of the 10 measurements.

2.7. Transmission electron microscopy (TEM)

The observations were recorded using a JEM 200CX (Jeol, Japan) microscope operating at 100 kV and equipped with a digital camera. The brightness, contrast and gamma corrections were performed using the standard software. The nanoparticles were diluted 100 times, and 5 μL of the aqueous solutions was dropped onto a copper TEM grid (300 mesh) coated with a carbon film.

2.8. Drug loading and encapsulation efficiency

After washing steps, the total quantity of DOX and DTXL loaded into the NPs was determined by the difference between the total DOX and DTXL feeding. The total DOX content was calculated after quantitative acid hydrolysis in 1 M HCl. After incubation for 1 h at 50 °C, doxorubicinone (aglycon of DOX) was extracted with chloroform. The organic phase was evaporated to dryness and the remaining solid was completely dissolved in acetonitrile and analyzed using a gradient-based HPLC analyzer (Shimadzu, Japan) with a reverse-phase Chromolith Performance RP-18e column (100×4.6, a water-acetonitrile eluent with an acetonitrile gradient of 0–100 vol.%, flow rate = 1.0 mL·min^{-1}) with fluorescence detection for DOX (excitation at 488 nm and emission at 560 nm) [27]. The total DTXL content in the NPs was determined by dissolving all NP components with ACN, then using the same HPLC system with UV detection at 227 nm [20]. Typically, 100 μL NP was used for the HPLC analysis. The drug-loading (*LC*) and the drug-loading efficiency (*LE*) were calculated using the following equations:

$$LC(\%) = \frac{\text{drug amount in nanoparticles}}{\text{mass of nanoparticles}} \times 100, \quad (5)$$

$$LE(\%) = \frac{\text{drug amount in nanoparticles}}{\text{drug feeding}} \times 100. \quad (6)$$

2.9. Release experiments

The release experiments were carried out at 37 °C in a pH-adjusted incubation media (pH 7.4 and 5.0). Aliquots (500 μL) of the core-shell NPDTXL-DOX were loaded into 36 Slide-A-Lyzer MINI dialysis microtubes with 10 kDa MWCO (Pierce, Rockford, IL), and the solution was dialyzed against 4 L of pH-adjusted PBS buffer under gentle stirring. The release media was changed periodically to reduce possible DTXL precipitation and/or drug-diffusion equilibrium. The drug release experiments were performed in triplicate. At each sampling time, three microtubes were removed from the dialysis system, and from each microtube 0.1 mL was sampled and in the particles remaining drugs were extracted using the aforementioned method. The reported data are expressed as the quantity of released DOX and DTXL (calculated from the decrease of the drug content in the particles) relative to the total DOX and DTXL content in the NPDTXL-DOX. No degradation products were detected during the analysis.

2.10. Stability of the nanoparticles in simulated physiological media

The stability of the NPDTXL-DOX NPs in diluted human plasma was examined as previously described [28]. The NPs were incubated in 10% *v*/*v* human plasma (Sigma-Aldrich, Czech Republic) at 37 °C under gentle stirring in a concentration of 1 mg·mL^{-1}. At each sampling time, an aliquot of the NPs was collected, and the DLS measurements were performed in triplicate to probe the hydrodynamic radius and size polydispersity index of the entities.

2.11. In vivo antitumor activity

The antitumor efficacy of the NPs was evaluated in C57BL/6 (B/6) mice inoculated with syngeneic T cell lymphoma EL-4 (ATCC TIB-39). The B/6 mice were purchased from the animal facility of the Institute of Physiology, Academy of Sciences of the Czech Republic, *v. v. i.* The mice were housed in accordance to the approved guidelines and food and water were given ad libitum. The animal room was maintained at 20 °C. The experimental designs were in accordance with the Act on Experimental Work with Animals (Decrees No. 311/97; 117/87, and Act No. 246/96) of the Czech Republic, which is fully compatible with the corresponding European Union directives.

The mice were randomly assigned to either an experimental or control group and they were injected subcutaneously into the shaven right ridge with 1×10^5 EL-4 cells to produce continuously growing solid tumors. The tumor sizes were measured using calipers in two perpendicular diameters every 2 days and expressed as tumor volume $V = a\times b^2/2$ (a = longer diameter, b = shorter diameter). The survival time was regularly scored. The NPs were administered (i.e., the therapeutic regime of the treatment was employed) when the tumors were well established (5–8 mm in diameter, 7 or 8 days after transplantation). The core-shell NPs were intravenously injected as two equal doses (totaling 10 mg DOX(equivalent)/kg and 20 mg DTXL(equivalent)/kg). The doses were determined according to the body weights of the mice as estimated at the time of drug administered. Groups of 8 mice were used for each treatment.

3. Results and discussion

The molecular structures of poly(butylene succinate-*co*-butylene dilinoleate) PBS/PBDL (core-forming) and *N*-(2-hydroxypropyl) methacrylamide PHPMA-based polymers (shell-forming) and the schematic representation of the prepared NPs are depicted in Fig. 1.

The macromolecular characteristics of the polymers are summarized in Table 1.

The number-average molecular weight (M_n) of the PBS/PBDL was estimated as 32.0 kDa using SEC with a reasonable degree of polydispersity ($M_w/M_n = 1.76$). The composition of the copolyester was previously discussed [19,20] and was determined from the ^{1}H NMR data using the relative integrals of SA arising from PBS and the dimerized fatty acid from PBDL. The monomer composition ratio was calculated as 3:1 (PBS:PBDL), which leads to a weight segment composition of ~50/50 *w*/*w*. The characteristic signals of "couplings" in the ^{1}H-NMR and ^{13}C-NMR spectra were not found confirming a statistical distribution of the monomer units. This finding was also supported by the ^{13}C NMR spectra, which described the division of the carbonyl groups (C═O) in the copolymer, with an area of ~64 ppm. Both carbonyl group signals correspond to the 3:1 ratio.

The PHPMA-chol precursor was prepared via the free radical terpolymerization of HPMA with comonomers bearing hydrazide groups and hydrophobic cholesterol substituents in a 77% yield. The obtained amphiphilic copolymer had a molecular weight (M_w) of 17.2 kDa, a $M_w/M_n = 1.92$ with a cholesterol content of ~2.3 mol% estimated as the optimal content for enabling sufficient coating of hydrophobic NPs [19]. The DOX·HCl was attached to the polymer

Table 1
Macromolecular characteristics of the synthesized polymers.

Entry	M_n (10^3 g·mol^{-1})[a]	M_w/M_n[a]	Cholesterol amount (mol%)[b]	DOX (*wt*.%)[c]
PBS/PBDL	32.0	1.76	–	–
PHPMA-chol	17.2	1.92	2.3	–
PHPMA-chol-DOX	21.1	1.65	2.3	10.1

[a] Measured by SEC.
[b] Determined by ^{1}H NMR.
[c] Measured by UV/Vis spectrophotometry.

precursor via a hydrazone bond (10.1% w_{DOX}/w_{HPMA}) resulting in the conjugate PHPMA-chol-DOX ($M_w = 21.1$ kDa, $M_w/M_n = 1.65$). The PHPMA-based polymers were synthesized with M_w values below the renal threshold ($M_w \approx 50$ kDa) allowing the polymer to undergo renal clearance and avoid accumulation after in vivo administration [23].

In comparison with well-known standard polyesters such as poly(ε-caprolactone) (PCL), poly(L-lactide-co-glycolide) (PLGA) and poly(L-lactic acid) (PLA), the spherical, surfactant-free PBS/PBDL NPs have recently been shown to carry a higher paclitaxel quantity (~6–7% $w_{drug}/w_{polymer}$). The nanoparticles were highly swollen by water and bulk erodible after approximately two weeks due to their porous structure [20], which accelerates the hydrolysis process, an attractive characteristic for drug delivery applications [29–31].

Unlike polymeric micelles, which are in dynamic equilibrium with free unimers, polymeric nanoparticles made from hydrophobic polyester or copolyesters are frozen-state colloidal particles. Therefore, no critical aggregation concentration can be observed ensuring their in vivo stability in the bloodstream [32–34].

The sub-200-nm diameter biodegradable and biocompatible NPs were prepared through self-assembly of the PBS/PBDL and the PHPMA-based copolymers (PHPMA-chol and PHPMA-chol-DOX). The concentrations of the PBS/PBDL and of the PHPMA-based polymers were optimized to obtain sub-200-nm diameter core-shell NPs [19]. The formation of the polymeric nanoparticles can be explained by the nucleation–aggregation mechanism [35]. Thus, when the solution is sufficiently saturated, the critical nuclei of pure solute form and grow by capturing solute molecules from their surroundings. Nevertheless, impure nuclei formation is expected in the presence of the PHPMA-based polymers dissolved in the water phase because the PHPMA-chol or PHPMA-chol-DOX will nucleate along with the PBS/PBDL. Accordingly, the PHPMA-based polymers act as system stabilizers and are therefore responsible for the interface between the hydrophobic PBS/PBDL core and the external aqueous environment reducing the surface tension between the water phase and the organic polymer solution leading consequently to the formation of smaller and narrowly distributed nanoparticles.

The DLS measurements revealed the assembly of well-defined low-dispersity core-shell NPs after the elimination of the organic solvent. Fig. 2 depicts the autocorrelation functions (a) and the respective distributions of R_H (b) for NP0, NP1 and NPDTXL-DOX.

In all cases, reasonably narrowly distributed nanoparticles were obtained with relaxation modes corresponding to the diffusive motion of the nanoparticles as characterized by the q^2-dependence of the relaxation frequency Γ (Fig. 2(c)) [36]. The polydispersity index calculated using cumulant analysis [24] remained below 0.1 (PDI < 0.1). The physicochemical characteristics of the NPs are summarized in Table 2.

The size of the core-shell NPs (R_H) was found to remain below the cut-off size for the leaky pathological vasculature ($2R_H < 200$ nm) making them potential candidates for use in targeted cancer chemotherapy via passive solid tumor accumulation due to the EPR effect [15]. The values of the zeta potential ($\zeta \approx -32$ mV) determined for NP0, NP1 and NPDTXL are negative suggesting good dispersion stability in an aqueous environment. The negative ζ-potentials prevent any aggregation of the particles by their electrostatic repulsion forces. The negative ζ-potentials are attributed to the delocalization of the negative charges of the ester bonds [37] and to the negative charges of the partially ionized carboxylic groups of polyester based in the fatty acids [20,38].

In contrast, the average ζ-potentials determined for NPDOX and NPDTXL-DOX were positive and are explained by the presence of DOX on the outer shell of the NPs, where the amino groups of the DOX neutralize the negative ζ-potential [39].

The formation of spherical core-shell nanoparticles was confirmed by transmission electron microscopy (TEM). Fig. 3 indicates that the NPs consist of an electron-dense compact core and a thicker shell which is highly diffused [19].

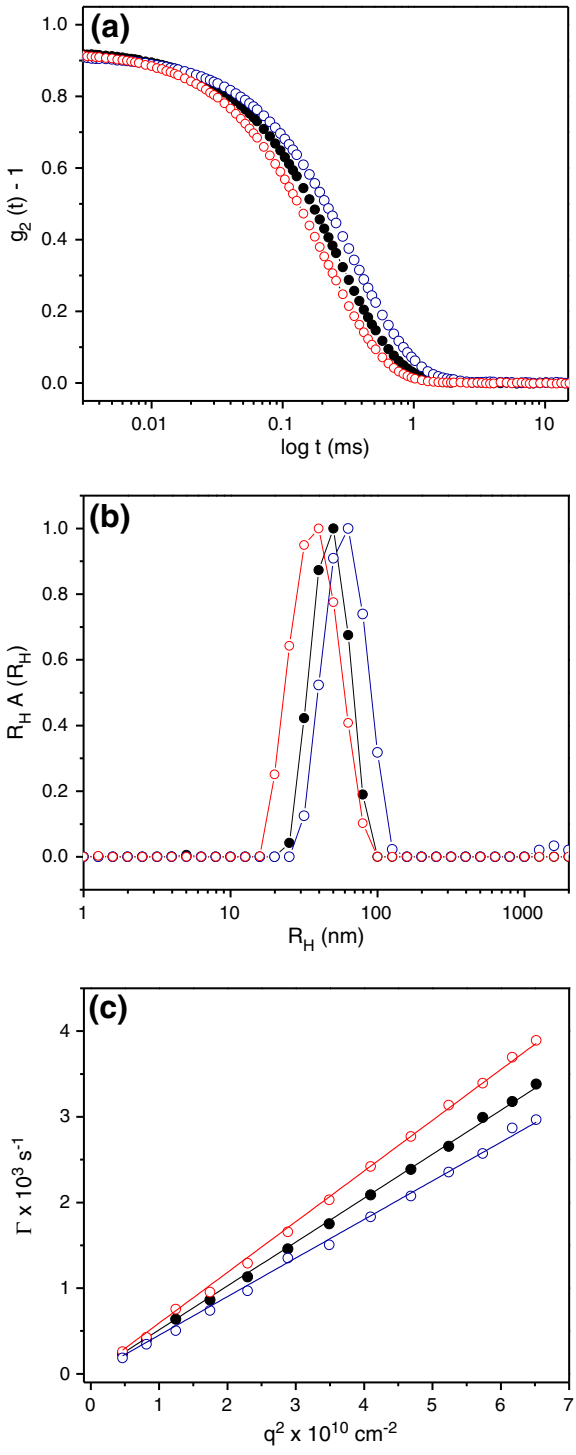

Fig. 2. Autocorrelation functions $g_2(t)$ measured at 90° (a), respective distributions of R_H as revealed by the REPES analysis (b) and q^2-dependence of Γ (c) for NP0 (●), NP1 (○) and NPDTXL-DOX (○) in water at 25 °C.

The representative SLS data of the core-shell NP1 and NPDTXL-DOX are provided in Fig. 4. The combination of SLS and DLS is appropriate for measuring their hydrodynamic dimensions and provides information on the shape and inner structure of the scattering objects.

The radius of gyration (R_G) of the NPs and their molecular weights $M_{w(NP)}$ were estimated from the slope of the curves and from the inverse of the intercepts. The data are provided in Table 1. A comparison to the naked NP0 confirms that the parameters R_H, R_G, and $M_{w(NP)}$ and the density (d) of the NPs are affected by the drug entrapment (DTXL) and by the presence of the hydrophilic shell. The

Table 2
Physicochemical characteristics of the prepared NPs.

Entry	R_H (nm)	Dispersity[a]	ζ (mV)	$M_{w(NP)}$ (10^7 g·mol^{-1})	R_G (nm)	d (g·mol^{-1})
NP0	46.0	0.10	−32.0	12.9	47.0	0.46
NP1	41.0	0.09	−26.0	4.2	38.0	0.24
NPDTXL-DOX	56.0	0.09	+17.0	23.3	61.0	0.53
NPDOX	54.0	0.08	+15.0	21.7	59.0	0.55
NPDTXL	44.0	0.06	−21.0	6.4	40.0	0.30

[a] Estimated using the cumulant analysis of the autocorrelation functions monitored at 90°.

reduction in the size and density of NP1 compared with NP0 is clear, and the hydrophobic drug encapsulation is responsible for reducing the R_G of the entities (comparing NP0 to NPDTXL) due to the collapsing (shrinkage of the NPs) promoted by favorable drug-copolyester hydrophobic interactions [20]. In contrast, the presence of the protonated drug (DOX) is responsible for the increase in the NP sizes (NPDOX and NPDTXL-DOX) which is most likely related to the formation of a thicker hydrophilic shell.

The simultaneous release profile of DTXL and DOX was investigated further. The anticancer drugs act mechanistically on cancer cells in distinct ways. Therefore, it is important to allow the NPs to release the individual drugs independently, enabling them to attack cancer cells via their independent mechanisms of action. The DTXL and DOX loading capacity and loading efficiency in the NPDTXL-DOX NPs were determined using Eqs. (5) and (6), respectively. The determined values were ~5.5% $w_{DTXL}/w_{NPDTXL\text{-}DOX}$ (~56 μg of DTXL per mg of nanoparticles) corresponding to a loading efficiency of 95%. The DOX loading capacity was equal to 1.7% $w_{DOX}/w_{NPDTXL\text{-}DOX}$ (~17.0 μg of DOX per mg of nanoparticles) corresponding to a loading efficiency of 98%. The overall loading capacity of the NPs was ~7.2% ($w_{Drugs}/w_{NPDTXL\text{-}DOX}$).

The release experiments were conducted at 37 °C and pH 7.4 (to simulate conditions during transport in blood) and at pH 5.0 (a buffer modeling the acidic cytosolic or endosome conditions in tumor cells). The profiles are given in Fig. 5. A sustained release of the DTXL was observed in which 39% and 31% of the loaded DTXL were released within the first 12 h of incubation at pH 7.4 and pH 5.0, respectively.

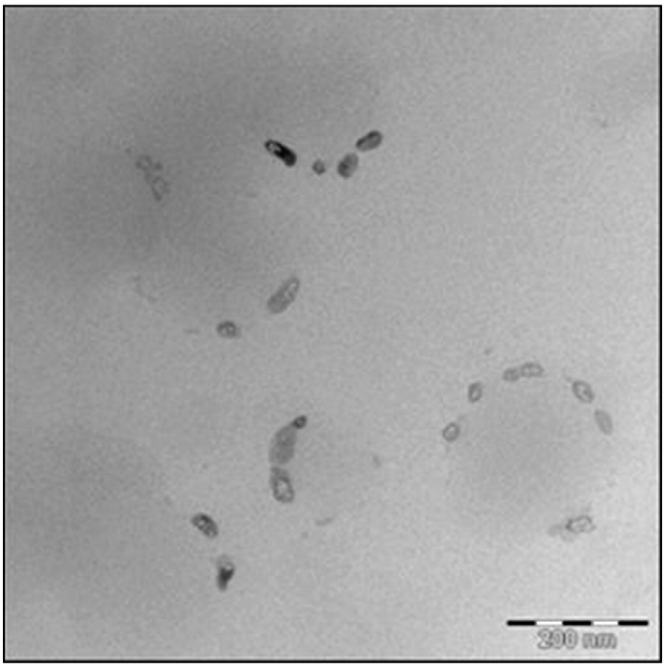

Fig. 3. TEM image of NPDTXL-DOX.

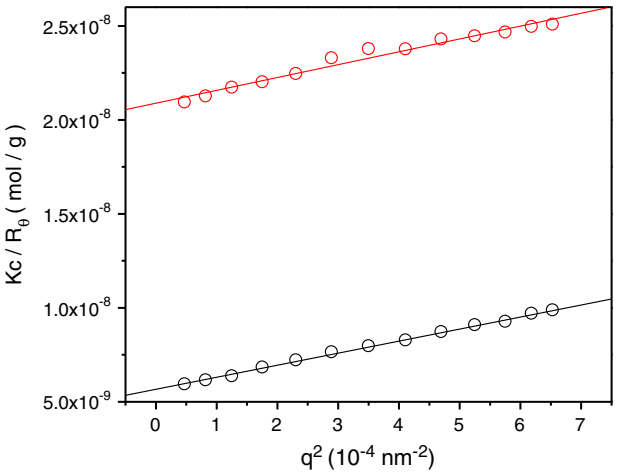

Fig. 4. Static light scattering measurements (Kc/R_θ vs. q^2) for NP1 (○) and NPDTXL-DOX (○) in water.

The remaining DTXL was slowly released with only 56% and 49% released at pH 7.4 and pH 5.0, respectively, within 48 h of incubation. The slow DTXL pharmacokinetics are attributed to the hydrophobicity of the manufactured PBS/PBDL core and to the poor water solubility (~0.025 μg·mL^{-1}) of DTXL. In the present case, the drug release is also supposed to be controlled by the diffusion of the drug through the polymer matrix and by the hydrolysis of the biodegradable PBS/PBDL copolymer [20]. However, a reasonably small quantity of DOX (10%) was released during the same period at pH 7.4, with more than 87% being released within the same period at a pH mimicking the intracellular environment (pH 5.0). The release data demonstrates that during the systemic circulation only marginal quantities of drugs are released before reaching the solid tumor environments via the EPR effect mechanism. Conversely, the DOX is quickly released at pH 5.0 with ~42% of the loaded DOX released within first 12 h and nearly total release of the anticancer drug within 48 h fulfilling the criteria for a pH-triggered drug release mechanism. Therefore, the core-shell NPDTXL-DOX nanoparticles exhibit the physicochemical properties required for practical application as nanocarriers in passive tumor-targeted drug delivery. The fastest DOX release profile at pH 5.0 and the slow DTXL release kinetics strongly hint that the co-delivery system can provide a synergistic effect for the treatment of solid tumors.

Furthermore, the efficient NP accumulation in the solid tumor sites requires extended circulating capabilities to enable a time-dependent extravasation of the nanoparticles through the leaky tumor

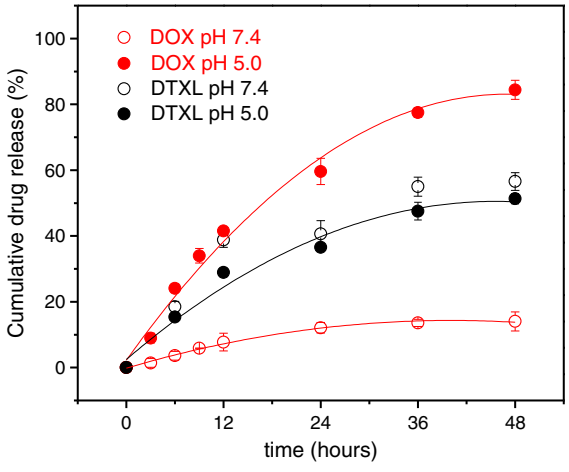

Fig. 5. DTXL and DOX release profiles from core-shell NPDTXL-DOX at pH 5.0 (DTXL ●; DOX ●) and pH 7.4 (DTXL ○; DOX ○). The values represent average ± s.d. (n = 3).

microvasculature and impaired or missing lymphatic drainage. The long-term stability of the NPs in serum is therefore a pre-requisite for the use of polymeric nanoparticles in vivo [19,40]. To confirm the serum stability of the NPDTXL-DOX NPs, they were incubated in 10% (*v*/*v*) diluted human plasma in PBS. The serum stability of the NPs was monitored by evaluating any possible changes in their hydrodynamic size and scattering intensity over time [28]. Fig. 6 shows the temporal stability of the NPs in blood plasma as a function of the incubation time.

The size and scattering intensity patterns of the nanocarrier system do not change within the first 24 h suggesting that the NPs are highly stable against aggregation in the simulated physiological media. The slight increase in hydrodynamic radius ($2R_H = 122$ nm) should be related to the adsorption of a protein monolayer because the average size of the dissolved single proteins is ~8 nm [41].

The stability of the NPs is promoted by the presence of the hydrophilic PHPMA shell once the HPMA copolymers deserve hydrophilicity rendering the adsorption of plasma proteins energetically unfavorable. The serum stability demonstrates the efficiency of the PHPMA coating for protecting the NPs in vitro against aggregation.

The anticancer activity of the NPs was evaluated in the mouse syngeneic lymphoma model. The developed tumors killed the untreated mice within 28–32 days (the mean survival time was 30 days, SD = 1.87, median survival = 28.5 days, n = 8). The NPs were administered in two doses (2×5 mg DOX(equivalent)/kg) on the 7th and 8th day after tumor transplantation. The NPDTXL-DOX treatment was substantially more effective in the mice inoculated with EL-4 T cell lymphoma than treatment with free drugs or with single-loaded NPs (NPDTXL or NPDOX) as presented in Fig. 7. After 30 days of treatment using NPDTXL or NPDOX, the tumor growth was reduced by ~50% and ~65%, respectively, compared with the controls ($p<0.005$). The NPDTXL-DOX NPs inhibited tumor growth by ~90% compared with the controls (30 days, $p<0.001$) or by ~30% compared with NPDTXL and NPDOX NPs ($p<0.005$). The co-delivery also suppressed tumor growth more efficient than the delivery of either free DOX or free DTXL at the same dose concentrations.

Along with the reduction in tumor growth, the survival time of the animals was also extended over that of the untreated controls (Fig. 7(b)). The efficacy of the combination chemotherapy (NPDTXL-DOX) in comparison with NPDTXL and NPDOX (dose-equivalent) was evident. The mice treated with core-shell NPDTXL-DOX survived significantly longer than the untreated control or separately administered DOX and DTXL. This might indicate a synergistic effect [42] requiring further investigation.

The NPDOX nanoparticles appear to have an equal antitumor efficacy as the free DOX, which contradicts our previous results related to the PHPMA-hydrazone-DOX conjugates in which a superior efficacy was observed [43,44]. This result may be attributed to the higher dose (e.g., 75 mg, 2×25 mg or 25 mg eq./kg) administered in our previous work. Because the efficacy of the treatment is significantly dose-dependent, an increase in the antitumor activity of NPDOX and NPDTXL-DOX can be expected at doses higher than 2×5 mg eq./kg.

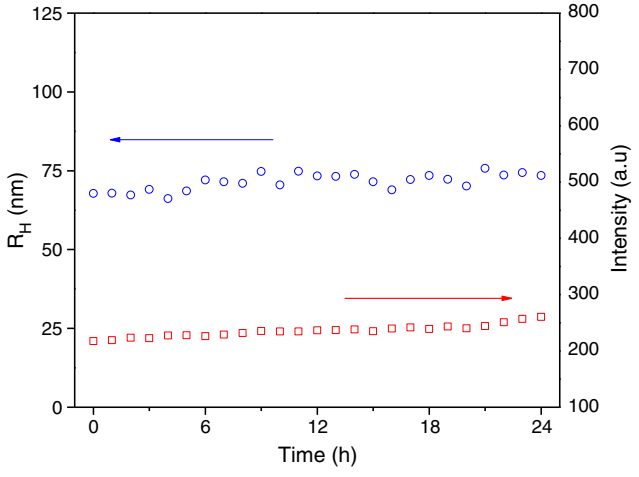

Fig. 6. R_H and light-scattering intensity as a function of the incubation time for NPDTXL-DOX incubated in diluted human plasma.

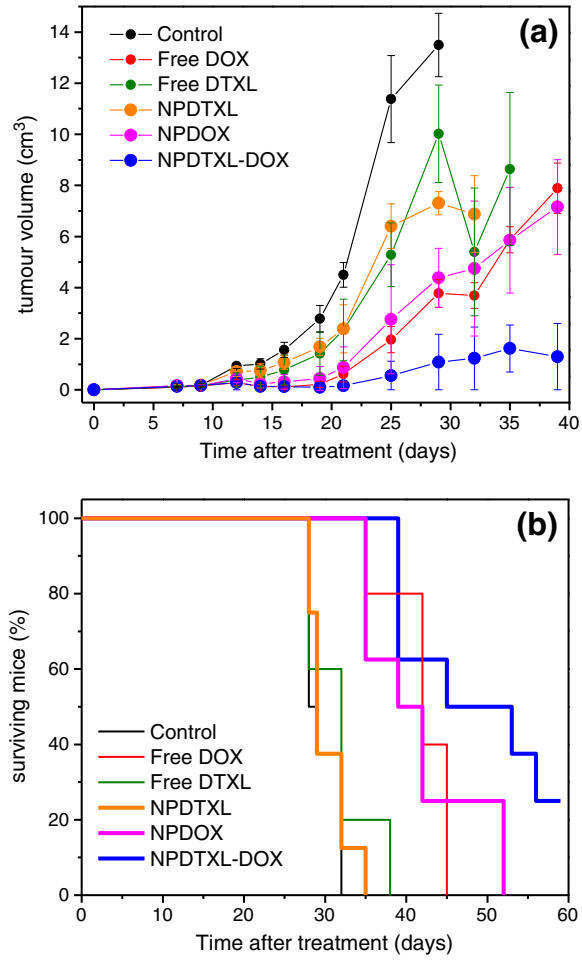

Fig. 7. In vivo effect of core-shell NPs on the growth of T cell lymphoma EL-4 (a), Kaplan–Meier survival plot of mice (b); NPDTXL (—) 2×5 mg DOX(equivalent)/kg, NPDOX (—) and NPDTXL-DOX (—) 2×5 mg DOX(equivalent)/kg, Free DTXL (—) 2×5 mg DOX(equivalent)/kg; and Free DOX (—) 2×5 mg DOX(equivalent)/kg, untreated control (—) (Student's *t*-test; $P<0.005$).

The EL-4 T cell lymphoma model is particularly aggressive and known for its leaky tumor vasculature. This model is one in which the enhanced polymer-drug accumulation via EPR mechanism has been observed [23]. Cancer treatments using free DTXL and NPDTXL were quite ineffective. The poor efficacy of NPDTXL is supposed to be related to the aggressiveness of the EL4 T cell lymphoma model, which is also most likely less sensitive to DTXL treatment. Additionally, the prolonged degradation time of PBS/PBDL (~2 weeks) and the favorable DTXL-PBS/PBDL hydrophobic interactions lead to a slow release of the hydrophobic drug in the acidic intracellular environment of the tumor cells as evidenced by the in vitro release data (Fig. 5).

Recently, the potential of combination chemotherapy using doxorubicin and paclitaxel has been evaluated in vitro in A549 (human lung cancer), B16 (mouse melanoma) and HepG2 (human hepatocellular carcinoma) [42] cells in which the highest activity was obtained when the release kinetics were similar and rapid (total release within 48 h). The same drug combination was loaded onto polymersomes, and its efficacy was evaluated in vivo in the human breast carcinoma xenograft model [45,46]. A more pronounced shrinkage of the tumors was observed when all of the drugs were released within 24 h. Based on

the literature, the rapid and equal release rate of both drugs is favorable for combination therapy in cancer cells. Due to the particular characteristics of the core-shell NPs and different types of drug attachment (physical and covalent), the rate of drug release from the NPs was unequal for DOX and DTXL. However, due to many variables affecting the success of the therapy (e.g., the pharmacokinetics (depending on the molecular characteristics of the NPs), the type of tumor cells (rapid or slow growth, resistant or sensitive to drug/drugs used) and the specific tumor characteristics and tumor leakiness) no simple explanation can be given for the optimal release kinetics suitable for combination therapy.

In summary, the developed method for preparing polymer-coated NPs combines the desirable characteristics of polymeric NPs and HPMA-based polymer drug conjugates: (*i*) high drug encapsulation, (*ii*) DOX pH-triggered drug release and (*iii*) combinatorial chemotherapy. A simultaneous controlled release of two chemotherapeutics has been achieved through the physical entrapment of DTXL into the degradable PBS/PBDL copolyester core and the covalent attachment of DOX to the HPMA-based copolymer via pH-sensitive hydrazone bonding. The cargo capacity and relative drug ratios are amenable to fine-tuning by varying the quantity of bound drug during the HPMA copolymer synthesis and NP formulation. Multivalency of the PHPMA polymer precursor also allows the potential attachment of targeting moieties to enable the combination of passive and active NP targeting. This article aimed to provide an alternative to combination chemotherapy using NPs formed by degradable polyesters coated with HPMA copolymer-drug conjugates, rather than bringing conclusive evidence of possible synergistic effects among the chosen anticancer drugs.

4. Conclusion

Biodegradable polymeric sub-200-nm diameter core-shell nanoparticles consisting of a biodegradable hydrophobic copolyester core and a non-immunogenic and non-toxic hydrophilic shell have been prepared for the delivery of multiple anti-cancer drugs to solid tumors. The nanoparticles were prepared using a combination of a single-step nanoprecipitation and self-assembly protocols and were characterized, in detail, using light-scattering and imaging analysis. The payload capability of the studied core-shell nanoparticles was confirmed since they can deliver high quantities of docetaxel and doxorubicin releasing the therapeutics at a sustained rate or via a pH-triggered pathway with in vivo efficacy in the treatment of mice bearing EL-4 T cell lymphoma. Moreover, the multivalency of the HPMA copolymer in the NP shell enables further development of targeting strategies based on the use of cell membrane receptor-specific ligands attached to the NP surfaces for in vivo multi-target and combination therapies.

Acknowledgments

This research was supported by the grant agency of the Academy of Sciences of the Czech Republic (grant no. IAAX00500803) and the grant agency of the Czech Republic (grant no. GA202/09/2078 and P207/11/P551). F.C.G. acknowledges financial support from FAPESP (grant 2010/06348-0). The authors are grateful to Dr. Miroslav Šlouf from the Institute of Macromolecular Chemistry AS CR for the TEM measurements.

References

[1] R.K. Jain, T. Stylianopoulos, Delivering nanomedicines to solid tumors, Nat. Rev. Drug Discov. 7 (2010) 653–664.
[2] J.C.-M. Hu, L. Zhang, Nanoparticle-based combination therapy toward overcoming drug resistance in cancer, Biochem. Pharmacol. 83 (2012) 1104–1111.
[3] T. Lammers, V. Subr, K. Ulbrich, P. Peschke, P.E. Huber, W.E. Hennink, G. Storm, Simultaneous delivery of doxorubicin and gemcitabine to tumors in vivo using prototypic polymeric drug carriers, Biomaterials 30 (2009) 3466–3475.
[4] F. Greco, M.J. Vincent, Polymer-drug conjugates: current status and future trends, Front. Biosci. 13 (2008) 2744–2756.
[5] T. Lammers, V. Subr, K. Ulbrich, W.E. Hennink, G. Storm, F. Kiessling, Polymeric nanomedicines for image-guided drug delivery and tumour-targeted combination therapy, Nano Today 5 (2010) 197–212.
[6] H. Krakovicova, T. Etrych, K. Ulbrich, HPMA-based polymer conjugates with drug combination, Eur. J. Pharm. Sci. 37 (2009) 405–412.
[7] M.J. Vicent, F. Greco, R.I. Nicholson, A. Paul, P.C. Griffiths, R. Duncan, Polymer therapeutics designed for a combination therapy of hormone-dependent cancer, Angew. Chem. 44 (2005) 4061–4066.
[8] H. Kostkova, T. Etrych, B. Říhova, K. Ulbrich, Synergistic effect of HPMA copolymer-bound doxorubicin and dexamethasone in vivo on mouse lymphomas, J. Biocom. Bioconj. Pol. 26 (2011) 270–286.
[9] J.C.-M. Hu, S. Aryal, L. Zhang, Nanoparticle-assisted combination therapies for effective cancer treatment, Ther. Deliv. 1 (2010) 323–334.
[10] L. Zhang, A.F. Radovic-Moreno, F. Alexis, F.X. Gu, P.A. Basto, V. Bagalkot, S. Jon, R.S. Langer, Co-delivery of hydrophobic and hydrophilic drugs from nanoparticle-aptamer bioconjugates, ChemMedChem 2 (2007) 1268–1271.
[11] N. Kolishetti, S. Dhar, P.M. Valencia, L.Q. Lind, R. Karnik, S.J. Lippard, R. Langer, O.C. Farokhzad, Engineering of self-assembled nanoparticle platform for precisely controlled combination drug therapy, Proc. Natl. Acad. Sci. U. S. A. 107 (2011) 17939–17944.
[12] S. Aryal, J.C.-M. Hu, L. Zhang, Combinatorial drug conjugation enables nanoparticle dual-drug delivery, Small 6 (2010) 1442–1448.
[13] R. Misra, S.K. Sahoo, Coformulation of doxorubicin and curcumin in poly-(D, L-lactide-co-glycolide) nanoparticles suppresses the development of multidrug resistance in K562 cells, Mol. Pharm. 8 (2011) 852–866.
[14] A. Bernardi, R.L. Frozza, E. Jäger, F. Figueiró, L. Bavaresco, C. Salbego, A.R. Pohlmann, S.S. Guterres, A.M.O. Battastini, Selective cytotoxicity of indomethacin and indomethacin ethyl ester-loaded nanocapsules against glioma cell lines: an in vitro study, Eur. J. Pharmacol. 586 (2008) 24–34.
[15] J. Fang, H. Nakamura, H. Maeda, The EPR effect: unique features of tumor blood vessels for drug delivery, factors involved, and limitations and augmentation of the effect, Adv. Drug Del. Rev. 3 (2011) 136–151.
[16] K.R. Whiteman, V. Subr, K. Ulbrich, V.P. Torchilin, Poly(HPMA)-coated liposomes demonstrate prolonged circulation in mice, J. Liposome Res. 11 (2001) 153–164.
[17] S. Kamei, J. Kopeček, Prolonged blood circulation in rats of nanospheres surface-modified with semitelechelic poly[*N*-(2-hydroxypropyl)methacrylamide], Pharm. Res. 12 (1995) 663–668.
[18] N.K. Green, C.W. Herbert, S.J. Hale, A.B. Hale, V. Mautner, R. Harkins, T. Hermiston, K. Ulbrich, K.D. Fisher, L.W. Seymour, Extended plasma circulation time and decreased toxicity of polymer-coated adenovirus, Gene. Therapy 11 (2004) 1256–1263.
[19] E. Jäger, A. Jäger, T. Etrych, F.C. Giacomelli, P. Chytil, A. Jigounov, J.-L. Putaux, B. Říhová, K. Ulbrich, P. Štěpánek, Self-assembly of degradable polyester and reactive HPMA-based polymers into nanoparticles as an stealth drug delivery system alternative, Soft Matter 8 (2012) 9563–9575.
[20] A. Jäger, D. Gromadzki, E. Jäger, A. Kozlowska, M. El Fray, L. Kobera, J. Brus, B. Říhová, K. Ulbrich, P. Štěpánek, Novel "soft" biodegradable nanoparticles prepared from aliphatic based monomers as a potential drug delivery system, Soft Matter 8 (2012) 4343–4354.
[21] P. Chytil, T. Etrych, J. Kříž, V. Šubr, K. Ulbrich, *N*-(2-hydroxypropyl)methacrylamide-based polymer conjugates with pH-controlled activation of doxorubicin for cell-specific or passive tumour-targeting. Synthesis by RAFT polymerisation and physicochemical characterisation, Eur. J. Pharm. Sci. 41 (2010) 473–482.
[22] T. Etrych, T. Mrkvan, P. Chytil, Č. Koňák, B. Říhová, K. Ulbrich, *N*-(2-hydroxypropyl) methacrylamide-based polymer conjugates with pH-controlled activation of doxorubicin. I. New synthesis, physicochemical characterization and preliminary biological evaluation, J. Appl. Pol. Sci. 109 (2008) 3050–3061.
[23] P. Chytil, T. Etrych, Č. Koňák, M. Šírová, T. Mrkvan, J. Bouček, B. Říhová, K. Ulbrich, New HPMA copolymer-based drug carriers with covalently bound hydrophobic substituents for solid tumour targeting, J. Control. Release 127 (2008) 121–130.
[24] P. Štěpánek, in: W. Brown (Ed.), Dynamic Light Scattering, Oxford University Press, New York, 1993, pp. 177–240.
[25] Č. Koňák, V. Šubr, R. Laga, K. Ulbrich, Coating of DNA/poly(L-lysine) complexes by covalent attachment of poly[N-(2-hydroxypropyl)methacrylamide], Biomacromolecules 7 (2006) 122–130.
[26] H. Dautzenberg, A. Zintchenko, Č. Koňák, T. Reschel, V. Šubr, K. Ulbrich, Polycationic graft copolymers as carriers for oligonucleotide delivery. Complexes of oligonucleotides with polycationic graft copolymers, Langmuir 17 (2001) 3096–3102.
[27] T. Etrych, P. Chytil, M. Jelínková, B. Říhová, K. Ulbrich, Synthesis of HPMA copolymers containing doxorubicin bound via a hydrazone linkage. Effect of spacer on drug release and in vitro cytotoxicity, Macromol. Biosci. 2 (2002) 43–52.
[28] F.C. Giacomelli, P. Štěpánek, C. Giacomelli, V. Schmidt, E. Jäger, A. Jäger, K. Ulbrich, pH-triggered block copolymer micelles based on a pH-responsive PDPA (poly [2-(diisopropylamino)ethyl methacrylate]) inner core and a PEO (poly(ethylene oxide)) outer shell as a potential tool for the cancer therapy, Soft Matter 7 (2011) 9316–9325.
[29] M.J. Campolongo, D. Luo, Old polymers learn new tracts, Nat. Materials 8 (2009) 447–448.
[30] K.S. Soppimath, T.M. Aminabhavi, A.R. Kulkarni, W.E. Rudzinski, Biodegradable polymeric nanoparticles as drug delivery devices, J. Control. Release 70 (2002) 1–20.
[31] J.M. Chan, P.M. Valencia, L. Zhang, R. Langer, O.C. Farokhzad, Polymeric nanoparticles for drug delivery, Methods Mol. Biol. 624 (2010) 163–175.

[32] C. Zheng, M. Zheng, P. Gong, D. Jia, P. Zhang, B. Shi, Z. Sheng, Y. Ma, L. Cai, Indocyanine green-loaded biodegradable tumor targeting nanoprobes for in vitro and in vivo imaging, Biomaterials 33 (2012) 5603–5609.
[33] A. Schädlich, H. Caysa, T. Mueller, F. Tenambergen, C. Rose, A. Göpferich, J. Kuntsche, K. Mäder, Tumor accumulation of NIR fluorescent PEG-PLA nanoparticles: impact of particle size and human xenograft tumor model, ACS Nano 5 (2011) 8710–8720.
[34] S. Sengupta, D. Eavarone, I. Capila, G. Zhao, N. Watson, T. Kiziltepe, Temporal targeting of tumour cells and neovasculature with a nanoscale delivery system, Nature 436 (2005) 568–572.
[35] J. Aubry, F. Ganachaud, J.-P.C. Addad, B. Cabane, Nanoprecipitation of polymethylmethacrylate by solvent shifting: 1. Boundaries, Langmuir 25 (2009) 1970–1979.
[36] P. Štěpánek, Static and dynamic properties of multiple light-scattering, J. Chem. Phys. 99 (1993) 6384–6393.
[37] F. Quaglia, L. Ostacolo, G. De Rosa, M.I. La Rotonda, M. Ammendola, G. Nese, G. Maglio, R. Palumbo, C. Vauthier, Nanoscopic core-shell drug carriers made of amphiphilic triblock and star-diblock copolymers, Int. J. Pharm. 324 (2006) 56–66.
[38] V.M. Weiss, T. Naolou, G. Hause, J. Kuntsche, J. Kressler, K. Mäder, Poly(glycerol adipate)-fatty acid esters as versatile nanocarriers: from nanocubes over ellipsoids to nanospheres, J. Control. Release 158 (2012) 156–164.
[39] H.S. Yoo, K.H. Lee, J.E. Oh, T.G. Park, In vitro and in vivo anti-tumor activities of nanoparticles based on doxorubicin-PLGA conjugates, J. Control. Release 68 (2000) 419–431.
[40] L. Zhang, J.M. Chan, F.X. Gu, J.-W. Rhee, A.Z. Wang, A.F. Radovic-Moreno, F. Alexis, R. Langer, O.C. Farokhzad, Self-assembled lipid-polymer hybrid nanoparticles: a robust drug delivery platform, ACS Nano 2 (2008) 1696–1702.
[41] F.C. Giacomelli, P. Štěpánek, V. Schmidt, E. Jäger, A. Jäger, C. Giacomelli, Light scattering evidences of selective protein fouling on biocompatible block copolymer micelles, Nanoscale 4 (2012) 4504–4514.
[42] H. Wang, Y. Zhao, Y. Wu, Y.-L. Hu, K. Nan, G. Nie, H. Chen, Enhanced anti-tumor efficacy by co-delivery of doxorubicin and paclitaxel with amphiphilic methoxy PEG-PLGA copolymer nanoparticles, Biomaterials 32 (2011) 8281–8290.
[43] K. Ulbrich, T. Etrych, P. Chytil, M. Jelinkova, B. Rihova, HPMA copolymers with pH-controlled release of doxorubicin: in vitro cytotoxicity and in vivo antitumor activity, J. Control. Release. 87 (2003) 33–47.
[44] P. Chytil, T. Etrych, Č. Koňák, M. Šírová, T. Mrkvan, B. Říhová, K. Ulbrich, Properties of HPMA copolymer-doxorubicin conjugates with pH-controlled activation: effect of polymer chain modification, J. Control. Release 115 (2006) 26–36.
[45] F. Ahmed, R.I. Pakunlu, G. Srinivas, A. Brannan, F. Bates, M.L. Klein, T. Minko, D.E. Discher, Shrinkage of a rapidly growing tumor by drug-loaded polymersomes: pH-triggered release through copolymer degradation, Mol. Pharm. 3 (2006) 340–350.
[46] F. Ahmed, R.I. Pakunlu, A. Brannan, F. Bates, T. Minko, D.E. Discher, Biodegradable polymersomes loaded with both paclitaxel and doxorubicin permeate and shrink tumors, inducing apoptosis in proportion to accumulated drug, J. Control. Release. 116 (2006) 150–158.

Polymer Chemistry

PAPER

View Article Online
View Journal | View Issue

Cite this: *Polym. Chem.*, 2014, **5**, 3884

Novel poly(ethylene oxide monomethyl ether)-*b*-poly(ε-caprolactone) diblock copolymers containing a pH-acid labile ketal group as a block linkage†

S. Petrova,* E. Jäger, R. Konefał, A. Jäger, C. G. Venturini, J. Spěváček, E. Pavlova and P. Štěpánek

Received 24th January 2014
Accepted 13th February 2014

DOI: 10.1039/c4py00114a

www.rsc.org/polymers

A new biocompatible and biodegradable diblock copolymer that contains a specific acid-labile degradable linkage (acyclic ketal group) between the hydrophobic poly(ε-caprolactone) (PCL) and the hydrophilic poly(ethylene oxide monomethyl ether) (MPEO) blocks is described herein. A multi-step synthetic method that combines carbodiimide chemistry, a "click" reaction and ring-opening polymerization (ROP) was employed to successfully produce a series of MPEO-*b*-PCL diblock copolymers (herein referred to as $MPEO_{44}$-*b*-PCL_{17} and $MPEO_{44}$-*b*-PCL_{44}). 2-{[2-(2-Azidoethoxy)propan-2-yl]}ethan-1-ol was obtained as a linker between the two blocks through a three-step synthetic approach. Furthermore, a newly developed α-methoxy-ω-hydroxy-poly(ethylene oxide) that contains an acid-labile ketal linkage was designed as a macroinitiator *via* a "click" reaction for the sequential controlled ring-opening polymerization of ε-CL. The newly obtained compounds (precursors, macromer, macroinitiator and final diblock copolymers) were assessed by ^{1}H NMR, ^{13}C NMR and FT-IR spectroscopy and SEC analysis, which are described in this manuscript. Upon dissolution in a mild organic solvent, the $MPEO_{44}$-*b*-PCL_{17} block copolymer self-assembled in water–PBS into regular, spherical, stable nanoparticles (NPs). Furthermore, the presence of the acid-labile ketal linker enabled the disassembly of these nanoparticles in a buffer that simulated acidic cytosolic or endosomal conditions in tumour cells as evaluated by dynamic light scattering (DLS), nanoparticle tracking analysis (NTA) and transmission electron microscopy (TEM) images. This disassembly led to hydrolysis profiles that resulted in neutral degradation products.

Introduction

Currently, the priorities for the development of polymer therapeutics are strictly associated with the production of biocompatible, degradable polymeric nanostructures. The properties of these materials are defined by their structures, compositions, dimensions and functionalities. Over the past several decades, amphiphilic block copolymers (hydrophilic and hydrophobic blocks) have been extensively studied.[1–4] These copolymers are of great interest because of their ability to self-assemble in aqueous media to generate various structure types, shapes and sizes, ranging from nano- to micrometres.[5–7] It is well known that amphiphilic block copolymers are able to form nanosized spherical micelles with a core–shell architecture. The applications of these systems are associated with their several unique properties, such as the possibility of controlling the release of drugs,[8–10] matrices for three-dimensional tissue regeneration,[11–13] diagnostic agents[14,15] and DNA delivery.[16,17] In particular, self-assembled core–shell NPs from amphiphilic block copolymers have attracted considerable attention in the development of drug-delivery systems. Their hydrophobic core is used as a reservoir for lipophilic agents (drugs), whereas their hydrophilic corona creates a highly water-bound barrier that ensures colloidal stability, a reduction in the rate of opsonin adhesion and clearance of the particles from the body.[18] Another relevant consideration for the development of core–shell NPs for drug-release applications is the carriers' ability to release their cargo drug in a controlled manner upon arrival at the target site.[19] For these reasons, many researchers are paying special attention to the design of environmentally triggered polymeric nanoparticles that are capable of releasing the original molecules in their active forms under various chemical and physical stimuli, such as pH, light, temperature, enzyme concentration or redox gradients.[20–22] pH-sensitive degradable polymers have played an integral role in the advancement of drug-delivery technology, such as the delivery of protein-based vaccines and nucleic acids, in the treatment of acute

Institute of Macromolecular Chemistry v.v.i., Academy of Sciences of the Czech Republic, Heyrovsky Sq. 2, 162 06 Prague 6, Czech Republic. E-mail: petrova@imc.cas.cz; Tel: +420 296 809 296

† Electronic supplementary information (ESI) available. See DOI: 10.1039/c4py00114a

inflammatory diseases and especially for tumour targeting.[23,24] Considering the tumour-targeting field of drug delivery, the hydrophobic guest drug molecules must be retained in the inner particle core while in the bloodstream and then be rapidly released at the specific tumour sites.[25] A significant amount of research has demonstrated the association between acidic pH conditions and cancer, as the extracellular pH in most solid tumour sites is more acidic (ranging from pH 5.7 to 7.2) compared to that of normal tissues (buffered at pH 7.4).[26,27] Because of these pH differences, several pH-degradable polymers that contain different acid-labile linkers suitable for triggering drug release, such as ester,[28] hydrazone,[29] carboxydimethylmaleic,[30] orthoester,[31] imine,[32] β-thiopropionate,[33] vinylether,[34] and phosphoramidate,[35] have been widely studied. In particular, acid-degradable (co)polymers and NPs that contain multiple reactive functionalities, such as ketal/acetal labile linkages along the polymer backbone or as pendant groups, are of considerable interest. Ketals and acetals have been demonstrated to be more sensitive to the acidic environment of tumours and phagosomes than esters and hydrazones.[35] Moreover, these linkers are also more stable under physiological conditions (at pH $\sim$ 7.4) than the other aforementioned linkages.[36] In addition, pH-responsive systems containing acid-labile bonds that are degradable under mild acidic conditions, such as those of tumour sites, lead to tuneable hydrolysis profiles, which ultimately result in neutral degradation products that can be easily excreted, thereby avoiding accumulation and inflammatory responses.[37] Although novel and efficient pH-sensitive carriers that contain ketal/acetal linkages have great potential for drug delivery, synthetic challenges have limited the applications of these systems.

Herein, we report the synthesis of a novel class of well-defined biocompatible and biodegradable acid-labile poly(ethylene oxide monomethyl ether) (MPEO)-*b*-poly(ε-caprolactone) (PCL) diblock copolymers that contain ketal groups as block linkers. The PEO and PCL polymers were selected as building blocks because of their special interest for environmental, biomedical and pharmaceutical applications.[38–41] PCL is a aliphatic hydrophobic polyester with great potential as a biomaterial due to its unique combination of biodegradability and biocompatibility,[42] and PEO is a hydrophilic and very flexible biocompatible polymer that is non-toxic and easily eliminated from the body.[43] For the synthesis, an efficient multi-step pathway was employed, which resulted in new block copolymers with reasonable yields. Different synthetic routes (*i.e.*, carbodiimide chemistry, "click" reaction and ring-opening polymerization) were applied for the preparation of low-molecular-weight compounds as precursors for constructing the acid-labile ketal group of the MPEO-*b*-PCL diblock copolymers. In addition, the amphiphilic diblock copolymers self-assembled into regular spherical NPs in aqueous solution and under buffer-simulated physiological conditions (pH $\sim$ 7.4). These nanoparticles were found to be degraded into non-toxic compounds under buffer-simulated acidic cytosolic or endosomal conditions in tumour cells (pH $\sim$ 5.0), revealing their potential as systems that could find applications, *e.g.*, as acid-labile drug-delivery systems.

Experimental

Materials

Ethylene glycol (99%, Sigma-Aldrich), trimethyl orthoacetate (99%, Aldrich), *p*-toluenesulphonic acid monohydrate (98.5%, Fluka), 2-chloroethanol (99%, Aldrich), sodium azide (99%, Fluka), tetrabutylammonium bromide (TBABr, 99%, Fluka), pyridinium *p*-toluenesulphonate (PPTS, 99%, Fluka), 5-hexynoic acid (97%, Aldrich), 4-dimethylaminopyridine (DMAP, 99% Sigma-Aldrich), *N*,*N*′-dicyclohexylcarbodiimide (DCC, 99%, Fluka), CuBr (98%, Fluka), 2-methoxypropene (98%, Aldrich) and molecular sieves (5 Å, Sigma-Aldrich) were used without further purification. ε-Caprolactone (ε-CL, 99%, Sigma-Aldrich) was dried over CaH_2 with continuous stirring at room temperature for 48 h and distilled under reduced pressure before use. Tin(II) bis(2-ethylhexanoate) ($Sn(Oct)_2$, 95%, Aldrich, 0.06 M solution in toluene) and sodium hydroxide (NaOH) were used as received. MPEO ($M_n \sim 1800$ g mol^{-1}) was purchased from Fluka. Triethylamine (Et_3N) (≥99.5%, Sigma-Aldrich) was dried over CaH_2 and distilled under reduced pressure. CH_2Cl_2 (Sigma-Aldrich) was dried by refluxing over a benzophenone–sodium complex and distilled under an argon atmosphere. Toluene (99%, Labscan) and tetrahydrofuran (THF, 99%, Fluka) were refluxed for 24 h over CaH_2 under a dry argon atmosphere and then distilled. All other chemicals were used as received.

Synthesis of compounds 1–5

Compounds **1**,[44,45] **2**,[46] **3**,[45] **4**,[45] and **5**[47] were synthesised according to previous procedures, which are described in detail in the ESI.†

Synthesis of α-methoxy-ω-hydroxy-poly(ethylene oxide) containing a ketal group (compound 6)

The coupling of 2-{[2-(2-azidoethoxy)propan-2-yl]ethan-1-ol (**4**) (0.18 g, 7.78×10^{-4} mol) with α-methoxy-ω-alkyne-poly(ethylene oxide) (**5**) (1.4 g, 7.09×10^{-4} mol) bearing the alkyne was performed in a glass reactor containing dry THF (8 mL). CuI (0.015 g, 7.87×10^{-5} mol) and triethylamine (0.01 mL, 7.91×10^{-5} mol) were added to the polymer solution and allowed to react at 35 °C for 4 h. Subsequently, the reaction mixture was exposed to air, diluted with THF, and passed through a neutral alumina column to remove the copper catalysts. The macroinitiator was recovered by two precipitations in cooled diethyl ether. The product (**6**) was recovered as a white solid. Yield: 1.30 g, 93%.

Synthesis of the MPEO-*b*-PCL diblock copolymer containing a ketal group (compound 7)

In a typical synthesis, 0.127 g (5.7×10^{-5} mol) of α-methoxy-ω-hydroxy-poly(ethylene oxide) (**6**) containing a ketal group was introduced into a 50 mL glass reactor equipped with a magnetic stir bar. The macroinitiator was dissolved in dry toluene and dried three times by azeotropic distillation. A certain amount of freshly distilled ε-CL was added, and after heating, 0.1 mL of 0.06 M $Sn(Oct)_2$ was rapidly injected through a septum. The

polymerization was carried out for 48 h at 110 °C. The reactor was cooled to room temperature, and the reaction mixture was dissolved in toluene. The copolymer (**7**) was collected by precipitation in cooled diethyl ether, filtered and dried overnight under vacuum at 40 °C.

Characterisation techniques

^{1}H NMR and ^{13}C NMR spectra (300 and 75 MHz, respectively) were recorded using a Bruker Avance DPX 300 NMR spectrometer with $CDCl_3$ as the solvent at 25 °C. The chemical shifts are relative to TMS using hexamethyldisiloxane (HMDSO, $\delta = 0.05$ and 2.0 ppm from TMS in ^{1}H NMR and ^{13}C NMR spectra) as the internal standard. The M_n values of compounds **5–7** were determined by ^{1}H NMR spectroscopy. For compound **5**, the M_n was calculated according to eqn (1):

$$M_{n(NMR)} = [(I_b/4)/(I_d/2)] \times 44 + 31 + 95 \quad (1)$$

where I_b and I_d represent the integral values of the peaks at $\delta =$ 3.63 ppm (–CH_2–CH_2–O– of the PEO repeating unit) and at $\delta =$ 4.22 ppm (–CH_2–CH_2–O–C(O)), respectively. The values 31 and 95 represent the molecular weights of the two functional groups at the chain ends CH_3–O– and –C(O)–$C(CH_2)_3$–C≡CH, respectively. The M_n of the macroinitiator (**6**) was calculated according to eqn (2):

$$M_{n(NMR)} = [(I_b/4)/(I_g/2)] \times 44 + 31 + 284 \quad (2)$$

where I_b and I_g represent the integral values of the peaks at $\delta =$ 3.63 ppm (–CH_2–CH_2–O– of the PEO repeating unit) and at $\delta =$ 2.76 ppm (–O–C(O)–CH_2–CH_2–CH_2–), respectively. The values 31 and 284 are the molecular weights of the two functional groups at the chain ends CH_3–O– and –O–C(O)–$(CH_2)_3$–triazole ring–$(CH_2)_2$–$OC(CH_3)_2$–O–$(CH_2)_2$–OH, respectively. The M_n of the MPEO-*b*-PCL diblock copolymers (**7**) was determined by ^{1}H NMR using eqn (3)

$$M_{n(NMR)}\,(\text{MPEO-}b\text{-PCL}) = [(I_r/2)/(I_b/4)] \times DP_{MPEO} \times 114 + M_{n(NMR)}\,(\text{macroinitiator}) \quad (3)$$

where I_r and I_b represent the integral values of the methylene protons of PCL (r) (Fig. 2, top) and of the methylene protons of PEO (b). The value 114 is the molecular weight of the ε-CL unit, DP_{MPEO} is the degree of polymerization of the macroinitiator, and $M_{n(NMR)}$ is the number-average molecular weight of the macroinitiator. Infrared spectra were obtained using a PerkinElmer Spectrum 100 equipped with a universal ATR (attenuated total reflectance) accessory with a diamond crystal. In all cases, the resolution was 4 cm^{-1} and the spectra were averaged over 16 scans. The samples were prepared in the form of KBr pellets. The number-average molecular weights (M_n),

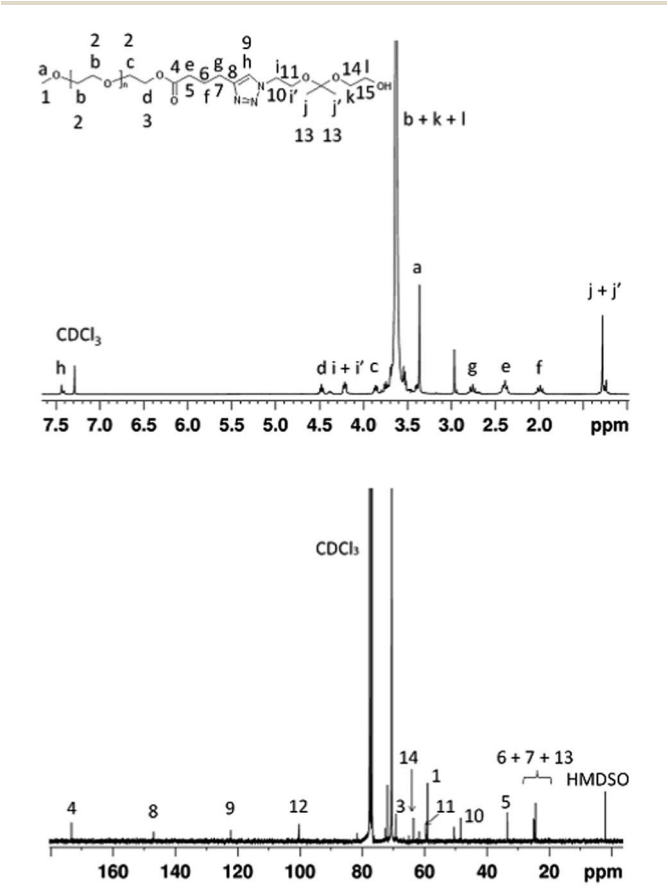

Fig. 1 ^{1}H (top) and ^{13}C (bottom) NMR spectra of the α-methoxy-ω-hydroxy-PEO containing a ketal group in $CDCl_3$.

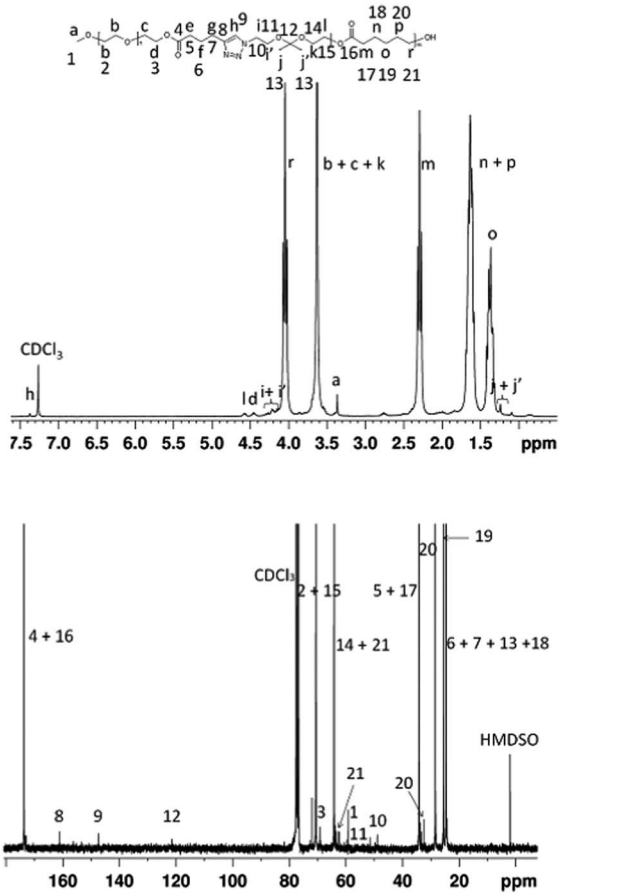

Fig. 2 ^{1}H (top) and ^{13}C (bottom) NMR spectra of the MPEO-*b*-PCL diblock copolymer in $CDCl_3$.

weight-average molecular weights (M_w), and polydispersity indices (M_w/M_n) of the prepared macromer, macroinitiator and block copolymers were determined by size exclusion chromatography (SEC). The analyses were performed using an SDS 150 pump (Watrex, Czech Republic) equipped with refractometric (Shodex RI-101, Japan) and UV (Watrex UVD 250, Czech Republic) detectors. The separation system consisted of two PLgel MIXED-C columns (Polymer Laboratories) and was calibrated with polystyrene standards (PSS, Germany). THF was used as the mobile phase at a flow rate of 1.0 mL min^{-1} at 25 °C. Data collection and processing were performed using the Clarity software package.

Nanoparticle preparation

NPs were prepared using the nanoprecipitation protocol. A preheated (40 °C) acetone solution (5 mL) containing the MPEO-*b*-PCL block copolymer (10 mg) was added drop-wise (EW-74900-00, Cole-Parmer®) into a pre-heated (40 °C) Milli-Q® water solution (10 mL, pH ~ 7.4). The pre-formed NPs were allowed to self-assemble, and then the solution was transferred to a dialysis tube (MWCO = 3500) and dialysed against 5 L of water (pH ~ 7.4) for 24 hours. The final concentration was adjusted to 1 mg mL^{-1} using phosphate-buffered saline (PBS) at pH ~ 7.4.

Nanoparticle characterisation

The NPs were characterised by DLS and NTA. The DLS measurements were performed using an ALV CGE laser goniometer consisting of a 22 mW HeNe linearly polarised laser operating at a wavelength (λ = 632.8 nm), an ALV 6010 correlator, and a pair of avalanche photodiodes operating in the pseudo cross-correlation mode. The samples were filtered through 0.45 μm PVDF membranes (Millex-HV, Millipore®) loaded into 10 mm diameter glass cells and maintained at 25 or 37 ± 1 °C. The data were collected using the ALV Correlator Control software, and the counting time was 30 s. To avoid multiple light scattering, the samples were diluted 100-fold before the measurements.[48] The measured intensity correlation functions $g_2(t)$ were analysed using the algorithm REPES (incorporated in the GENDIST program),[49] resulting in the distributions of relaxation times shown in an equal area representation as $\tau A(\tau)$. The mean relaxation time or relaxation frequency ($\Gamma = \tau^{-1}$) is related to the diffusion coefficient (D) of the nanoparticles as $D = \frac{\Gamma}{q^2}$, where $q = \frac{4\pi n \sin(\theta/2)}{\lambda}$ is the scattering vector with n representing the refractive index of the solvent and θ representing the scattering angle. The hydrodynamic radius (R_H) or the distribution of R_H was calculated using the well-known Stokes–Einstein relation:

$$R_H = \frac{k_B T}{6\pi\eta D} \quad (4)$$

where k_B is the Boltzmann constant, T is the absolute temperature, and η is the viscosity of the solvent. The NTA analyses were performed using the NanoSight LM10 & NTA 2.0 Analytical Software (NanoSight, Amesbury, England). The samples were diluted (4000×, Milli-Q® water or PBS, pH ~ 7.4 and 5.0) and injected into the sample chamber with a syringe (25 °C). The NTA apparatus combines a light scattering microscope with a laser diode (635 nm) camera charge-coupled device, which allows viewing and recording of the NPs in solution. Each video clip was captured over 60 s. The NTA software is able to identify and track individual NPs (10–1000 nm), which are in Brownian motion, and relate their particle movement to a sphere with an equivalent R_H, as calculated using the Stokes–Einstein relation (eqn (4)). The size distribution was expressed by the span value, which was calculated using eqn (5).

$$\text{Span} = \frac{d_{(0.9)} - d_{(0.1)}}{d_{(0.5)}} \quad (5)$$

where $d_{(0.9)}$, $d_{(0.1)}$ and $d_{(0.5)}$ are the diameters at 90%, 10% and 50% cumulative volumes, respectively.

Transmission electron microscopy (TEM)

TEM observations were performed on a Tecnai G2 Spirit Twin at 120 kV (FEI, Czech Republic). The NPs were diluted 100-fold, and 2 μL of the aqueous solution was dropped onto a copper TEM grid (300 mesh) coated with a thin, electron-transparent carbon film. The solution was removed by touching the bottom of the grid with filter paper. This rapid removal of the solution was performed after 1 min to minimise oversaturation during the drying process; this step was found to be necessary to preserve the structure of the NPs. The NPs were negatively stained with uranyl acetate (2 μL of a 1 wt% solution was dropped onto the dried NPs and removed after 15 s in the same manner described above). The sample was left to completely dry at ambient temperature and then observed *via* a TEM using bright-field imaging. Under these conditions, the micrographs displayed a negatively stained background with bright spots, which correspond to the investigated NPs.

Results and discussion

A new synthetic pathway was developed to obtain well-defined amphiphilic copolymers that contain acid-labile, degradable ketal linkages as block linkers that are highly sensitive to pH under physiological conditions. The synthesis of the biocompatible, biodegradable, acid-labile MPEO-*b*-PCL was designed using, for the first time, the combination of a "click" reaction with DCC chemistry and ROP (Scheme 1). This strategy provides new insights into the combination of new "click" chemistry reactions with the classic synthetic pathways in polymer chemistry.

Synthesis of compounds 1 to 5

The compounds ethylene glycol monoacetate (**1**)[44,45] (Fig. S1†), 2-azidoethanol (**2**)[46] (Fig. S2†), 2-{[2-(2-azidoethoxy)propan-2-yl]oxy}ethyl acetate (**3**)[45] (Fig. S3†), 2-{[2-(2-azidoethoxy)propan-2-yl]ethan-1-ol (**4**)[45] (Fig. S4†) and α-methoxy-ω-alkyne-poly(ethylene oxide) (**5**)[47] (Fig. S5†) were synthesised according to previous reports and were characterised by ^{1}H and ^{13}C NMR, FT-IR spectroscopy and SEC analysis (**5**), which are described in detail in the ESI.†

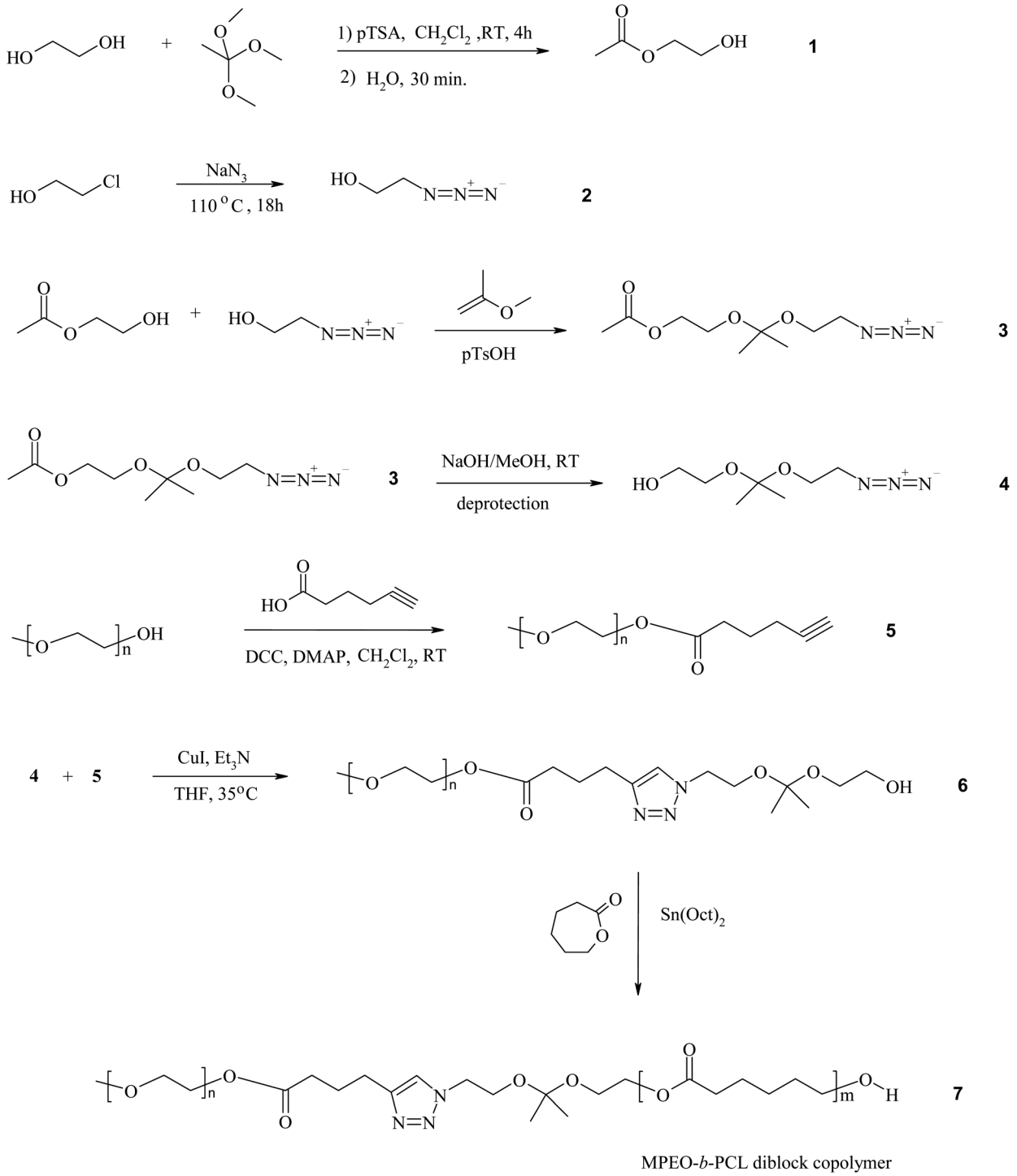

Scheme 1 Synthetic route for the preparation of MPEO-*b*-PCL diblock copolymers.

Synthesis of α-methoxy-ω-hydroxy-poly(ethylene oxide) containing a ketal group (compound 6)

The α-methoxy-ω-hydroxy-poly(ethylene oxide) containing a ketal group (**6**) was prepared as a macroinitiator through a "click" reaction between α-methoxy-ω-alkyne-PEO (**5**) and 2-{[2-(2-azidoethoxy)propan-2-yl]ethan-1-ol (**4**) (see Scheme 1). The azide–alkyne Huisgen cycloaddition was performed in the presence of CuI and Et_3N. After purification, the obtained macroinitiator was characterised by ^1H and ^{13}C NMR, FT-IR spectroscopy and SEC analysis. The ^1H NMR spectrum (Fig. 1, top) confirms that the "click" reaction was complete due to the disappearance of the characteristic signal for the alkyne end-group at $\delta = 1.96$ ppm (h) (Fig. S5†) and the appearance of a new proton signal from the triazole ring at $\delta = 7.40$ ppm (h) in Fig. 1 (top). The signal observed at $\delta = 1.28$ ppm (j + j′) is assigned to

Table 1 Macromolecular characteristics of functional MPEO

MPEO samples	Conversion[a] (%)	M_n[b] (NMR)	M_n[c] (SEC)	M_w/M_n[d] (SEC)
MPEO	—	1800	1464	1.23
Macromer	87	2200	1710	1.24
Macroinitiator	82	2320	1760	1.31

[a] Conversion was calculated by ^{1}H NMR spectroscopy (Fig. S5† and 1, top). [b] M_n was calculated by ^{1}H NMR spectroscopy according to eqn (1) and (2). [c] M_n was determined by SEC calibrated with PS standards. [d] M_w/M_n was determined by SEC calibrated with PS standards.

the six protons of the dimethyl ketal group –OC(CH$_3$)$_2$–O– and demonstrates that the ketal group remains unaffected during the azide–alkyne Huisgen cycloaddition. Furthermore, a singlet signal attributed to CH$_3$–O– was observed at $\delta = 3.39$ ppm (a), and other signals were observed at $\delta = 2.76$ (g), $\delta = 2.39$ (e) and $\delta = 1.96$ ppm (f). Additional signals located in the vicinity of the EO ($\delta = 3.63$ ppm) were also identified: $\delta = 2.85$ ppm (c) is a typical signal of –CH$_2$–CH$_2$–O–C(O), $\delta = 4.21$ ppm (i + i′) is attributed to –N–CH$_2$–CH$_2$–O–, and $\delta = 4.47$ ppm (d) is characteristic of –CH$_2$–CH$_2$–O–C(O). The conversion of the "click" reaction was calculated from the relative intensities of the signals characteristic of both –O–C(CH$_3$)$_2$–O– (j + j′, $\delta = 1.28$ ppm) and –CH$_2$–O–C(O) (d, $\delta = 4.47$ ppm) groups in the ^{1}H NMR spectrum, which gives a quantitative value of ~82% (Table 1).

The ^{13}C NMR spectrum (Fig. 1, bottom) of the α-methoxy-ω-hydroxy-PEO containing a ketal group is further evidence for the successful achievement of the "click" cycloaddition. Signals corresponding to the dimethyl ketal group at $\delta = 24.32$ ppm (**13**) and from the fully substituted carbon –OC(CH$_3$)$_2$–O– at 100.33 ppm (**12**) were clearly observed. Other significant signals were observed at high chemical shifts at $\delta = 122.22$ (**9**) and $\delta = 146.97$ ppm (**8**), which correspond to the carbons from the triazole ring –CH$_2$–CH═CH–N–, and at $\delta = 173.29$ ppm (**4**), which is attributed to the carbonyl carbon from the –CH$_2$–O–C(O)–(CH$_2$)$_3$– group.

Moreover, the effectiveness of the "click" cycloaddition reaction to afford 1,2,3-triazole as a product was confirmed by FT-IR spectroscopy (Fig. S7b†). Complete disappearance of the peak corresponding to the azide group at 2102 cm^{-1} was observed, which indicates the completion of the reaction. The identification of C–N stretching frequencies is generally a very difficult task because the mixing of bands is possible in this region.[50] The absorption bands observed at 1553, 1469 and 1455 cm^{-1} are due to stretching vibrations between carbon and nitrogen atoms. The characteristic absorption band of C–N observed at 1361 cm^{-1} confirms the formation of the triazole ring. Absorption bands for the carbon–hydrogen groups were also observed, thus resulting in C–H stretching absorption in the 2992 to 2700 cm^{-1} region of the IR spectrum. Moreover, in the spectrum of compound **6**, a weak –C═O stretching band at 1735 cm^{-1} was observed, indicating the presence of a carbonyl ester group. Furthermore, distinctive bands from the ether groups of the EO repeating units at 1107 cm^{-1} were also observed (Fig. S7b†). The SEC chromatogram from the corresponding macroinitiator obtained after the cycloaddition reaction shows a monomodal distribution, as indicated by the overlap of the SEC traces (dotted line in Fig. S8†). The molecular weight of the resulting product remains unchanged, except for a slight increase in polydispersity. Nevertheless, after the reaction, the SEC chromatogram from α-methoxy-ω-hydroxy-MPEO containing a ketal group (**6**) clearly demonstrates the absence of side products with higher M_n values that could be formed as a result of alkyne homocoupling.

Synthesis of the MPEO-*b*-PCL diblock copolymer containing a ketal group (compound 7)

The MPEO-*b*-PCL diblock copolymers (**7**) were successfully synthesised by ROP from the ε-CL monomer. The previously synthesised α-methoxy-ω-hydroxy-poly(ethylene oxide) containing a ketal group (**6**) was used as a macroinitiator in the presence of Sn(Oct)$_2$ as a catalyst. The lengths of the PCL blocks were controlled by regulating the ε-CL/macroinitiator molar ratio. After purification, the MPEO-*b*-PCL diblock copolymers were characterised by ^{1}H and ^{13}C NMR, FT-IR spectroscopy and SEC analysis. The structure and composition of the obtained diblock copolymers were also confirmed by FT-IR spectroscopy. The ^{1}H NMR spectrum of the diblock copolymer (Fig. 2, top) shows characteristic signals for protons belonging to ε-CL and EO repeating units. The signals for the methylene protons of the ε-CL units were detected at $\delta = 4.06$ ppm (r) –CH$_2$–OC(O)–, $\delta = 2.29$ ppm (m) –C(O)CH$_2$–, $\delta = 1.58$ ppm (n + p) –C(O)–CH$_2$–CH$_2$–CH$_2$–CH$_2$– and $\delta = 1.34$ ppm (o) –C(O)–CH$_2$–CH$_2$–CH$_2$–. The methylene protons of the EO repeating units were observed at $\delta = 3.63$ ppm (b), whereas the singlet signal is attributed to the CH$_3$–O– appeared at $\delta = 3.39$ ppm (a). The signal observed at $\delta = 1.31$ ppm (j + j′) attributed to the six protons of the dimethyl ketal group –OC(CH$_3$)$_2$–O– and the resonance signal at $\delta = 7.37$ ppm (h) assigned to the triazole ring demonstrate that the ketal group and the triazole ring remain unaffected following the ROP. Furthermore, there were signals in the spectrum at $\delta = 4.57$ ppm (l), attributed to methylene protons from the –CH$_2$–O–C(O)– fragment; at $\delta = 4.45$ ppm (d), assigned to the last monomer unit of PEO; and at $\delta = 4.21$ ppm (i + i′), attributed to the methylene protons from the fragment between the triazole ring and the ketal group –N–CH$_2$–CH$_2$–O–C(CH$_3$)$_2$–O–. Low intensity signals at $\delta = 2.76$ (g), 2.50 (e) and 2.00 ppm (f) for the protons from the –OC(O)–CH$_2$–CH$_2$–CH$_2$– triazole ring were also present. The experimental degree of ε-CL polymerization agrees well with the theoretical values (Table 2). The ^{13}C NMR spectrum (Fig. 2, bottom) of the diblock copolymers shows

Table 2 Macromolecular characteristics of MPEO-*b*-PCL diblock copolymers

Sample	M_n[a] (NMR)	M_n[b] (NMR)	M_n[c] (SEC)	M_w/M_n[d] (SEC)
MPEO$_{44}$-*b*-PCL$_{17}$	4000	5400	3130	1.45
MPEO$_{44}$-*b*-PCL$_{44}$	7000	6830	7570	1.43

[a] M_n was calculated by the monomer conversion; $M_n = [M]_0/[I]_0 \times 114 + M_n$ α-methoxy-ω-hydroxy-MPEO containing a ketal group (**6**). [b] M_n was calculated by ^{1}H NMR spectroscopy according to eqn (2). [c] M_n is relative to PS standards. [d] M_w/M_n is relative to PS standards.

carbon signals that are consistent with the desired structure. The most important carbon signals are highlighted, *i.e.*, the signals that correspond to carbons from the dimethyl ketal group at $\delta =$ 24.39 ppm (**13**) and the quaternary carbon from the same group –OC$(CH_3)_2$–O– at $\delta = 121.50$ ppm (**12**). Other significant signals were observed at higher frequencies and slightly shifted in comparison with the ^{13}C NMR spectrum from α-methoxy-ω-hydroxy-PEO containing a ketal (**6**) (Fig. 1, bottom). These signals appear at $\delta = 147.44$ (**9**) and $\delta = 161.1$ ppm (**8**) for the triazole ring –CH_2–CH=CH–N– and at $\delta = 173.58$ ppm (**4** + **16**) for the carbon from the carbonyl group –CH_2–O–C(O)–$(CH_2)_3$– next to PEO and for the carbon from carbonyl group in PCL. All of the other remaining signals are attributed to the carbon atoms from the diblock copolymer structure.

Similar bands for the characteristic peaks were found for all samples in the FT-IR spectra (Fig. S7c†).

The molecular weights and polydispersity indices of the synthesised MPEO-*b*-PCL diblock copolymers were determined by SEC. The analysis clearly shows that the obtained curves are monomodal, confirming that the ketal group was not degraded during the ROP of ε-CL. A slight asymmetry is observed at longer elution times in the SEC curve (regular line in Fig. S9†), which strongly suggests that some unreacted MPEO is present. The molecular characteristics of the diblock copolymers are listed in Table 2.

Polymer nanoparticles (NPs)

As a proof-of-concept, polymer NPs were prepared from the block copolymers, and their behaviours under different simulated physiological conditions were evaluated in detail by DLS and NTA. The visual appearance of the colloidal particles immediately after the injection of the MPEO-*b*-PCL block copolymer solutions into water was size-dependent and did not change after the dilution with PBS (pH ~ 7.4) (data not shown). For $MPEO_{44}$-*b*-PCL_{17}, the resulting colloidal solution was fully transparent, whereas the solution was slightly opalescent for the $MPEO_{44}$-*b*-PCL_{44} block copolymer. This result is a visual indication that the particles produced by the nanoprecipitation protocol using the $MPEO_{44}$-*b*-PCL_{44} block copolymer are larger than the particles produced using the $MPEO_{44}$-*b*-PCL_{17} block copolymer.[51] Fig. 3 shows the distribution of R_H for $MPEO_{44}$-*b*-PCL_{17} and $MPEO_{44}$-*b*-PCL_{44} block copolymer micelles after the dialysis process and dilution with PBS, as measured by DLS. The distribution of R_H for $MPEO_{44}$-*b*-PCL_{17} appears as only one single distribution of R_H relative to the presence of the polymer micelles in PBS solution with an average of $R_H = 32.1$ nm (Fig. 3, blue circles). Furthermore, the polydispersity of the $MPEO_{44}$-*b*-PCL_{17} micelles is very low as estimated through the cumulant analysis ($\mu/\Gamma^2 = 0.08 \pm 0.007$). However, for the $MPEO_{44}$-*b*-PCL_{44} block copolymer, a bimodal distribution of R_H was observed with average sizes of $R_H = 18.5$ nm and 99.5 nm, respectively (Fig. 3, red circles). Because the ketal linkage does not affect the physico-chemical properties of the MPEO-*b*-PCL diblock copolymers, the main factors that control the particle size and morphology in crystalline amphiphilic block copolymers that self-assemble in water are the preparation methodology and the polymer properties,

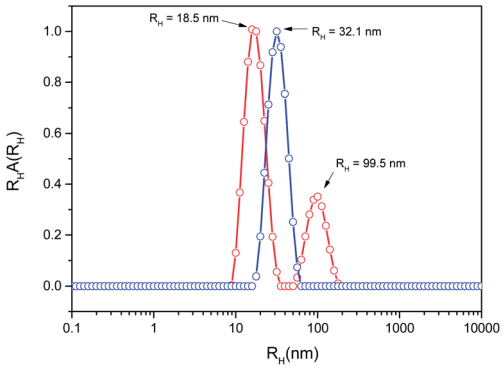

Fig. 3 Distributions of R_H for (○) $MPEO_{44}$-*b*-PCL_{17} and (○) $MPEO_{44}$-*b*-PCL_{44} NPs prepared by the nanoprecipitation protocol and diluted in PBS (pH ~ 7.4), both at a concentration of 1 mg mL^{-1}.

such as the molecular weight and the relative block length.[52] Although the study of the particles' morphology is far beyond the scope of the current investigation, some comparisons with the literature data could be performed. Similar particle sizes were found in a previous study for micelles of the PEO-*b*-PCL diblock copolymer with the same block length prepared through the dialysis method.[53,54] For the PEO_{44}-*b*-PCL_{44} diblock copolymer, mixtures between spherical and cylindrical micelles were found to coexist after dialysis when observed by TEM.[53] Spherical micelles with diameters in the range of 35 ± 5 nm were observed concomitantly with cylinders with a broad size range (greater than 100 nm) and polydispersity. Similar results were obtained by others authors[55] by using the same block and block lengths. The observed bimodal size distribution of R_H for the PEO_{44}-*b*-PCL_{44} block copolymer is related to a morphological mixture of at least two types of particles. According to the aforementioned literature, the most probable morphological structures are the mixture between spherical micelles with an average size of $D_H = 37.0$ nm and cylindrical and/or worm-like micelles with $D_H = 199$ nm. On the other hand, for PEO_{44}-*b*-PCL_{17} block copolymer assemblies, single monodisperse spherical micelles are obtained in most cases.

Note that thermodynamically stable polymeric NPs with hydrodynamic diameters ($2R_H = D_H$) within the range of 20 to 60 nm have been shown to be ideal for tumour drug-delivery applications.[56] They are within the size range that enables renal clearance to be avoided ($D_H > 10$ nm), thereby providing the NPs a potentially prolonged blood circulation time and, considering that their size is below the cut-off size of the leaky pathological vasculature ($D_H < 200$ nm), specific accumulation in solid tumour tissue due to the enhanced permeation and retention (EPR) effect.[57] Moreover, in addition to the role of the particle size in the EPR effect, another important aforementioned target in cancer therapy is the acidic cytosolic or endosomal conditions in tumour cells. Therefore, the sensibility of the polymer NPs containing the acid-labile ketal group was tested by DLS in acidic media (pH ~ 5) under physiological conditions (37 °C) using the $MPEO_{44}$-*b*-PCL_{17} block copolymer. $MPEO_{44}$-*b*-PCL_{17} block copolymer NPs were chosen for evaluating the ketal linkage sensibility *in vitro* because they presented a monodisperse single distribution of R_H with a

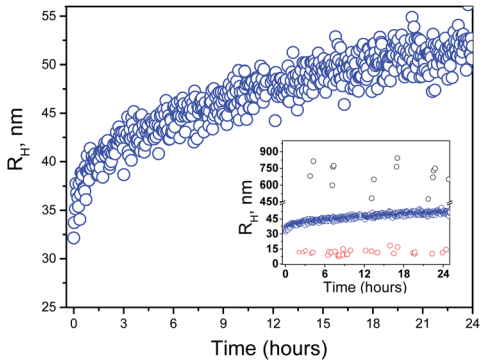

Fig. 4 Temporal dependence on the R_H distribution of $MPEO_{44}$-*b*-PCL_{17} NPs at pH ~ 5.0 and 37 °C. The inset illustrates the R_H distribution as a function of time for (○) aggregate NPs, (○) free PEO chains and (○) loose aggregates.

$D_H = 64.2$ nm, which is within the optimal size for drug-delivery applications. As shown in Fig. 3, the absence of a mixture between distinct morphological structures facilitates the experimental procedures and data analysis. Fig. 4 shows the distribution of R_H for the $MPEO_{44}$-*b*-PCL_{17} block copolymer NPs at pH ~ 5.0 and 37 °C as a function of time.

The results clearly show an increase in the average size of the micellar NPs from $R_H = 32.1$ nm to R_H 52.6 nm in 24 hours, which corresponds to an increase in D_H of approximately 41 nm. To obtain a thorough size distribution and to gain more information to accurately analyse the distribution of monodisperse and polydisperse samples than can be obtained through DLS,[58,59] the $MPEO_{44}$-*b*-PCL_{17} NPs were analysed using NTA at 25 °C. This technique is a powerful tool that complements DLS, and it is particularly valuable for the detection and accurate sizing of a broad range of population ratios. After 24 hours, the $MPEO_{44}$-*b*-PCL_{17} block copolymer NPs showed mean particle sizes of 96 nm and 118 nm under pH ~ 7.4 and pH ~ 5.0, respectively. Fig. 5 depicts the size distributions for the NPs, in which the value of $d(0.1)$ was 64 nm, $d(0.5)$ was 92 nm and $d(0.9)$ was 128 nm (pH ~ 7.4) and $d(0.1)$ was 61 nm, $d(0.5)$ was 92 nm and $d(0.9)$ was 209 nm (pH ~ 5.0). According to eqn (2), these cumulative volumes give span values of 0.69 and 1.57 for pH ~ 7.4 and pH ~ 5.0, respectively.

In addition, it is possible to verify for the $MPEO_{44}$-*b*-PCL_{17} block copolymer NPs the presence of only one sharp peak at pH ~ 7.4 (Fig. 5, upper) and three peaks at pH ~ 5.0 (Fig. 5 bottom). Similarly, the TEM images (Fig. 6) showed a comparable increase in the size of the $MPEO_{44}$-*b*-PCL_{17} block copolymer NPs at pH ~ 5.0 (Fig. 6b) when compared to the NPs at pH ~ 7.4 (Fig. 6a) after 24 hours. The particle sizes determined from the TEM images are clearly smaller than those determined by scattering techniques. This discrepancy can be explained by a combination of two effects: (i) during sample preparation, the particles undergo dehydration and may shrink, and (ii) scattering techniques report an intensity-average dimension, whereas TEM reports a number-average dimension. Therefore, TEM images generally yield smaller sizes relative to DLS data.[60]

The increases in particle size and size distribution, as shown by both scattering techniques and TEM, are strong evidence for

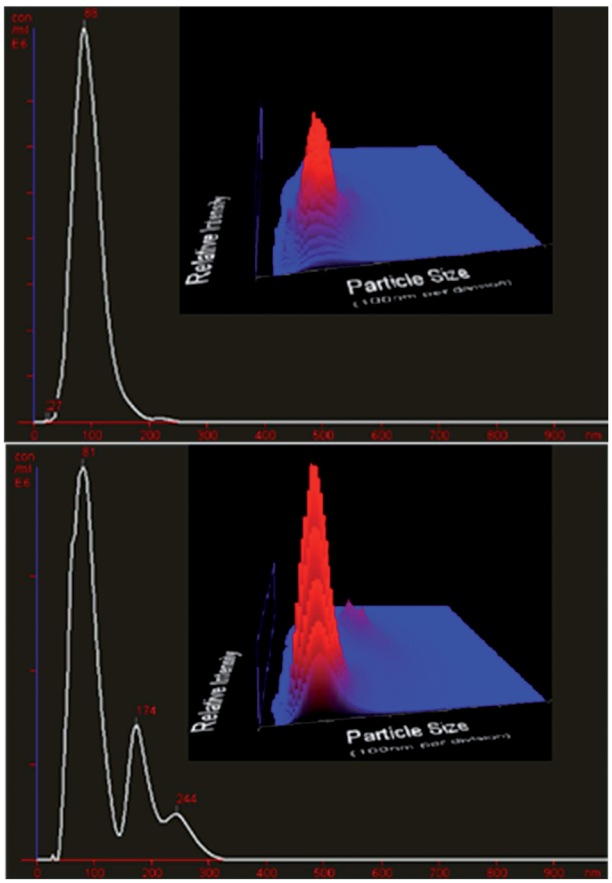

Fig. 5 Size distribution from NTA for the $MPEO_{44}$-*b*-PCL_{17} NPs under pH ~ 7.4 (upper) and pH ~ 5.0 (bottom) after 24 h.

micellar aggregation over time. The aggregation mechanism could be explained through the hydrolysis of the acid-labile ketal linkage in the $MPEO_{44}$-*b*-PCL_{17} block copolymer micelles at pH 5.0. While the hydrolysis of the ketal group occurs at the interface between the PCL core and the PEO shell inside the micelles, the free hydrolysed PEO chains begin to be released into the media (inset of Fig. 4). The decrease in the density of surface PEO chains leads to a decrease in the steric hindrance of the particles and to an increase in the hydrophobicity of the particles, and consequently, particle aggregation.[23] The linear relationship observed between the relaxation rates (Γ) and the square of the wave vector (q^2) for the particles before (37 °C and pH ~ 7.4) and after 24 hours (37 °C and pH ~ 5.0) demonstrates that both NPs and their aggregates are spherical (Fig. S10† and 6), and no distinct micellar structures were observed by DLS, NTA and TEM. Furthermore, no changes in the particle size distributions were observed for the $MPEO_{44}$-*b*-PCL_{17} block copolymer micelle by DLS at pH ~ 7.4 for 24 hours, confirming that the particles are selective to environments with mild acidic conditions (from pH ~ 5 to ~ 6.5) such as tumour tissues (Fig. S11†). Moreover, the degradation of the $MPEO_{44}$-*b*-PCL_{17} diblock copolymer was confirmed by ^{13}C NMR spectroscopy. For the NMR study, 40–50 mg of the $MPEO_{44}$-*b*-PCL_{17} diblock copolymer was dissolved in 0.6 mL of deuterated chloroform followed by the addition of 25 μl of hydrochloric acid-d (DCl).

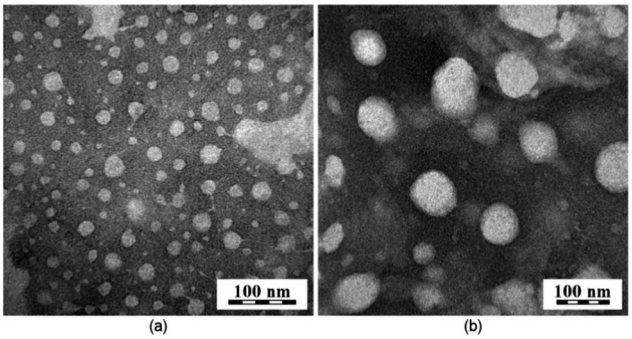

Fig. 6 TEM images of $MPEO_{44}$-*b*-PCL_{17} NPs at pH ~ 7.4 (a) and at pH ~ 5.0 (b) after 24 h.

The degradation was determined based on the disappearance of the signal from the ketal linkage between the PEO and PCL blocks. Fig. S12† shows the ^{13}C NMR spectra of the $MPEO_{44}$-*b*-PCL_{17} copolymer (a) before and (b) after the addition of DCl. The ^{13}C NMR spectra reveal the complete disappearance of the carbon signal from the ketal group linker $-OC(CH_3)_2-O-$ at $\delta =$ 121.50 ppm (**12**, Fig. S12†) after the addition of DCl (**12**, Fig. S12b†). This observation is strong evidence that hydrolytic degradation occurs in the ketal linkage of the $MPEO_{44}$-*b*-PCL_{17} diblock. Unfortunately, the usual degradation products resulting from the acid hydrolysis of a ketal group, such as acetone,[22] could not be detected in the ^{13}C NMR spectrum. Their signal is hidden under that of the ε-CL repeating units in the ^{13}C NMR. According to the ^{13}C NMR spectra, no changes were observed in the signal from ε-CL repeating units after the addition of DCl. The signals from the methylene carbons $-CO-(CH_2)_5-O-$ (**17** to **21** from $\delta = 20$ to $\delta = 65$ ppm, Fig. S12†) and from the carbonyl group (**16** at $\delta = 173$ ppm, Fig. S12†) related to the PCL segments remain unchanged. Moreover, no new signal from side products that could derive from the hydrolysis of ester bonds related to the PCL segments was detected after the acid addition. However, a visible decrease in the methylene signal $-O-(CH_2)_2-O-$ (**2** at $\delta = 70$ ppm, Fig. S12b†) related to MPEO units was observed in the ^{13}C NMR spectra. The decrease in the signal of the MPEO units is related to the experimental procedures. After the addition of DCl to the $MPEO_{44}$-*b*-PCL_{17} block copolymer solution in $CDCl_3$, the NMR tube was vigorously shaken. The formation of an emulsion composed of droplets of D_2O containing the MPEO blocks dissolved in the internal phase and the PCL blocks dissolved in the outer phase ($CDCl_3$, organic phase) spontaneously occurs. While hydrolysis of the ketal group occurs, the released PCL segments are dissolved in the outer organic phase ($CDCl_3$), whereas the MPEO blocks remain dissolved in the emulsion droplets (D_2O) with restricted mobility. The restriction in the mobility of the MPEO chains dissolved in the D_2O droplets decreases the signal intensity in the ^{13}C NMR spectra.[61]

Conclusions

Through the combination of carbodiimide chemistry and ROP mechanisms with a "click" reaction, novel pH-sensitive amphiphilic block copolymers containing acid-labile ketal groups as block linkers were successfully synthesised using a multi-step stage-by-stage synthetic strategy. The acid-cleavable linkage in the block copolymer backbone was used as a junction point for the design of hydrophilic PEO and hydrophobic PCL segments. For this purpose, a 2-{[2-(2-azidoethoxy)propan-2-yl]} ethan-1-ol compound, with a specific degradable linkage (acyclic ketal group), was synthesised for the first time. Subsequently, α-methoxy-ω-hydroxy-PEO containing a ketal group was prepared as a macroinitiator through a "click" reaction between previously synthesised α-methoxy-ω-alkyne-PEO and 2-{[2-(2-azidoethoxy)propan-2-yl]}ethan-1-ol. The obtained macroinitiator was applied for the sequential controlled ROP of ε-CL in the presence of $Sn(Oct)_2$. Different ratios of ε-caprolactone/hydroxyl were used to obtain copolymers with different PCL block lengths. Good control, purity and conversion over each obtained product were achieved without degradation of the acid-labile ketal group. Upon dissolution in a mild organic solvent, the $MPEO_{44}$-*b*-PCL_{17} block copolymer self-assembled in water–PBS into regular spherical NPs, and the presence of the acid-labile ketal group linker allowed the NPs to disassemble and aggregate in buffer that simulated acidic cytosolic or endosomal conditions in tumour cells (pH ~ 5.0), as evaluated by DLS and NTA analyses and TEM images. The synthesised block copolymers could be used in a variety of applications, *e.g.*, as pH-triggered release and drug-delivery systems.

Acknowledgements

This research was supported by the Grant Agency of the Czech Republic (P208/10/1600). E.J., R.K., and A.J. acknowledge Charles University (Prague, CZ) for the financial support and for the opportunity to pursue their Ph.D. studies. C. G. Venturini acknowledges the Program Science Without Borders CAPES/Brazil (Process number 2293/13-7). Electron microscopy was supported through grant TACR TE01020118.

References

1 Y.-Y. Won, H. T. Davis and F. S. Bates, *Science*, 1999, **283**, 960–963.
2 J. K. Kim, E. Lee, Z. G. Huang and M. Lee, *J. Am. Chem. Soc.*, 2006, **128**, 14022–14023.
3 E. Busseron, Y. Ruff, E. Moulin and N. Giuseppone, *Nanoscale*, 2013, **5**, 7098–7140.
4 D. E. Cola, C. Lefebvre, A. Deffieux, T. Narayanan and R. Borsali, *Soft Matter*, 2009, **5**, 1081–1090.
5 A. H. Gröschel, F. H. Schacher, H. Schmalz, O. V. Borisov, E. B. Zhulina, A. Walther and A. H. E. Müller, *Nat. Commun.*, 2012, **3**, 1–11.
6 T. Smart, H. Lomas, M. Massgnani, M. V. Flores-Merino, L. R. Perez and G. Battaglia, *Nano Today*, 2008, **3**, 38–46.
7 R. B. Grubbs and Z. Sun, *Chem. Soc. Rev.*, 2013, **42**, 7436–7445.
8 X.-B. Xiong, A. Falamarzian, S. M. Garg and A. Lavasanifar, *J. Controlled Release*, 2011, **155**, 248–261.

9 W. Shao, K. Miao, H. Liu, C. Ye, J. Du and Y. Zhao, *Polym. Chem.*, 2013, **4**, 3398–3410.
10 W. Wang, H. Sun, F. Meng, S. Ma, H. Liu and Z. Zhong, *Soft Matter*, 2012, **8**, 3949–3956.
11 W. J. Li, C. T. Laurencin, E. J. Caterson, R. S. Tuan and K. K. Frank, *J. Biomed. Mater. Res.*, 2001, **60**, 613–621.
12 W. J. Li, K. G. Danielson, P. G. Alexander and R. S. Tuan, *J. Biomed. Mater. Res., Part A*, 2003, **67**, 1105–1114.
13 C. Drew, X. Wang, L. A. Samuelson and J. Kumar, *J. Macromol. Sci., Part A: Pure Appl.Chem.*, 2003, **40**, 1415–1422.
14 S. V. Trubetskoy, *Adv. Drug Delivery Rev.*, 1999, **37**, 81–88.
15 V. P. Torchilin, *Colloids Surf., B*, 1999, **16**, 305–319.
16 K. Miyata, N. Nishiyama and K. Kataoka, *Chem. Soc. Rev.*, 2012, **41**, 2562–2574.
17 J. H. Jeong and T. G. Park, *J. Controlled Release*, 2002, **82**, 159–166.
18 Y. Ymamoto, Y. Nagasaki, Y. Kato, Y. Sugiyama and K. Kataoka, *J. Controlled Release*, 2001, **77**, 27–38.
19 A. Rösler, G. W. M. Vandermeulen and H.-A. Klok, *Adv. Drug Delivery Rev.*, 2001, **53**, 95–105.
20 Q. Zhang, N. R. Ko and J. K. Oh, *Chem. Commun.*, 2012, **48**, 7542–7552.
21 E. G. Kelley, J. N. L. Albert, M. O. Sullivan and T. H. Epps, *Chem. Soc. Rev.*, 2013, **42**, 7057–7071.
22 S. Binauld and M. H. Stenzel, *Chem. Commun.*, 2013, **49**, 2082–2102.
23 F. C. Giacomelli, P. Štěpánek, C. Giacomelli, V. Schmidt, E. Jäger, A. Jäger and K. Ulbrich, *Soft Matter*, 2011, **7**, 9316–9325.
24 S. Mura, J. Nicolas and P. Couvreur, *Nat. Mater.*, 2013, **12**, 991–1003.
25 E. Jäger, A. Jäger, P. Chytil, T. Etrych, B. Říhova, F. C. Giacomelli, P. Štěpánek and K. Ulbrich, *J. Controlled Release*, 2013, **165**, 153–161.
26 I. F. Tannock and D. Rotin, *Cancer Res.*, 1989, **49**, 4373–4384.
27 H. Yin, E. S. Lee, D. Kim, K. H. Lee, K. T. Oh and Y. H. Bae, *J. Controlled Release*, 2008, **126**, 130–138.
28 S. Sengupta, D. Eavarone, I. Capila, G. Zhao, N. Watson, T. Kiziltepe and R. Sasisekharan, *Nature*, 2005, **436**, 568–572.
29 S. Aryal, C. J. Hu and L. Zhang, *ACS Nano*, 2010, **4**, 251–258.
30 H. Mok, J. W. Park and T. G. Park, *Bioconjugate Chem.*, 2008, **19**, 797–801.
31 A. P. Griset, J. Walpole, R. Liu, A. Gaffey, Y. L. Colson and M. W. Grinstaff, *J. Am. Chem. Soc.*, 2009, **131**, 2469–2471.
32 B. Wang, C. Xu, J. Xie, Z. Yang and S. Sun, *J. Am. Chem. Soc.*, 2008, **130**, 14436–14437.
33 M. M. Ali, M. Oishi, F. Nagatsugi, K. Mori, Y. Nagasaki, K. Kataoka and S. Sasaki, *Angew. Chem., Int. Ed.*, 2006, **45**, 3136–3140.
34 Y. Li and P. I. Lee, *Int. J. Pharm.*, 2010, **383**, 45–52.
35 S. D. Khaja, S. Lee and N. Murthy, *Biomacromolecules*, 2007, **8**, 1391–1395.
36 J. Siepmann and A. Göpferich, *Adv. Drug Delivery Rev.*, 2001, **48**, 229–247.
37 J. H. Jeong, S. W. Kim and T. G. Park, *Bioconjugate Chem.*, 2003, **14**, 473–479.
38 M. A. R. Meier, S. N. H. Aerts, B. B. P. Staal, M. Rasa and U. S. Schubert, *Macromol. Rapid Commun.*, 2005, **26**, 1918–1924.
39 S. Petrova, I. Kolev, S. Miloshev, M. D. Apostolova and R. Mateva, *J. Mater. Sci.: Mater. Med.*, 2012, **23**, 1225–1234.
40 J. Wu and C.-C. Chu, *Acta Biomater.*, 2012, **8**, 4314–4323.
41 J. Nicolas, S. Mura, D. Brambila, N. Mackiewicz and P. Couvreur, *Chem. Soc. Rev.*, 2013, **42**, 1147–1235.
42 J. Rieger, P. Dubois, R. Jérôme and C. Jérôme, *Langmuir*, 2006, **22**, 7471–7479.
43 N. Kumar, M. N. V. Ravikumar and A. J. Domb, *Adv. Drug Delivery Rev.*, 2001, **53**, 23–44.
44 M. Oikawa, A. Wada, F. Okazaki and S. J. Kusumoto, *J. Org. Chem.*, 1996, **61**, 4469–4471.
45 R. A. Shenoi, B. F. L. Lai and J. N. Kizhakkedathu, *Biomacromolecules*, 2012, **13**, 3018–3030.
46 O. Norberg, L. Deng, T. Aastrup and M. Yan, *Anal. Chem.*, 2011, **83**, 1000–1007.
47 H. Freichels, V. Pourcelle, R. Auzély-Velty, J. Marchand-Brynaert and C. Jérôme, *Biomacromolecules*, 2012, **13**, 760–768.
48 P. Štěpánek, *J. Chem. Phys.*, 1993, **99**, 6384–6393.
49 J. Jakes, *Czech. J. Phys.*, 1988, **38**, 1305.
50 V. Krishnakumar and J. R. Xavier, *Spectrochim. Acta, Part A*, 2004, **60**, 709–714.
51 A. M. de Oliveira, E. Jäger, A. Jäger, P. Štěpánek and F. C. Giacomelli, *Colloids Surf., A*, 2013, **436**, 1092–1102.
52 A. Choucair and A. Eisenberg, *Eur. Phys. J. E*, 2003, **10**, 37–44.
53 Z.-X. Du, J.-T. Xu and Z.-Q. Fan, *Macromolecules*, 2007, **40**, 7633–7637.
54 P. Schuetz, M. J. Greenall, J. Bent, S. Furzeland, D. Atkins, M. F. Butler, T. C. B. McLeishd and D. M. A. Buzza, *Soft Matter*, 2011, **7**, 749–759.
55 S. M. Loverde, M. L. Klein and D. E. Discher, *Adv. Mater.*, 2012, **24**, 3823–3830.
56 H. Cabral, Y. Matsumoto, K. Mizuno, Q. Chen, M. Murakami, M. Kimura, Y. Terada, M. R. Kano, K. Miyazono, M. Uesaka, N. Nishiyama and K. Kataoka, *Nat. Nanotechnol.*, 2011, **6**, 815–823.
57 H. Maeda, H. Nakamura and J. Fang, *Adv. Drug Delivery Rev.*, 2013, **65**, 71–79.
58 V. Filipe, A. Hawe and W. Jiskoot, *Pharm. Res.*, 2010, **27**, 796–810.
59 A. E. James and J. D. Driskell, *Analyst*, 2013, **138**, 1212–1218.
60 A. Jäger, D. Gromadzki, E. Jäger, F. C. Giacomelli, A. Kozlowska, L. Kobera, J. Brus, B. Říhova, M. El Fray, K. Ulbrich and P. Štěpánek, *Soft Matter*, 2012, **8**, 4343–4354.
61 J. Spěváček, *Makromol. Chem., Rapid Commun.*, 1982, **3**, 697–703.

Journal Name

ARTICLE

pH-triggered release of paclitaxel from nanoparticles made from biodegradable block copolymer containing ketal groups between polymer blocks

Received 00th January 20xx,
Accepted 00th January 20xx

DOI: 10.1039/x0xx00000x

www.rsc.org/

Eliézer Jäger,[a,b]* Anita Höcherl,[a] Alessandro Jäger,[a,b] Svetlana Petrova,[a]* Cristina Garcia Venturini,[a] Olga Janoušková,[a] Rafał Konefał,[a,b] Ewa Pavlova,[a] Karel Ulbrich[a] and Petr Štěpánek[a]

The potential of biodegradable self-assembled MPEO-*b*-PCL nanoparticles (NPs) containing hydrolytically labile linkage (acyclic ketal group) between the hydrophobic PCL and the hydrophilic MPEO blocks for paclitaxel delivery and their *in vitro* cytostatic activity has been explored on model cancer cells. The amphiphilic diblock copolymer poly(ethylene oxide monomethyl ether) (MPEO)-*b*-poly(ε-caprolactone) (PCL) block copolymers containing a ketal group as block linker dissolved in organic solvent (acetone) undergoes nanoprecipitation in phosphate buffer saline (PBS, pH ~ 7.4) and self-assemble into regular spherical NPs after solvent elimination. The NPs structure was characterized in detail by dynamic (DLS), static (SLS), nanoparticle tracking analysis (NTA) and transmission electron microscopy (TEM). The acid-labile ketal linker enabled the disassembly of the nanoparticles in a buffer simulating acidic environment in endosomal (pH ~ 5.0 to ~ 6.0) and lysosomal (pH ~ 4.0 to ~ 5.0) cell compartments resulting in the release of paclitaxel (PTX) and formation of neutral degradation products. The *in vitro* cytotoxicity studies showed an important increase in activity of the paclitaxel-loaded particles compared to the free paclitaxel. The particle's size below the cut-off of the leaky pathological vasculature (particle diameter below 100 nm) and the ability to release a drug at the endosomal pH with concomitant high cytotoxicity makes them suitable candidates for cancer therapy, namely for the treatment of solid tumours where the NPs can selectively accumulate due to Enhanced Permeability and Retention (EPR) effect.

Introduction

The design of amphiphilic block copolymers (composed of hydrophilic and hydrophobic blocks) has been extensively studied.[1-4] These copolymers are of great interest because of their ability to self-assemble in aqueous media generating particles of various structure types, shapes and sizes, ranging from nano- to micrometres.[5-6] By careful tuning of the amphiphilic block copolymers' properties (such as the molecular weight and the relative block length),[7] self-assembled nano-sized spherical micellar nanoparticles (NPs) with a core-shell architecture[8] can be generated.

One key feature of these materials is associated with their capability to bear the lipophilic drug and release it in a controlled manner[9,10] as their hydrophobic core works as reservoir for lipophilic agents (drugs). Equally important is their hydrophilic corona which provides a highly water-bound barrier to ensure colloidal stability, reduction in the rate of opsonin adhesion and uptake by cells of RES, which prolongs the blood circulation life time.[11] In addition, self-assembled NPs gain much more relevance in biomedical applications especially if they are tailored to be degradable as a response to external stimuli. Such stimulus may be the enzymatic removal of protecting groups,[12] light,[13] temperature,[14] redox gradient[15] or change of pH.[16] Especially delivery platforms that enable a targeted release of chemotherapeutics at sites of pH imbalance have the potential for high therapeutic impact.[17] The ability to generate a triggered nanoparticle response (*e.g.* release of cargo) at selective pH is of particular interest, *e.g.*, in the targeted delivery to tumors, as the extracellular pH at solid tumor sites is generally more acidic (ranging from pH 5.7 to 7.2) than in normal tissue (buffered at pH 7.4).[18,19] Variations in pH are also encountered when nanoparticles are internalized by cells *via* endocytosis where the pH usually drops to as low as 5.0 - 6.0 in endosomes and 4.0 - 5.0 in lysosomes.[20]

Several polymers responsive to pH-sensitive hydrolysis that contain different acid-labile linkers suitable for triggering drug release, such as ester,[21] hydrazone,[22] orthoester,[23] imine,[24] ketal and acetal,[25] have been widely studied. In particular, acid-degradable (co)polymers and NPs that contain ketal/acetal labile linkers, situated along the polymer backbone or as pendant groups enabling drug attachment, are

[a] Institute of Macromolecular Chemistry v.v.i., Academy of Sciences of the Czech Republic, Heyrovsky Sq. 2, 162 06 Prague 6, Czech Republic.
[b] Charles University Prague, Faculty of Natural Sciences, Hlavova 2030, Prague 12840 2, Czech Republic.
E-mail: jager@imc.cas.cz; petrova@imc.cas.cz; Tel: +420 296 809 296.

† Footnotes relating to the title and/or authors should appear here.
Electronic Supplementary Information (ESI) available: [details of any supplementary information available should be included here]. See DOI: 10.1039/x0xx00000x

of considerable interest. In many cases they showed to be more sensitive to the acidic environment of tumors and phagosomes than esters and hydrazones.[26] Furthermore, these linkers can also be more stable under physiological conditions (pH ~ 7.4) than the other aforementioned linkers.[27]

Although novel and efficient pH-sensitive carriers with ketal/acetal linkers have great potential for drug delivery, synthetic challenges have often limited their applications. In this way, we recently reported the synthesis of a novel class of well-defined biocompatible and biodegradable poly(ethylene oxide monomethyl ether) (MPEO)-*b*-poly(ε-caprolactone) (PCL) block copolymers containing an acid-labile ketal group as block linker.[28] The PEO and PCL polymers were selected as building blocks because of their special suitability for environmental, biomedical and pharmaceutical applications.[29-31] PCL is an aliphatic hydrophobic polyester with great potential as a biomaterial due to its unique combination of biodegradability and biocompatibility,[32] and PEO is a hydrophilic and very flexible biocompatible polymer that is non-toxic and easily eliminated from the body.[33]

Herein, we report the potential of NPs as a tumor-specific drug delivery carrier. The NPs were prepared from a new biocompatible and biodegradable diblock copolymer containing an acid-labile linkage (acyclic ketal group) between the hydrophobic PCL and the hydrophilic MPEO blocks and they contained the cytotoxic drug paclitaxel loaded in hydrophobic core by hydrophobic interactions. Drug release and cytotoxic activity of the NPs were evaluated on human HeLa carcinoma cells. Due to the specific chemical structure, the block copolymer NPs disassemble and release the drug cargo under mildly acidic conditions (which simulate the acidic environment in endosomal and lysosomal compartments), exerting *in vitro* cytostatic efficacy on HeLa human cervical carcinoma cell line. The ketal linkage hydrolysis results in neutral degradation products that can be easily excreted, thereby avoiding accumulation and likely inflammatory responses. These important features of the presented novel MPEO-*b*-PCL block copolymer are discussed in the paper.

Results and discussion

In the first step the low-molecular-weight compounds as precursors for constructing the acid-labile ketal group as a biodegradable linkage between blocks for further polymerization of the MPEO-*b*-PCL block copolymers through an efficient multi-step pathway containing different synthetic routes (*e.g.*, carbodiimide chemistry, "click" reaction and ring-opening polymerization) were prepared.[28] The block copolymers were synthesized using a newly developed *α*-methoxy-*ω*-hydroxy-poly(ethylene oxide) that contains the acid-labile ketal linkage (incorporated *via* a "click" reaction) as a macroinitiator for the sequential controlled ring-opening polymerization of ε-CL (Fig. S1, ESI and Mat. and Methods). These new synthetic pathways were developed to obtain well-defined acid-labile block copolymer NPs which release hydrophobic drug with increased rate at relevant mild acidic conditions. This should raise potential PTX toxicity to cancer cells, while after releasing the cargo, the nanocarriers are further disassembled into environmentally neutral degradation products.

We chose the $MPEO_{44}$-*b*-PCL_{17} (the subscripts refer to the degree of polymerization of each block) as a well-defined and characterized copolymer forming the delivery system. Due to carefully calibrated block copolymer properties, such as the molecular weight and the relative block length, the $MPEO_{44}$-*b*-PCL_{17} block copolymer self-assembles in PBS (pH ~ 7.4) forming single spherical nanoparticles (discussed hereafter). The structure of the block copolymer is depicted in Fig.1.

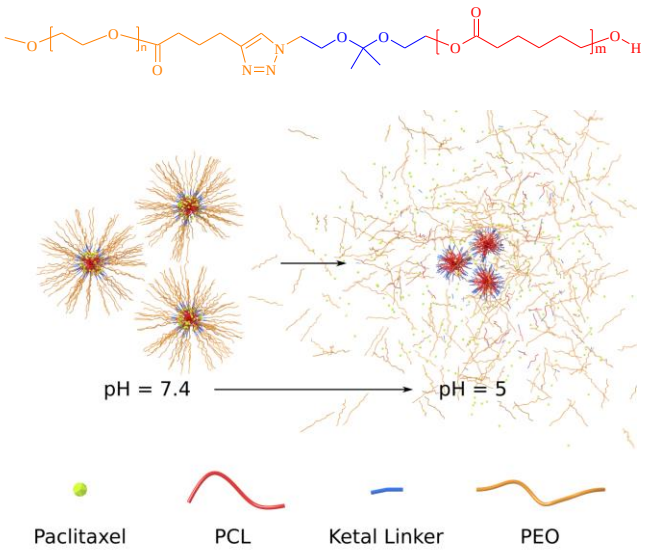

Fig. 1. Molecular structure of the pH-triggered acid-labile block copolymer $MPEO_{44}$-*b*-PCL_{17} (top) and the schematic nanoparticles assembly/disassembly mechanism at pH ~ 5.0 (bottom).

The composition of the $MPEO_{44}$-*b*-PCL_{17} block copolymer was characterized using ^{1}H and ^{13}C NMR and is shown in Table 1 and Fig. S1 and S2 (ESI). The SEC analysis (Fig. S3) shows that the obtained distribution curve for the copolymer is monomodal, confirming that the ketal group was not degraded during the ring-opening polymerisation (ROP) of ε-CL as it was also confirmed by the ^{1}H and ^{13}C NMR (Fig. S2 top and bottom, ESI). The macromolecular characteristics of the block copolymer are listed in Table 1.

Table 1. Macromolecular characteristics of the $MPEO_{44}$-*b*-PCL_{17} block copolymer.

Sample	M_n,[a] (NMR)	M_n,[b] (NMR)	M_n,[c] (SEC)	M_w/M_n,[d] (SEC)
$MPEO_{44}$-*b*-PCL_{17}	4000	5400	3130	1.45

[a] M_n was calculated by the monomer conversion; $M_n = [M]_o/[I]_o \times 114 + M_n$ *α*-methoxy-*ω*-hydroxy-MPEO containing a ketal group (**Fig. S1** and **S2**, **ESI**).
[b] M_n was calculated by ^{1}H NMR spectroscopy according to Eq. 2 (**ESI**).
[c] M_n and [d] M_w/M_n values are relative to PS standards (**Fig. S3**, **ESI**).

After the dissolution upon organic solvent the $MPEO_{44}$-*b*-PCL_{17} diblock copolymer undergoes nanoprecipitation and self-assembles into regular spherical NPs in PBS containing the PTX chemotherapeutic drug (see Mat. and Methods). The SLS and DLS measurements revealed the assembly of well-defined low-dispersity NPs after solvent evaporation (Fig. 2). A plot of the relaxation frequency (Γ) versus the square of the scattering vector (q^2) gives a linear relationship, indicative of the Brownian diffusion of spherical particles (Fig. 2a). The slope through the origin yields the diffusion coefficient and by using the Stokes-Einstein equation (eq. 5, Mat. and Methods), an apparent R_H of 32.1 nm was determined, which is in good agreement with the data from fixed angle measurements (Fig. 2b). From the Zimm analysis of the SLS data (see Mat. and Methods) the values of the radius of gyration (R_G) were determined from the slope of the curve as being equal to 28.3 nm. It is well established that the R_G/R_H ratio is related to the shape of NPs in solution. The obtained R_G/R_H ratio was equal to 0.88, thus being compatible with the formation of spherical block copolymer NPs.[16,34] ELS measurements at pH 7.4 (PBS buffer) showed an average ζ-potential for the studied block copolymer NPs close to neutrality (~ - 0.5 mV).

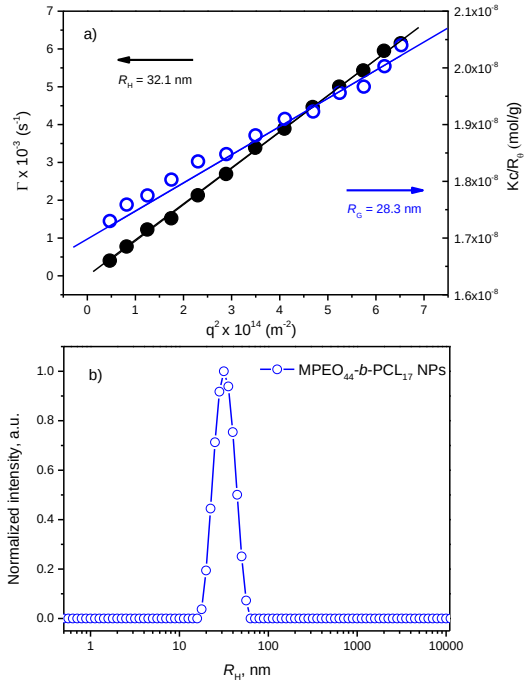

Fig. 2. Measurement of angular dependence by DLS (●) and SLS (○) of the $MPEO_{44}$-*b*-PCL_{17} NPs prepared using the nanoprecipitation protocol (a) and normalized intensity size distribution of the $MPEO_{44}$-*b*-PCL_{17} NPs measured at angle 90° at a concentration of 1 mg·mL^{-1} in PBS (pH ~ 7.4) and at 37 °C (b).

Thermodynamically stable polymeric NPs with a hydrodynamic diameter ($2R_H = D_H$) of ~ 64 nm were obtained. These NPs are perfectly suited for drug-delivery *by* specific accumulation in solid tumor tissue by the EPR effect, because the optimal particle size for EPR effect is usually stated to be ~ 20 to 70 nm.[34] Another important aforementioned target in cancer therapy is the acidic environment in endosomal (pH ~ 5.0 to ~ 6.0) and lysosomal (pH ~ 4.0 to ~ 5.0) compartments. Therefore, the sensibility of the polymer NPs containing the acid-labile ketal group was tested by NTA in acidic media (pH ~ 5.0; 37 °C) (Fig. 3).

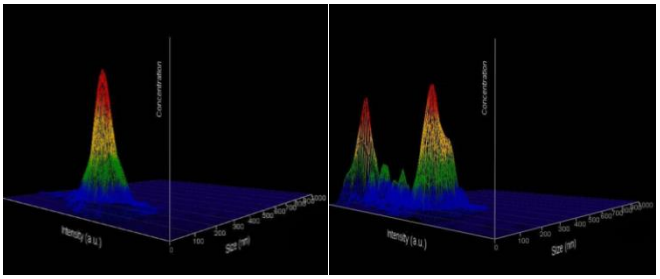

Fig. 3. Size distribution as obtained from NTA for the $MPEO_{44}$-b-PCL_{17} NPs after 72 h at pH ~ 7.4 (left) and pH ~ 5.0 (right).

NTA is a powerful tool and it is particularly valuable for the detection and accurate sizing of a broad range of population ratios because it simultaneously depicts the particles' size, concentration (number) and intensity distribution on the same measurement.[36,37] After 72 h of incubation, the results show the presence of only one peak at pH ~ 7.4 (Fig. 3, left) and the presence of several peaks at pH ~ 5.0 (Fig. 3, right) mostly located at lower and larger sizes. The broadening in particle size and size distribution as shown by NTA is an evidence of NPs disassembly and aggregation[16] over time, which is a result of the hydrolysis of the acid-labile ketal linkage.[28] The hydrolysis of the $MPEO_{44}$-*b*-PCL_{17} block copolymer was also characterized by SEC analysis (Fig. S3 red lines, ESI) and ^{13}C NMR spectroscopy (Fig. S4, ESI). Firstly the SEC chromatograms confirmed the hydrolysis due the appearance of peaks from the macromers around the region of the PEO macromer (Fig. S3 blue line, ESI). Secondly, the degradation was confirmed by ^{13}C NMR spectroscopy based on the disappearance of the carbon signal from the ketal group linker between the PEO and PCL blocks (Fig. S4, ESI). The hydrolysis of the ketal linker occurs at the interface between the PCL core and the PEO shell inside the NPs. The free hydrolyzed PEO chains are gradually released into the medium (smaller size peaks; Fig. 3, right). The particle aggregation (bigger size peaks; Fig. 3, right) is the result of the increased hydrophobicity of the particles due to the hydrolysis of the hydrophilic PEO macromer (see SEC and ^{13}C NMR Fig. S3 resp. Fig. S4).[28] It is important to note that no changes in the particle size distributions were observed for the $MPEO_{44}$-*b*-PCL_{17} block copolymer NPs, as observed by NTA and at pH ~ 7.4 during 72 hours, confirming that the particles are responsive to mild acidic conditions (pH ~ 5.0).

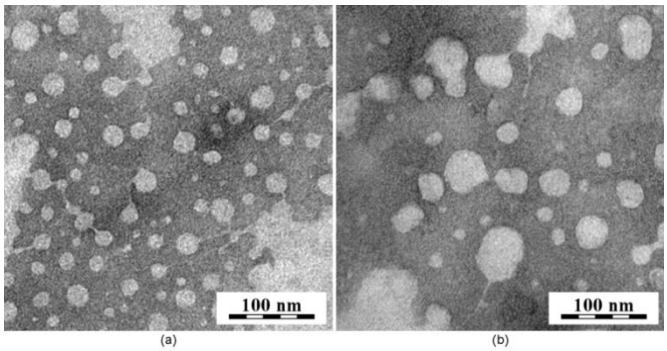

Fig. 4. TEM images of $MPEO_{44}$-*b*-PCL_{17} at pH ~ 7.4 (a) and pH ~ 5.0 (b) after 24 h incubation.

Similarly, the TEM images (Fig. 4) showed a comparable increase in the size of the $MPEO_{44}$-*b*-PCL_{17} block copolymer NPs at pH ~ 5.0 (Fig. 4b) when compared to the NPs at pH ~ 7.4 (Fig. 4a) after 24 hours. Subsequently, the release profile of the chemotherapeutic PTX was investigated under the same aforementioned conditions (pH ~ 5.0; 37 °C), which mimic the target acidic environment in endosomal and lysosomal compartments. The release experiments at 37 °C were conducted also at pH 7.4 to simulate conditions during transport in blood and in normal healthy tissues (Fig. 5). The drug release profile is clearly pH-sensitive. The results suggest that at pH ~ 5.0 the block copolymer NPs are activated and consequently destabilized physically (pH-triggered disassembly-aggregation, Fig. 3), thus accelerating the release of the drug. The drug cargo is released almost twice as efficiently (~ 70 % released) within 72 h at pH ~ 5.0 (mimicking intracellular environment) than at physiological conditions of pH ~ 7.4. On the other hand, at pH ~ 7.4, ~ 36 % of the drug loaded into the NPs cores is released.

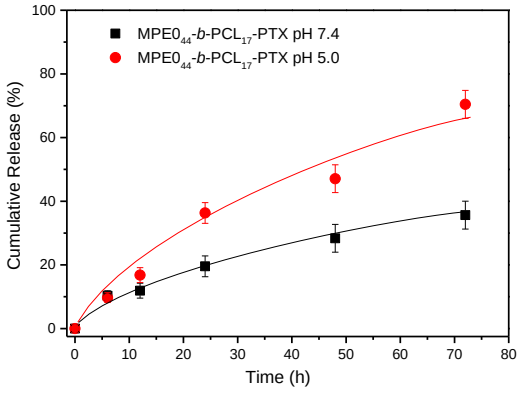

Fig. 5. Paclitaxel release profiles from $MPEO_{44}$-*b*-PCL_{17}-PTX NPs at pH 5.0 (●) and 7.4 (■).

The drug-release profile is considered not optimal; however, a yet faster release is expected in contact with more complex media such as the serum-supplied cell culture medium. To investigate the inhibitory effect on tumor cells, the $MPEO_{44}$-*b*-PCL_{17} NPs were loaded with the antitumor drug PTX with an overall cargo rate around 2.0 *wt*% (loading efficiency of 92 %, see Mat. and Methods). The cell viability assay was used to document *in vitro* cytotoxicity as a classical approach to evaluate the direct effect of the drug carrier NPs on target cancer cells. HeLa cell line was selected as a widely used and well-studied cancer cell model system. The drug-loaded NPs were incubated with the HeLa cells and the *in vitro* cytotoxicity after 24 h and 48 h of incubation was assessed by alamarBlue® assay. After 48 h incubation with the cells, the PTX-loaded $MPEO_{44}$-*b*-PCL_{17} NPs exhibited significantly stronger toxicity than the free drug (Fig. 6b). In contrast, the drug-free NPs showed only negligible cytotoxicity to the cancer cells (Fig. S5). This increased cytotoxicity of the drug-carrying NPs compared to the free drug is supposedly owed to endocytotic uptake;[38] at low drug concentrations (below 1 $\mu g \cdot ml^{-1}$, see Fig. 6b) the endocytotic uptake of the drug-loaded nanocarriers would be more efficient than the uptake of free drug into the cells. With increasing drug concentration this effect becomes less prominent (see Fig. 6b). Once internalized *via* endocytosis the PTX-loaded nanocarriers swiftly and efficiently release their cargo, when the enzymes and acidic conditions in endosomes trigger the cleavage of the pH-sensitive acyclic ketal bond.[39,40] Drug-free $MPEO_{44}$-*b*-PCL_{17} NPs were also tested up to the applied maximal concentration (0.67 $mg \cdot mL^{-1}$) with no significant cytotoxic activity (Fig. S5). Last but not least, the negligible toxicity of the unloaded-$MPEO_{44}$-*b*-PCL_{17} NPs emphasized that the presented nanocarrier system produces no toxic degradation products; and at any rate the products (PCL and PEO) are well known (FDA-approved) as environmentally friendly blocks.

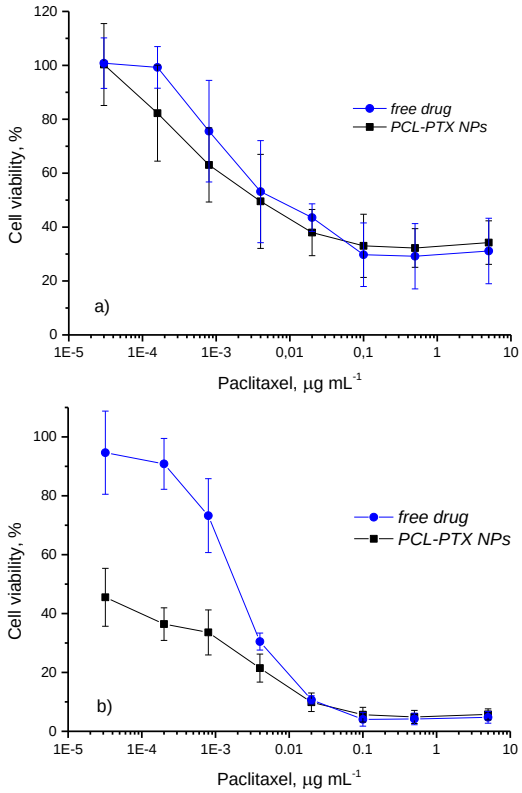

Fig. 6. Viability of HeLa cells after 24 h (a) and 48 h (b) of incubation with different concentrations of free PTX (blue circles) and PTX-loaded $MPEO_{44}$-*b*-PCL_{17} NPs (black squares).

Conclusions

In summary, well-defined nanoparticles prepared by the self-assembly of the new amphiphilic $MPEO_{44}$-*b*-PCL_{17} block copolymer in aqueous solution were presented. The NPs structure was characterized in detail by DLS, SLS, NTA and TEM. On decreasing pH the acid-labile ketal linker enabled the disassembly of the nanoparticles in a buffer that simulated the acidic environment in endosomal and lysosomal

compartments. As a result the chemotherapeutic paclitaxel was released and the polymer particles disintegrated into neutral degradation products as confirmed by SEC and ^{13}C NMR and by *in vitro* cell viability tests. In addition, the *in vitro* cell viability experiments demonstrated the great potential of the pH-triggered NPs as drug-delivery system in cancer therapy; the *in vitro* cytotoxicity studies showed an important increase in activity of the NP-loaded with drug and the free-drug NPs are degraded into well-known and FDA-approved by-products and itself introduces no toxicity to cells. The particle's hydrophilic surface coat and size below the cut-off size of the leaky pathological vasculature (NPs sizes < than 100 nm) predetermined the NPs for long circulation and efficient accumulation in solid tumours due to EPR effect and together with the ability to release a drug at the endosomal pH with concomitant high cytotoxicity makes them suitable candidates for cancer therapy.

Experimental section

Materials

Chemicals were purchased from Sigma-Aldrich at the highest purity and if not stated otherwise, were used as received.

Synthesis of *α*-methoxy-*ω*-hydroxy-poly(ethylene oxide) macromer containing a ketal group

The *α*-methoxy-*ω*-hydroxy-poly(ethylene oxide) macromere containing a ketal group was prepared as a macroinitiator through a "click" reaction between *α*-methoxy-*ω*-alkyne-PEO and 2-{[2-(2-azidoethoxy)propan-2-yl]ethan-1-ol. The azide-alkyne Huisgen cycloaddition was performed in the presence of CuI and Et_3N. The conversion of the "click" reaction was calculated from the relative intensities of the signals characteristic of both -O-C$(CH_3)_2$-O- (j + j', δ = 1.28 ppm) and –CH_2-O-C(O) (d, δ = 4.47 ppm) groups in the ^1H NMR spectrum, which gives a quantitative value of ~ 82 %.[28]

Synthesis of $MPEO_{44}$-*b*-PCL_{17} diblock copolymer containing a ketal group

The $MPEO_{44}$-*b*-PCL_{17} diblock copolymers were successfully synthesized by ROP from the ε-CL monomer. The previously synthesized *α*-methoxy-*ω*-hydroxy-poly(ethylene oxide) containing a ketal group (above) was used as a macroinitiator in the presence of $Sn(Oct)_2$ as catalyst. The PCL block length was controlled by regulating the ε-CL/macroinitiator molar ratio. After purification, the $MPEO_{44}$-*b*-PCL_{17} diblock copolymer was characterised using ^1H and ^{13}C NMR, and SEC analysis.[28]

Characterisation Techniques

^1H NMR and ^{13}C NMR spectra (300 and 75 MHz, respectively) were recorded using a Bruker Avance DPX 300 NMR spectrometer with $CDCl_3$ as the solvent at 25 °C. The chemical shifts are relative to TMS using hexamethyldisiloxane (HMDSO, δ = 0.05 and 2.0 ppm from TMS in ^1H NMR and ^{13}C NMR spectra) as the internal standard. The M_n of the synthesized macromers and final block copolymers were determined by ^1H NMR spectroscopy accordingly previously published.[28]

The M_n values of the macromer and of the block copolymer were determined by ^1H NMR spectroscopy. For the macromer, the M_n was calculated according to eqn (1):

$$M_{n(NMR)} = [(Ib/4)/(Ig/2)] \times 44 + 31 + 284 \quad (1)$$

where Ib and Ig represent the integral values of the peaks at δ = 3.63 ppm (–CH_2–CH_2–O– of the PEO repeating unit) and at δ = 2.76 ppm (–O–C(O)–CH_2–CH_2–CH_2–), respectively. The values 31 and 284 are the molecular weights of the two functional groups at the chain ends CH_3–O– and –O–C(O)–$(CH_2)_3$–triazole ring–$(CH_2)_2$–OC$(CH_3)_2$–O–$(CH_2)_2$–OH, respectively.

The M_n of the MPEO-*b*-PCL diblock copolymer was determined by ^1H NMR using eqn (2):

$$M_{n(NMR)}\,(\text{MPEO-}b\text{-PCL}) = [(Ir/2)/(Ib/4)] \times DPMPEO \times 114 + M_{n(NMR)}\,(\text{macroinitiator}) \quad (2)$$

where Ir and Ib represent the integral values of the methylene protons of PCL (r) (Fig. S2, top) and of the methylene protons of PEO (b). The value 114 is the molecular weight of the ε-CL unit, DPMPEO is the degree of polymerization of the macroinitiator, and $M_{n(NMR)}$ is the number-average molecular weight of the macroinitiator.

Nanoparticle preparation

A preheated (40 °C) acetone solution (2.0 mL) containing the $MPEO_{44}$-*b*-PCL_{17} block copolymer (5.0 mg) and the chemoterapeutic PTX (0.1 mg) was added drop-wise (EW-74900-00, Cole-Parmer®) into a pre-heated (40 °C) PBS solution (4 mL, pH ~ 7.4). The pre-formed NPs were allowed to self-assemble, and then the solvent was evaporated under reduced pressure. The final concentration was adjusted to 1 mg·mL^{-1} (NPs) using PBS at pH ~ 7.4. Given the high loading no further purification was carried out.[16,42]

Size exclusion chromatography (SEC)

The SEC analyses were performed using an SDS 150 pump (Watrex, Czech Republic) equipped with refractometric (Shodex RI-101, Japan) and UV (Watrex UVD 250, Czech Republic) detectors. The separation system consisted of two PLgel MIXED-C columns (Polymer Laboratories) and was calibrated with polystyrene standards (PSS, Germany). THF was used as the mobile phase at a flow rate of 1.0 mL·min^{-1} at 25 °C. Data collection and processing were performed using the Clarity software package.

Drug Loading and drug loading efficiency

The amount of the chemotherapeutic paclitaxel was determined according previously validated method.[16,42] PTX loaded into the NPs was measured by HPLC (Shimadzu, Japan) using a reverse-phase column Chromolith Performance RP-18e (100 × 4.6 mm, eluent water-acetonitrile with acetonitrile gradient 0 - 100 vol %, flow rate = 1.0 ml·min^{-1}). Firstly 100 µL of the drug-loaded NPs was collected from the bulk sample, filtered (0.45 µm) and diluted to 900 µL with

Acetonitrile (Lach-ner, Czech Republic). Such procedure led to NPs dissolution. Afterwards, 20 µL of the final sample was injected through a sample loop. PTX was detected at 227 nm using ultraviolet (UV) detection. The drug-loading content (*LC*) and the drug-loading efficiency (*LE*) were calculated by using the following equations:

$$LC\ (\%) = \frac{drug\ amount\ in\ nanoparticles}{mass\ of\ nanoparticles} x\,100 \quad (3)$$

$$LE\ (\%) = \frac{drug\ amount\ in\ nanoparticles}{drug\ feeding} x\,100 \quad (4)$$

Drug Release Experiments

The *in vitro* release of PTX from the block copolymer NPs was studied in pH-adjusted release media (pH ~ 7.4 and ~ 5.0) at 37 °C. Aliquots (500 µL) of drug loaded block copolymer micelles in PBS were loaded into 36 Slide-A-Lyzer MINI dialysis microtubes with MWCO 10000 (Pierce, Rockford, IL). These microtubes were dialyzed against 4 L of pH-adjusted PBS buffer gently stirred. The drug release experiments were done in triplicate. At each sampling time, it was removed three microtubes from the dialysis system and 300 µL from each microtube was sampled and diluted to 1.0 mL by using Acetonitrile (Lach-ner, Czech Republic). The PTX content at each sampling time was then determined *via* HPLC by applying the same procedure used to determine *LC* and *LE*.

Nanoparticle characterisation

The NPs were characterised using DLS, SLS and NTA. The DLS measurements were performed using an ALV CGE laser goniometer consisting of a 22 mW HeNe linear polarized laser operating at a wavelength (λ = 632.8 nm), an ALV 6010 correlator, and a pair of avalanche photodiodes operating in the pseudo cross-correlation mode. The samples were loaded into 10 mm diameter glass cells and maintained at 37 $\pm$ 1 °C. The data were collected using the ALV Correlator Control software and the counting time was 45 s. The measured intensity correlation functions $g_2(t)$ were analysed using the algorithm REPES (incorporated in the GENDIST program)[43] resulting in the distributions of relaxation times shown in equal area representation as τA(τ). The mean relaxation time or relaxation frequency ($\Gamma = \tau^{-1}$) is related to the diffusion coefficient (D) of the nanoparticles as $D = \frac{\Gamma}{q^2}$ where $q = \frac{4\pi n \sin\frac{\theta}{2}}{\lambda}$ is the scattering vector being n the refractive index of the solvent and θ the scattering angle. The hydrodynamic radius (R_H) or the distributions of R_H were calculated by using the Stokes-Einstein relation:

$$R_H = \frac{k_B T}{6\pi\eta D} \quad \text{(eq. 5)}$$

being k_B the Boltzmann constant, T the absolute temperature and η the viscosity of the solvent.

In the static light scattering (*SLS*), the scattering angle was varied from 30 to 150° with a 10° stepwise increase. The absolute light scattering is related to weight-average molar mass ($M_{w(NP)}$) and to the radius of gyration (R_G) of the nanoparticles by the Zimm formalism represented as:

$$\frac{K_c}{R_\theta} = \frac{1}{M_{w(NP)}}\left(1 + \frac{R_{Gq}^2}{3}\right) \quad \text{(eq. 6)}$$

where K is the optical constant which includes the square of the refractive index increment (dn/dc), R_θ is the excess normalized scattered intensity (toluene was applied as standard solvent) and c is the polymer concentration given in mg·mL^{-1}. The refractive index increment (dn/dc) of the MPEO$_{44}$-*b*-PCL$_{17}$ NPs in PBS (0.140 mL·g^{-1}) was determined using a Brice-Phoenix differential refractometer operating at λ = 632.8 nm.

The NTA analyses were performed using the NanoSight LM10 & NTA 2.0 Analytical Software (NanoSight, Amesbury, England). The samples were diluted (4000 x - Milli Q® water or PBS ~ 7.4 and ~ 5.0) and injected into the sample chamber with a syringe (25 °C). The NTA apparatus combines light scattering microscopy with a laser diode (635 nm) camera charge-coupled device, which allows viewing and recording of the NPs in solution. Each video clip was captured over 60 s. The NTA software is able to identify and track individual NPs (10 - 1000 nm), which are in Brownian motion, and relate this particle movement to a sphere with an equivalent R_H, as calculated using the Stokes-Einstein relation (eq. 5).

Cell Culture and *in vitro* experiments

The HeLa cells were cultivated in Dulbecco's Modified Eagle's Medium (DMEM) supplemented with 10% fetal calf serum, 100 units of penicillin and 100 µg·mL^{-1} of streptomycin (Life Technology, CZ). The cells were grown in a humidified incubator at 37 °C with 5 % CO_2. For the cytotoxicity assay, 5000 cells per well were seeded in duplicates in 96 flat bottom well plates in 100 µL of media 24 h before adding the NPs. For adding of the particles the volume was calibrated to 80 µL, and 20 µL of the 5-times concentrated dilution of PTX or particle dispersion were added per well to a final PTX concentration ranging from 10^{-5} to 5 µg·mL^{-1}. All dilutions were made in full incubation medium under thorough mixing of each dilution step. The sample concentrations of the PTX-loaded particles were adjusted to contain the same total amount of PTX as the samples with free PTX. The cells were incubated with free drug or NPs for 24 h or 48 h. Then 10 µL of alamarBlue® cell viability reagent (Life Technologies, Czech Republic) were added to each well and incubated a minimum for 3 h at 37 °C. The fluorescence of the reduced marker dye was read with a Synergy H1 plate reader (BioTek Instruments, US) at excitation 570 and emission 600 nm. The fluorescence intensity of the control samples (with no drug or particles added) was set as a marker of 100 % cell viability. The fluorescence signal of "0% viability samples" (where all cells were killed by addition of hydrogen peroxide) was used as background and subtracted from all values prior to calculations. The non-toxic character of the blank particles without drug was shown by incubation of cells up to 0.67 mg·L^{-1} of blank particles. This

corresponds to the amount of polymer that is contained in the samples of drug-loaded particles with 5 $\mu g \cdot L^{-1}$ total PTX content. For the cell experiments the PTX-dilutions in incubation medium were made from a PTX stock solution of 120 $\mu g \cdot mL^{-1}$ in PBS/DMSO (96.5 : 3.5 *v*/*v*).[41] Precipitation of the hydrophobic PTX out of the cell culture medium can therefore be excluded because the PTX was previously fully dissolved in a PBS/DMSO solution (96.5 : 3.5 *v*/*v*) and subsequently diluted in the serum-supplied medium under thorough mixing. Consequently, even at maximal PTX-concentration of 5 $\mu g \cdot mL^{-1}$, the final DMSO concentration in the incubation medium was below 0.2% and therefore no effect on cell vitality in the applied setup.[42,44] All the cells experiments are average of at least 4 measurements ($n \geq 4$).

Acknowledgements

This research was supported by the Norwegian Financial Mechanism 2009-2014 under Project contract no 7F14009. C. G. Venturini acknowledges the Program Science Without Borders CAPES/Brazil (Process number 2293/13-7).

References

1 Y.-Y. Won, H.T. Davis, F.S. Bates, *Science* 1999, **283**, 960.
2 E. Penott-Chang, A. Walther, P. Millard, A. Jãger, E. Jãger, A.H.E Müller, S.S. Guterres, A.R. Pohlmann, *J. Biomed. Nanotechnol*., 2012, **8**, 1.
3 E. Busseron, Y. Ruff, E. Moulin, N. Giuseppone, *Nanoscale* 2013, **5**, 7098.
4 R. Šachl, M. Uchman, P. Matějíček, K. Procházka, M. Štěpánek, M. Špírkova, *Langmuir* 2007, **6**, 3395.
5 A.H. Gröschel, F.H. Schacher, H. Schmalz, O.V. Borisov, E.B. Zhulina, A. Walther, A.H.E. Müller, *Nat. Commun*., 2012, **3**, 1.
6 N. Suthiwangcharoen and R. Nagarajan, *RSC Adv*., 2014, **4**, 10076.
7 A. Choucair and A. Eisenberg, *Eur. Phys. J. E*., 2003, **10**, 37.
8 N. Yeole, S. N. Raju Kutcherlapati, T. Jana, *RSC Adv*., 2014, **4**, 2382.
9 X.-B. Xiong, A. Falamarzian, S.M. Garg, A. Lavasanifar, *J. Control. Release* 2011, **155**, 248.
10 W. Shao, K. Miao, H. Liu, C. Ye, J. Du, Y. Zhao, *Polym. Chem*., 2013, **4**, 3398.
11 Y. Ymamoto, Y. Nagasaki, Y. Kato, Y. Sugiyama, K. Kataoka, *J. Control. Release* 2001, **77**, 27.
12 Hrubý, M., Etrych, T., Kučka, J., Forsterová, M., Ulbrich, K. *J. Appl. Pol. Sci*., 2006, **101**, 3192.
13 H-J. Li, H-X. Wang, C-Y. Sun, J-Z. Du, J. Wang, *RSC Adv*., 2014, **4**, 1961.
14 M.I. Gibson and R.K. O'Reilly, *Chem. Soc. Rev*., 2013, **42**, 7204.
15 D. Jeanmaire, J. Laliturai, A. Almalik, P. Carampin, R. d'Arcy, E. Lallana, R. Evans, R.E.P. Winpenny, N. Tirelli, *Pol. Chem*., 2014, **5**, 1393.
16 F.C. Giacomelli, P. Stepánek, C. Giacomelli, V. Schmidt, E. Jãger, A. Jãger, K. Ulbrich, *Soft Matter*, 2011, **7**, 9316.
17 Y. Wang, K. Zhou, G. Huang, C. Hensley, X. Huang, X. Ma, T. Zhao, B.D. Sumer, R.J. DeBerardinis, J. Gao, *Nat. Mater*. 2013, **12**, 991.
18 I. F. Tannock and D. Rotin, *Cancer Res*., 1989, **49**, 4373.
19 H. Yin, E. S. Lee, D. Kim, K. H. Lee, K. T. Oh and Y. H. Bae, *J. Control. Release* 2008, **126**, 130.
20 E.S. Lee and Y.H. Bae. *J. Control. Release* 2008, **132**, 164.
21 S. Sengupta, D. Eavarone, I. Capila, G. Zhao, N. Watson, T. Kiziltepe, R. Sasisekharan, *Nature* 2005, **436**, 568.
22 M. Hrubý, C. Koňak, K. Ulbrich, *J. Control. Release* 2005, **103**, 130.
23 V. Toncheva, E. Schacht, S.Y. Ng, J. Barr, J. Heller, *J. Drug Target*. 2003, **11**, 345.
24 B. Wang, C. Xu, J. Xie, Z. Yang, S. Sun, *J. Am. Chem. Soc*., 2008, **130**, 14436.
25 M.J. Heffernan and N. Murthy, *Bioconjugate Chem*., 2005, **16**, 1340.
26 S.D. Khaja, S. Lee, N. Murthy, *Biomacromolecules* 2007, **8**, 1391.
27 J. Siepmann and A. Göpferich, *Adv. Drug Del. Rev*., 2001, **48**, 229.
28 S. Petrova, E. Jäger, R. Konefal, A. Jäger, C.G. Venturini, J. Spěváček, E. Pavlova, P. Štěpánek, *Pol. Chem*., 2014, **5**, 3884.
29 S. Petrova, I. Kolev, S. Miloshev, M.D. Apostolova, R. Mateva, *J. Mater. Sci.: Mater. Med*., 2012, **23**, 1225.
30 J. Nicolas, S. Mura, D. Brambila, N. Mackiewicz, P. Couvreur, *Chem. Soc. Rev*., 2013, **42**, 1147.
31 J. Wu and C-C. Chu, *Acta Biomater*., 2012, **8**, 4314.
32 J. Rieger, P. Dubois, R. Jérôme, C. Jérôme, *Langmuir* 2006, **22**, 7471.
33 N. Kumar, M.N.V. Ravikumar, A.J. Domb, *Adv. Drug Deliv. Rev*., 2001, **53**, 23.
34 C.A. de Castro, B. Mattei, K.A. Riske, E. Jäger, A. Jäger, P. Stepánek, F.C. Giacomelli, *Langmuir* 2014, **30**, 9770.
35 H. Cabral, Y. Matsumoto, K. Mizuno, Q. Chen, M. Murakami, M. Kimura, Y. Terada, M. R. Kano, K. Miyazono, M. Uesaka, N. Nishiyama, K. Kataoka, *Nat. Nanotechnol*., 2011, **6**, 815.
36 V. Filipe, A. Hawe, W. Jiskoot, *Pharm. Res*., 2010, **27**, 796.
37 A.E. James and J.D. Driskell, *Analyst* 2013, **138**, 1212.
38 D. Li, Y. Zhang, S. Jin, J. Guo, H. Gao, C. Wang, *J. Mater. Chem. B*., 2014, 2, 5187.
39 G. Sahay, D.Y. Alakhova, A.V. Kabanov, *J. Control. Release* 2010, **145**, 182.
40 G.L. Li, J.Y. Liu, Y. Pang, R.B. Wang, L.M. Mao, D.Y. Yan, X.Y. Zhu, *Biomacromolecules* 2011, **12**, 2016.
41 E.A. Dubikovskaya, S.H. Thorne, T.H. Pillow, C.H. Contag, P.A. Wender, *Proc. Natl. Acad. Sci. U.S.A* 2008, **105**, 12128.
42 A. Jäger, E. Jäger, F. Surman, A. Höcherl, B. Angelov, K. Ulbrich, M. Dreschler, V.M. Garamus, C. Rodriguez-Emmenegger, F. Nallet, P. Štěpánek. *Pol. Chem*., 2015, DOI:10.1039/C5PY00567A.
43 J. Jakes, *Czech. J. Phys*., 1988, **38**, 1305.
44 A. B. Trivedi, N. Kitabatake, E. Do. *Agr. Biol. Chem*., 1990, **54**, 2961.

Polymer Chemistry

PAPER

View Article Online
View Journal | View Issue

Cite this: *Polym. Chem.*, 2015, **6**, 4946

Nanoparticles of the poly([*N*-(2-hydroxypropyl)]-methacrylamide)-*b*-poly[2-(diisopropylamino)ethyl methacrylate] diblock copolymer for pH-triggered release of paclitaxel†

Alessandro Jäger,*[a,e] Eliézer Jäger,*[a,e] František Surman,[a] Anita Höcherl,[a] Borislav Angelov,[a] Karel Ulbrich,[a] Markus Drechsler,[b] Vasil M. Garamus,[c] Cesar Rodriguez-Emmenegger,*[a] Frédéric Nallet[d] and Petr Štěpánek[a]

Received 17th April 2015,
Accepted 29th May 2015

DOI: 10.1039/c5py00567a

www.rsc.org/polymers

The potential of self-assembled nanoparticles (NPs) containing the fine tunable pH-responsive properties of the hydrophobic poly[2-(diisopropylamino)ethyl methacrylate] (PDPA) core and the protein repellence of the hydrophilic poly[*N*-(2-hydroxypropyl)methacrylamide] (PHPMA) shell for *in vitro* cytostatic activity has been explored on cancer cells. The amphiphilic diblock copolymer poly[*N*-(2-hydroxypropyl)methacrylamide]-*b*-poly[2-(diisopropylamino)ethyl methacrylate] (PHPMA-*b*-PDPA) synthesized by a reversible addition–fragmentation chain transfer (RAFT) technique allows for excellent control of the polymer chain length for methacrylamides. The PHPMA-*b*-PDPA block copolymer dissolved in an organic solvent (ethanol/dimethylformamide) undergoes nanoprecipitation in phosphate buffer saline (PBS, pH ~ 7.4) and self-assembles into regular spherical NPs after solvent elimination. The NPs' structure was characterized in detail by dynamic (DLS), static (SLS) and electrophoretic (ELS) light scattering, small angle X-ray scattering (SAXS), and cryo-transmission electron microscopy (cryo-TEM). The PHPMA chains prevented the fouling of proteins resulting in a remarkable stability of the NPs in serum. On decreasing pH the hydrophobic PDPA block becomes protonated (hydrophilised) in a narrow range of pH ($6.51 < pH < 6.85$; $\Delta pH \sim 0.34$) resulting in the fast disassembly of the NPs and chemotherapeutic drug release in a simulated acidic environment in endosomal and lysosomal compartments. A minimal amount of drug was released above the threshold pH of 6.85. The *in vitro* cytotoxicity studies showed an important increase in the activity of the NPs loaded with drug compared to the free drug. The particle's size below the cut-off size of the leaky pathological vasculature (less than 100 nm), the excellent stability in serum and the ability to release a drug at the endosomal pH with concomitant high cytotoxicity make them suitable candidates for cancer therapy, namely for treatment of solid tumours exhibiting high tumor accumulation of NPs due to the Enhanced Permeability and Retention (EPR) effect.

Introduction

A great deal of attention has been paid to block copolymers that when exposed to an aqueous environment self-assemble into highly organised nanoscale structures.[1,2] By changing the solvent selectivity or the insoluble-to-soluble block length ratio, one obtains thermodynamically favoured structures of various morphologies in solution.[3] Typical morphologies such as spheres, rods, lamellae and vesicles (polymersomes) can be easily prepared in a controlled manner in aqueous solutions through the self-assembly of asymmetric amphiphilic diblock copolymers.[4] Characterised by a bulky core and a relatively thin corona, the particles made by the self-assembly of highly asymmetric diblocks are frozen structures and do not dissociate under dilution.[5] Some of these structures such as

[a]*Institute of Macromolecular Chemistry v.v.i., Academy of Sciences of the Czech Republic, Heyrovsky Sq. 2, 162 06 Prague 6, Czech Republic. E-mail: ajager@imc.cas.cz, jager@imc.cas.cz, rodriguez@imc.cas.cz*
[b]*Laboratory for Soft Matter Electron Microscopy, Bayreuth Institute of Macromolecular Research, University of Bayreuth, D-95440 Bayreuth, Germany*
[c]*Helmholtz-Zentrum Geesthacht, Centre for Materials and Coastal Research, D-21502 Geesthacht, Germany*
[d]*Centre de Recherche Paul-Pascal, CNRS, Université de Bordeaux, 115 Avenue Schweitzer, F-33600 Pessac, France*
[e]*Department of Physical and Macromolecular Chemistry, Faculty of Science, Charles University in Prague, Albertov 2030, 128 40 Prague 2, Czech Republic*
†Electronic supplementary information (ESI) available. See DOI: 10.1039/c5py00567a

spheres and vesicles have attracted attention as versatile carriers for drug delivery.[6,7] They present improved colloidal stability under physiological conditions when compared to water soluble amphiphilic micelles and possess the ability to encapsulate or integrate a broad range of drugs. However, several problems arise related to the slow drug release if the drug is encapsulated in frozen colloidal particles, especially for applications such as drug release in cancer therapy. For an optimal therapy the hydrophobic guest drug molecules have to be seized into the inner particle core during circulation in the bloodstream and be quickly released at the specific tumour sites.[8] Recently, several types of pH-sensitive polymeric NPs have been investigated for such purposes[9,10] because the extracellular pH in most solid tumour tissues is more acidic (ranging from pH 6.7 to 7.1),[11,12] compared to the normal tissues (buffered at pH 7.4). Furthermore, variations in pH are also encountered when nanoparticles are internalized by cells *via* endocytosis, where the pH usually drops to as low as 5.0–6.0 in endosomes and 4.0–5.0 in lysosomes.[13]

For such a challenging task, taking into account the small pH window (ΔpH $\sim$ 0.4) in which the drug must be released, the 2-(diisopropylamino)ethyl methacrylate (DPA) based copolymers have recently proven to be valuable tools capable of fine tuning the release in the desired pH region, both *in vitro*[14] and *in vivo*[15] and quickly release the drug independently of its hydrophobicity[16] or hydrophilicity.[17] Nevertheless, regardless of the efficiency of the trigger mechanism involved in the drug release towards a successful cancer therapy, the nanocarrier must reach the tumor tissue first. However, nanoparticles in contact with the blood stream are rapidly coated with a corona of proteins which can impair the colloidal stability or can cause the particles to be eliminated *via* phagocytosis. This can only be circumvented by engineering the nanocarrier system to be "stealth" with a low particle size (between 10 and 100 nm) and having a sufficiently long circulation time to undergo passive specific accumulation in the tumor tissue through the EPR effect.[18] Recently published results from our group have demonstrated that unlike poly(ethylene glycol) PEG,[19] brushes of poly[*N*-(2-hydroxypropyl)methacrylamide] (PHPMA) withstand the fouling from blood plasma[20] and full blood.[21] The unmatched performance of PHPMA was also utilized to improve the circulation of hydrophobic nanoparticles with PHPMA-modified surfaces *in vitro*[22] and *in vivo.*[23]

Herein, for the first time, the potential of self-assembled NPs containing the fine tunable pH-responsive properties of the hydrophobic poly[2-(diisopropylamino)ethyl methacrylate] (PDPA) core and protein repellence of the hydrophilic PHPMA shell on *in vitro* cytostatic activity tested on cancer cells are reported. A diblock copolymer composed of hydrophobic PDPA and hydrophilic PHPMA was prepared by RAFT polymerisation. Poly[*N*-(2-hydroxypropyl)methacrylamide]-*b*-poly[2-(diisopropylamino)ethyl methacrylate] ($PHPMA_{25}$-*b*-$PDPA_{106}$) assembled forming nanoparticles. The novel NPs' self-assembly and structure were characterized in detail by cryo-TEM, SAXS, DLS, SLS and ELS light scattering techniques. Acidic physiological conditions trigger the disassembly of the novel NPs prepared from the block copolymer $PHPMA_{25}$-*b*-$PDPA_{106}$, thus controlling the release of their cargo, the chemotherapeutic paclitaxel (PTX), which results in a high cytostatic effect on HeLa cancer cells in *in vitro* studies.

Results and discussion

The block copolymer was prepared using RAFT polymerisation. A first block of PHPMA, (M_n = 3600 g mol^{-1}, M_w/M_n = 1.07; Scheme 1, Fig. S1 and S2†) was synthesised and used as a macro chain transfer agent. Subsequently a long second block of PDPA (M_n = 26 200 g mol^{-1}, M_w/M_n = 1.29) was grown from the macroCTA also by RAFT. RAFT polymerisation accounts for excellent living characteristics in the polymerization of methacrylamides. The block copolymer comprising a hydrophobic block (PDPA) and a hydrophilic block (PHPMA) favours the formation of stable NPs with a bulky core capable of encapsulating and controlling the release of the hydrophobic chemotherapeutic PTX.

The hydrophilic corona of PHPMA was utilized to protect the hydrophobic core from adsorption of proteins from blood (*vide infra*). An abrupt change in the light scattering intensity was observed during the titration experiments of the $PHPMA_{25}$-*b*-$PDPA_{106}$ diblock copolymer in aqueous solution simulating physiological conditions. The hydrophobic DPA block is protonated (hydrophilised) in a narrow range of pH (6.51 < pH < 6.85; ΔpH $\sim$ 0.34, Fig. 1a).

The markedly narrow window of pH at which the diblock copolymer (namely DPA block) can be protonated and the large change in scattering intensity and hydrodynamic diameter suggest that pH is a remarkably effective and precise trigger for assembly and disassembly of the system. The NPs were prepared by the solvent-shifting method, whereby the $PHPMA_{25}$-*b*-$PDPA_{106}$ block copolymer was dissolved in ethanol or dimethylformamide (concentration $\sim$ 1 mg mL^{-1}) and phosphate buffer saline (PBS, pH $\sim$ 7.4) was added dropwise to the organic solution under stirring until the aqueous weight fraction reached twice the weight of the organic phase. The organic solvent was removed by dialysis or evaporated under reduced pressure. DLS measurement of the diblock copolymer (before NP formation)

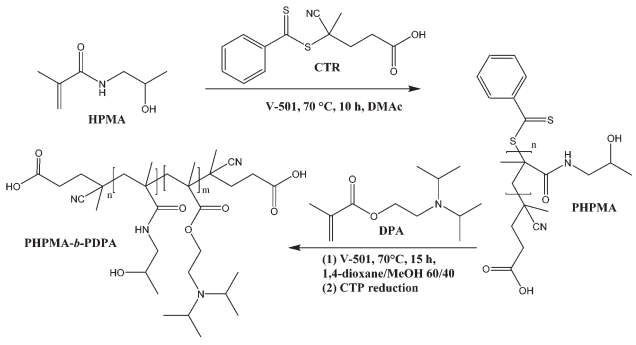

Scheme 1 Synthetic route and molecular structure of the $PHPMA_{25}$-*b*-$PDPA_{106}$ block copolymer with pH-triggered assembly/disassembly.

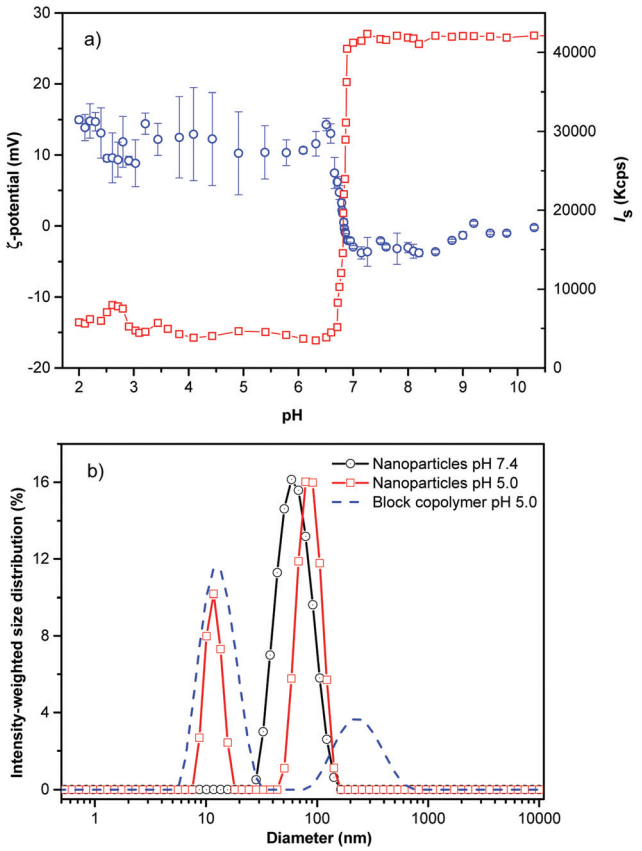

Fig. 1 (a) Zeta potential values (black circles) and overall scattering intensity (red squares) as a function of pH for the $PHPMA_{25}$-*b*-$PDPA_{106}$ block copolymer and (b) intensity-weighted size distribution for the $PHPMA_{25}$-*b*-$PDPA_{106}$ NPs at pH 7.4 (black circles), for the nanoparticles at pH 5.0 (red squares) and the single block copolymer at pH 5.0 (blue dashed lines) and 173° angle at a concentration of 1 mg mL^{-1} diluted in PBS at 37 °C.

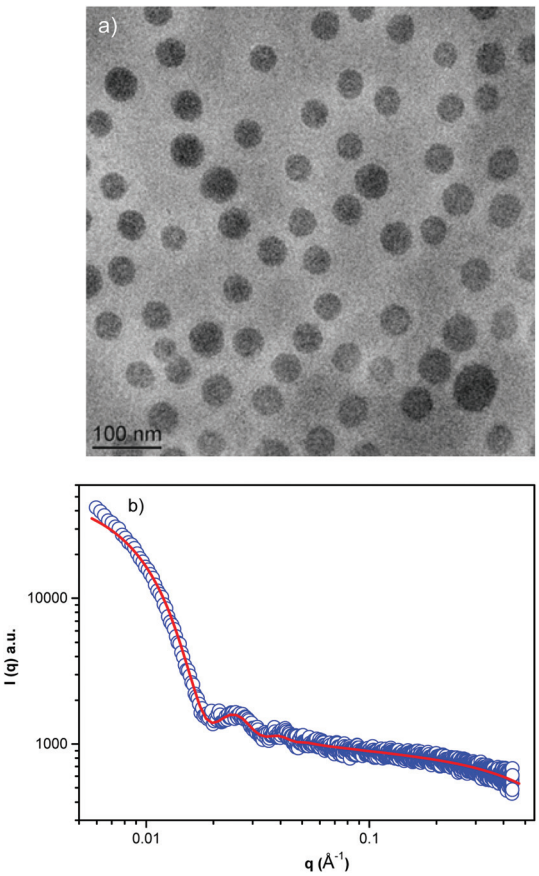

Fig. 2 Cryo-TEM image of the block copolymer NPs (a) and (b) small angle X-ray scattering profile in PBS, pH 7.4.

at pH 5.0 shows that most chains were fully dissolved with an average hydrodynamic diameter of $2R_H$ = 9.0 nm (Fig. 1b).

After PBS addition and solvent evaporation, the DLS shows a monomodal average size distribution referred to as the NPs' population ($2R_H$ = 52 nm, Fig. 1b, black circles) with low dispersity as was estimated by using the cumulant analysis (μ^2/Γ^2 = 0.120 ± 0.009), and as observed by Cryo-TEM (Fig. 2a). At pH 7.4 (PBS buffer) the average ζ-potential for the studied block copolymer nanoparticles is close to neutrality (~−2.5 mV) (Fig. 1a). Decreasing the pH below the pK_a (DPA) (6.51 < pH < 6.85), the system is rapidly protonated as evidenced by the positive ζ-potential, and mainly composed of molecularly dissolved block copolymer chains, besides a very small number of large aggregates (R_H ~ 125 nm). These aggregates represent about 25% of the intensity-weighted distribution, thus following the relationship $I_{sc} \sim cR^3$ the number of large particles can be calculated to be 0.0025% of the total number of objects scattering light in the system[16] (Fig. 1b). This negligible number of aggregates can be clearly visualized in the volume-weighted distribution of R_H shown in Fig. S5.†

Cryo-TEM images obtained at pH 7.4 reveal well-defined spherical NPs (Fig. 2a). The SAXS profile of the $PHPMA_{25}$-*b*-$PDPA_{106}$ block copolymer NPs (Fig. 2b) indicates the presence of flexible polymer chains described by Gaussian statistics at the outermost layer of the particles as evidenced in the high-*q* range profile corresponding to the PHPMA chains. These chains are, however, not visible in the Cryo-TEM image (Fig. 2a) due to poor contrast. To model the SAXS profile we utilized a superposition of Gaussian chains as the background and spherical nanoparticles:

$$I(q) \sim K^2(q, R, \Delta\eta) + \text{background}, \quad (1)$$

where

$$K(q, R, \Delta\eta) = \frac{4}{3}\pi R^3 \Delta\eta 3 \frac{\sin(qR) - qR\cos(qR)}{(qR)^3} \quad (2)$$

is the scattering from spherical NPs of radius R, $\Delta\eta$ is the difference between the scattering length density of the polymer and the solvent. A similar model was used previously to describe diverse systems.[23–25] The obtained nanoparticle radius R ~ 23 nm (diameter = $2R_H$ = 46 nm) is in good agreement with the DLS and Cryo-TEM data. Similarly, SLS measurements of NPs at pH = 7.4 (Fig. S3†) show R_G = 24 nm and $M_w \sim 1.2 \times 10^6$ g mol^{-1}.

The R_G/R_H ratio obtained by SLS and DLS data, gave access to the structural characteristics of the particles. It is well established that the NPs' R_G/R_H ratio values of 0.775, 1.78, and ≥2 have been reported for hard spheres, random coils and rod-like structures, respectively.[16,22,23,26] Furthermore, the R_G/R_H ratio of spherical objects depends on their inner structure and compactness, being close to 0.775 for compact spheres, 0.8–0.9 for block copolymer micelles due to solvation phenomena and 1.0 for hollow spheres and vesicles.[16,23,26] The R_G/R_H ratio found for the $PHPMA_{25}$-*b*-$PDPA_{106}$ NPs (R_G/R_H ~ 0.92) indicates that the particles had a core–shell-like structure.[16,27] Therefore, the most probable structural arrangement of the $PHPMA_{25}$-*b*-$PDPA_{106}$ NPs is a particle composed of a PDPA core surrounded by a PHPMA shell. These findings are in agreement with the SAXS measurements, which identify polymer chains with the Gaussian configuration at the outer region of the NPs. Furthermore, aggregation numbers with the same order of magnitude (~46 chains per particle) were also found for particles with such a structural composition.[16,24,27]

The efficient NP accumulation in the solid tumor tissue requires an extended circulating capability to enable a time-dependent extravasation of the NPs through the leaky tumor microvasculature (EPR effect). Therefore, long-term stability of the NPs in serum is a pre-requisite for the use of polymer NPs *in vivo*.[23,28,29] As a model of the possible detrimental interaction of the nanoparticles with proteins from blood, we incubated them in human plasma (10% in PBS). The stability of the NPs was monitored by evaluating any possible changes in their hydrodynamic size and scattering intensity over time.[23,26,29] Fig. 3a shows the temporal stability of the NPs in diluted human blood plasma as a function of the incubation time.

The size and scattering intensity patterns of the NPs do not change within the studied 36 h suggesting that the NPs are stable in the simulated but highly challenging media. The high stability of the NPs is based on their hydrophilic shell nature, improved colloidal stability and their unmatched resistance to protein adsorption.[16,20,29] By preventing any adsorption of proteins the NPs are virtually "invisible" in the blood milieux, which makes them a promising system for *in vivo* applications.[23,29–31]

Subsequently, the release profile of the chemotherapeutic PTX was investigated under conditions mimicking the acidic environment in endosomal and lysosomal compartments, pH ~ 5.0 and 37 °C. The release experiments at 37 °C were also conducted at pH 7.4 to simulate conditions during transport in blood and in normal healthy tissues (Fig. 3b). The drug release profile is clearly pH-sensitive in accordance with the physico-chemical studies presented above.

The results suggest that at pH ~ 5.0 (acidic environment in endosomal and lysosomal compartments) the block copolymer becomes protonated to form a polycation. The Coulombic repulsion among the chains disrupts the NPs which physically disassemble (pH-triggered disassembly, Fig. 1 and 3b), thus resulting in a 3.5 fold acceleration of the rate of release of the chemotherapeutic (~70%) within 24 h, (pH ~ 5.0) compared to physiological conditions (PBS). Moreover, ~21% of the drug

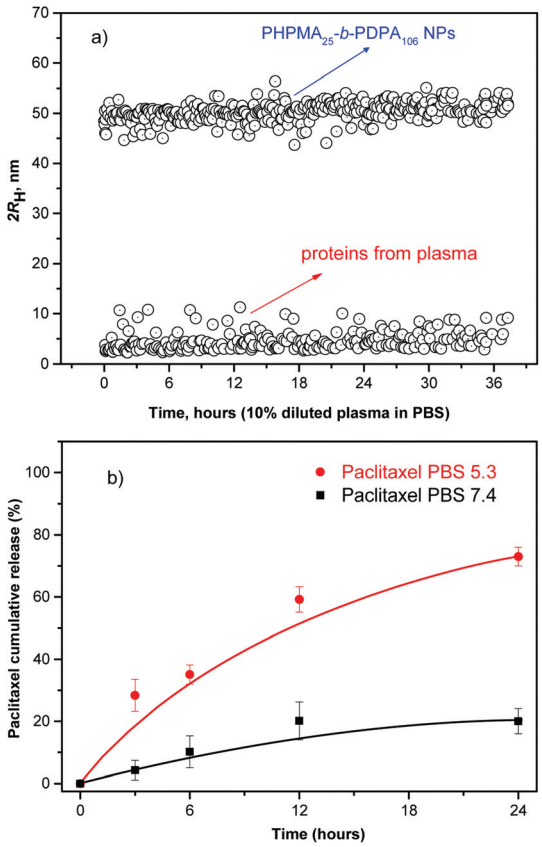

Fig. 3 (a) Size distribution in dissolved human plasma (10% v/v in PBS) for the $PHPMA_{25}$-*b*-$PDPA_{106}$ block copolymer NPs as a function of the incubation time and (b) drug release profiles from paclitaxel-loaded $PHPMA_{25}$-*b*-$PDPA_{106}$ block copolymer NPs at pH 7.4 (PBS, closed black squares) simulating transport in blood and at pH 5.3 (PBS, closed red circles) simulating the acidic environment in endosomal and lysosomal compartments at 37 °C.

was released from the intact NP cores when kept in PBS at pH 7.4. The release data demonstrate that during the systemic circulation minimal quantity of the drug would be released before reaching the solid tumor environment *via* the EPR effect. Conversely, the chemotherapeutic is readily released at pH 5.0 with ~70% of the loaded anticancer drug released within the first 24 h fulfilling the criteria[32] for a pH-triggered drug release mechanism exhibiting practical application as nanocarriers in passive tumor-targeted drug delivery.

To investigate the inhibitory effect on tumor cells, the pH-triggered $PHPMA_{25}$-*b*-$PDPA_{106}$ NPs were loaded with the anti-tumor drug PTX with an overall cargo rate around 2.5 wt% and a loading efficiency of 96% (see the Materials section and Methods section). Given the high loading (negligible free PTX) no further purification was carried out. The cell viability assay using alamarBlue® was used to examine the *in vitro* cytotoxicity as a classical approach to evaluate the direct effect of the drug-loaded NPs on target cancer cells. The HeLa cell line was selected as a widely used and well-studied cancer cell model system. The drug-loaded NPs were incubated with the HeLa

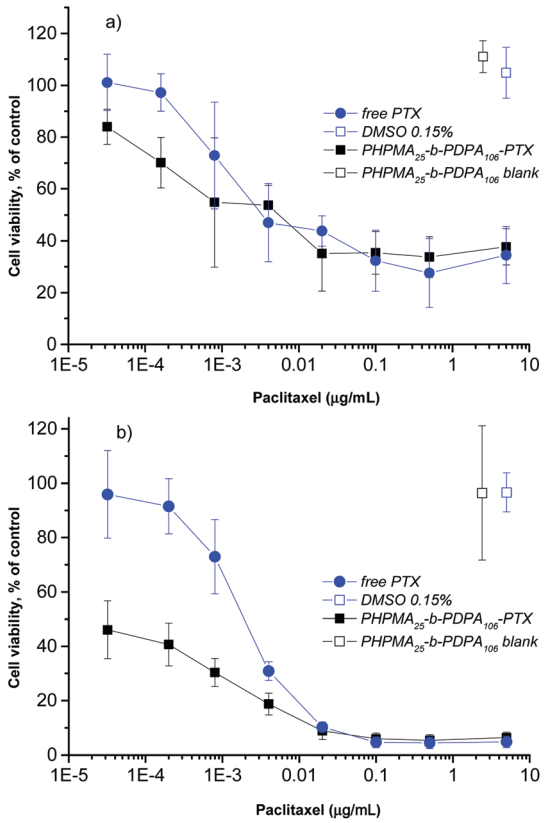

Fig. 4 Cell viability of HeLa cell line after 24 h (a) and 48 h (b) incubation with different concentrations of free PTX (closed blue circles) and PTX-loaded $PHPMA_{25}$-*b*-$PDPA_{106}$ (closed black squares) NPs. DMSO 0.15% (open blue squares) and blank $PHPMA_{25}$-*b*-$PDPA_{106}$ NPs (open black squares) were used as controls.

cells for 24 and 48 h. The *in vitro* cell viability experiments demonstrated that the PTX-loaded-$PHPMA_{25}$-*b*-$PDPA_{106}$ NPs exhibited a similar if not slightly stronger cytotoxic effect compared to the free drug after 24 h of incubation (Fig. 4a). After incubation over 48 h the superior toxicity of the PTX-loaded-$PHPMA_{25}$-*b*-$PDPA_{106}$ NPs compared to free PTX is clearly visible (Fig. 4b). The NPs (IC_{50} 0.1 ng mL^{-1}) exhibited significantly higher cytotoxicity than the free PTX (IC_{50} 1.7 ng mL^{-1}), which corresponds to the values stated in the literature for HeLa cells.[33,34] This increased cytotoxicity of the drug-carrying NPs compared to the free drug has been previously reported for analogous systems[35–39] and is supposedly the result of enhanced endocytotic uptake of NPs. In particular at low drug concentrations and higher incubation times (below 0.005 µg mL^{-1}, Fig. 4b), the endocytotic uptake of the PTX-loaded NPs is more efficient than the uptake of free drug into the cells.[36] A strong toxicity of the drug-loaded NPs after 48 h incubation correlates with the hypothesis that a significant amount of particles is already internalized in endosomal compartments within the first 24 h and that this is closely followed by a fast release of the drug (within 24 h approx. 70% of the drug was released under acidic conditions mimicking the conditions in endosomal and lysosomal compartments, see Fig. 3b). Drug-free $PHPMA_{25}$-*b*-$PDPA_{106}$ NPs were also tested up to the applied maximal concentration (0.4 mg mL^{-1}) with no significant cytotoxic activity (Fig. 4a and b, Fig. S4A and S4B†). After disassembly of the nanoparticles (pH < pK_a), the freely dissociated $PHPMA_{25}$-*b*-$PDPA_{106}$ chains present protonated amine groups to the cell. The toxicity of protonated amine groups has been described previously.[40] This may contribute to the high toxicity of the presented system. However, the data clearly showed evidence that the drug-free $PHPMA_{25}$-*b*-$PDPA_{106}$ particles have no relevant observable toxic effect on the cells (Fig. 4a and b, Fig. S4A and S4B†). Therefore the high efficiency of the drug delivery system is purely attributed to the efficient transport and release of the drug, and side effects of material toxicity can be excluded. It is important to highlight that the extracellular pH differences between the tumoral tissues and the healthy tissues are not just a characteristic of tumors but also ischemia, inflammation, renal failure or chronic obstructive pulmonary diseases that also share similar pH differences to their healthy counterparts. Therefore the HPMA-*b*-PDPA copolymer NPs may also find applications as drug carriers for their treatment.

Conclusions

In summary a diblock copolymer of PHPMA and PDPA was prepared by RAFT polymerisation. The diblock copolymer was assembled into spherical NPs consisting of a core of PDPA and a corona of PHPMA as evidenced by SLS, cryo-TEM and SAXS. Presumably, the PHPMA chains prevented the fouling of proteins resulting in a remarkable stability in serum. The reduction of the pH below 6.85 resulted in a rapid increase in the zeta-potential and the fast disassembly of the particles (size decrease in DLS). This was exploited as a trigger for the delivery of hydrophobic drugs into cancer cells. A minimal amount of drug was released above the threshold pH. The *in vitro* cytotoxicity studies showed an important increase in the activity of the NPs loaded with drug compared to the free drug.

The particle's size below the cut-off size of the leaky pathological vasculature ($2R_H$ < 100 nm), their excellent stability in serum and the ability to release a drug at the endosomal pH with concomitant high cytotoxicity make them suitable candidates for cancer therapy, namely for treatment of solid tumours exhibiting high tumor accumulation of NPs due to an effective EPR effect.

Experimental section

Materials

Monomer 2-(diisopropylamino)ethyl methacrylate (DPA, 97%) was purified by vacuum distillation prior to use. Monomer *N*-(2-hydroxypropyl)methacrylamide (HPMA) was synthesized according to the reference.[41] Initiator 4,4-azobis(4-cyanopentanoic acid) (V-501, Aldrich) was recrystallized from methanol

prior to use. The chain transfer agent, 4-cyano-4-(phenylcarbonothioylthio)pentanoic acid (CTP, Aldrich), was used as received. Solvents, methanol, dimethylacetamide and 1,4-dioxane were purchased from Lachner, dried over molecular sieves (3 Å) and distilled prior to use.

Methods

^{1}H NMR. The ^{1}H NMR spectra were recorded using a Bruker AMX-300 300 MHz spectrometer. PHPMA was dissolved in D_2O and $PHPMA_{25}$-*b*-$PDPA_{106}$ block copolymer in D_2O/DCl (pH 2).

Size exclusion chromatography (SEC). The number-average molecular weight (M_n) and its distribution (M_w/M_n) were obtained by SEC. SEC of the isolated copolymers was performed at 25 °C with two PLgel MIXED-C columns (300 × 7.5 mm, SDV gel with particle size 5 μm; Polymer Laboratories, USA) and with UV (UVD 305; Watrex, Czech Republic) and RI (RI-101; Shodex, Japan) detectors. The mixture of tetrahydrofuran/methanol 80/20 v/v% was used as a mobile phase at a flow rate of 1 mL min^{-1}. The molecular weight values were calculated using Clarity software (Dataapex, Czech Republic). Calibration with PMMA standards was used. The absolute number-average molar mass (M_n) and molar mass distribution (M_w/M_n) of PHPMA macroCTA were determined on a HPLC Shimadzu system equipped with a Superose 12™ column, UV, Optilab rEX differential refractometer and multiangle light scattering DAWN 8 (Wyatt Technology, USA) detectors. For these experiments, the 0.3 M sodium acetate buffer (pH 6.5) containing 0.5 g L^{-1} sodium azide was used as the mobile phase.

Synthesis of PHPMA macroCTA. In a Schlenk flask equipped with a magnetic stirrer bar, HPMA monomer (3 g, 21 mmol) and CTP (94 mg, 0.34 mmol) were dissolved in 17 mL of DMAc and deoxygenated by four freeze–pump–thaw cycles. Subsequently, 300 μL (0.167 mmol) of the initiator V-501 solution (78 mg, 0.5 mL DMAc) was added and another freeze–pump–thaw cycle was performed. The flask containing the pink solution was filled with argon and placed into an oil bath (70 °C) to start the polymerisation. After 10 h, the polymerisation was quenched by exposing the reaction mixture to air and liquid nitrogen. The polymerisation solution was precipitated in diethyl ether/acetone (3/1) mixture, filtered and vacuum dried to yield a pink solid (875 mg). The conversion was 36% as determined by ^{1}H NMR spectroscopy (Fig. S1B†). The obtained polymer was characterized by SEC M_n = 3600 g mol^{-1}, $Đ$ = 1.07 (Fig. S1A†).

Synthesis of poly(*N*-(2-hydroxypropyl)methacrylamide)-*b*-(2-(diisopropylamino)ethyl methacrylate) ($PHPMA_{25}$-*b*-$PDPA_{106}$). In a Schlenk flask equipped with a magnetic stirrer bar, PHPMA macroCTA (432 mg, M_n 3600, $Đ$ 1.07) was dissolved in MeOH (3 mL). The monomer DPA (2.56 g, 12 mmol) and 1,4-dioxane (4 mL) were added and the mixture was deoxygenated by four freeze–pump–thaw cycles. Subsequently, 100 μL (0.039 mmol) of the initiator V-501 solution (33 mg, 0.3 mL DMAc) was added and another freeze–pump–thaw cycle was performed. The flask containing the pink solution was filled with argon and placed into an oil bath (70 °C) to start the polymerisation. After 15 h, the polymerisation was quenched by exposing the reaction mixture to air rapidly cooling in liquid nitrogen. The polymer was isolated by dialysis using a Spectra-Por dialysis membrane MWCO 3500 against water (pH 2–3) for five days. The solution of polymer was lyophilized to yield a light pink solid. The conversion was 94% as determined by ^{1}H NMR spectroscopy. The dithiobenzoic ω-end group was removed by the method introduced by Perrier[42] using V-501 and the polymer isolated by dialysis and lyophilization to obtain a white solid. The obtained polymer was characterised by SEC M_n = 26 200 g mol^{-1}, $Đ$ = 1.29. The synthetic parameters and molecular weight data of polymers prepared *via* RAFT polymerization are described in Table TS1 (ESI†).

Scattering techniques

The dynamic light scattering (DLS) measurements were performed using an ALV CGE laser goniometer consisting of a 22 mW He–Ne linear polarized laser operating at a wavelength (λ = 632.8 nm), an ALV 6010 correlator, and a pair of avalanche photodiodes operating in the pseudo cross-correlation mode. The samples were loaded into 10 mm diameter glass cells and maintained at 25 ± 1 °C. The data were collected using the ALV Correlator Control software and the counting time was 30 s. The measured intensity correlation functions $g_2(t)$ were analysed using the algorithm REPES (incorporated in the GENDIST program)[43] resulting in the distributions of relaxation times shown in equal area representation as $\tau A(\tau)$. The mean relaxation time or relaxation frequency ($\Gamma = \tau^{-1}$) is related to the diffusion coefficient (D) of the nanoparticles as: $D = \frac{\Gamma}{q^2}$ where $q = \frac{4\pi n \sin\frac{\theta}{2}}{\lambda}$ is the scattering vector, n is the refractive index of the solvent and θ is the scattering angle. The hydrodynamic radius (R_H) or the distributions of R_H were calculated by using the well-known Stokes–Einstein relation:

$$R_H = \frac{k_B T}{6\pi\eta D} \quad (3)$$

where k_B is the Boltzmann constant, T is the absolute temperature and n is the viscosity of the solvent.

In the static light scattering (SLS), the scattering angle was varied from 30 to 150° with a 10° stepwise increase. The absolute light scattering is related to the weighted-average molar mass (M_w(NP)) and to the radius of gyration (R_G) of the nanoparticles by the Zimm formalism represented as:

$$\frac{K_c}{R_\theta} = \frac{1}{M_{w(NP)}}\left(1 + \frac{R_{Gq^2}}{3}\right) \quad (4)$$

where K is the optical constant which includes the square of the refractive index increment (dn/dc), R_θ is the excess normalized scattered intensity (toluene was applied as the standard solvent) and c is the polymer concentration given in mg mL^{-1}. The refractive index increment (dn/dc) of the $PHPMA_{25}$-*b*-$PDPA_{106}$ NPs in PBS (0.143 mL g^{-1}) was determined using a Brice–Phoenix differential refractometer operating at λ = 632.8 nm.

The small angle X-ray scattering (SAXS) experiments were performed on the P12 BioSAXS beamline at the PETRA III storage ring of the Deutsche Elektronen Synchrotron (DESY, Hamburg, Germany) at 20 °C using a Pilatus 2M detector and synchrotron radiation with a wavelength of λ = 0.1 nm. The sample-detector distance was 3 m, allowing for measurements in the q-range interval from 0.11 to 4.4 nm^{-1}. The q range was calibrated using the diffraction patterns of silver behenate. The experimental data were normalized to the incident beam intensity and corrected for the non-homogeneous detector response, and the background scattering of the solvent was subtracted. The solvent scattering was measured before and after the sample scattering to control for possible sample holder contamination. Eight consecutive frames comprising the measurement of the solvent, sample, and solvent were performed. No measurable radiation damage was detected by the comparison of eight successive time frames with 15 s exposures. The final scattering curve was obtained using the PRIMUS program by averaging the scattering data collected from the different frames. The automatic sample changer for sample volume 15 μL and filling cycle of 20 s was used.

pH titration

The pH titration was employed in order to determine the exact pK_a of the DPA block in the $PHPMA_{25}$-*b*-$PDPA_{106}$ block copolymer under simulated physiological conditions. The block copolymer sample (c = 0.2 mg mL^{-1}) was previously dissolved in Milli-Q water. The pH was pre-set to pH = 2.0 by adding small amounts of 0.1 mol L^{-1} HCl solution and the ionic strength was set to 0.15 mol L^{-1} by adding NaCl to the system. An MPT2 autotitrator connected to a Nano-ZS, Model ZEN3600 (Malvern, UK) zetasizer was used for automated measurement of the pH dependencies of the scattering intensity (I_s) and zeta potential (ζ). The I_s and ζ-potential were measured at an angle of 173° using a He–Ne 4.0 mW power laser operating at a wavelength of 633 nm. The equipment measures the electrophoretic mobility (U_E) of the solution and converts the value to ζ-potential (mV) through Henry's equation. The Henry's function was calculated through the Smoluchowski approximation using the DTS (Nano) program.

Cryogenic transmission electron microscopy (Cryo-TEM)

For cryo-TEM studies, a sample droplet of 2 μL was put on a lacey carbon film covered copper grid (Science Services, Munich, Germany), which was hydrophilized by glow discharge for 15 s. Most of the liquid was then removed with blotting paper, leaving a thin film stretched over the lace holes. The specimens were instantly shock frozen by rapid immersion into liquid ethane and cooled to approximately 90 K by liquid nitrogen in a temperature-controlled freezing unit (Zeiss Cryobox, Zeiss NTS GmbH, Oberkochen, Germany). The temperature was monitored and kept constant in the chamber during all the sample preparation steps. After the specimens were frozen, the remaining ethane was removed using blotting paper. The specimen was inserted into a cryo transfer holder (CT3500, Gatan, Munich, Germany) and transferred to a Zeiss EM922 Omega energy-filtered TEM (EFTEM) instrument (Zeiss NTS GmbH, Oberkochen, Germany). Examinations were carried out at temperatures around 90 K. The TEM instrument was operated at an acceleration voltage of 200 kV. Zero-loss-filtered images (ΔE = 0 eV) were taken under reduced dose conditions (100–1000 e nm^{-2}). All images were recorded digitally by a bottom-mounted charge-coupled device (CCD) camera system (Ultra Scan 1000, Gatan, Munich, Germany) and combined and processed with a digital imaging processing system (Digital Micrograph GMS 1.8, Gatan, Munich, Germany). All images were taken very close to focus or slightly under the focus (some nanometers) due to the contrast enhancing capabilities of the in-column filter of the used Zeiss EM922 Omega. In EFTEMs, deep underfocussed images can be totally avoided.

Preparation of the nanoparticles

To 2.5 mL of a solution of $PHPMA_{25}$-*b*-$PDPA_{106}$ (20 mg mL^{-1}) and paclitaxel (500 μg mL) in ethanol, 5.0 mL of PBS were added as a precipitant. The increase in the polarity of the solvent led to the aggregation of the polymer chains forming the NPs. The remaining ethanol was removed by evaporation and the final volume of the NPs was concentrated to 5 mg mL^{-1}. Drug-free NPs were prepared by the same way without adding paclitaxel.

Paclitaxel (PTX) drug loading and loading efficiency

The total amount of the chemotherapeutic PTX loaded into the nanoparticles was measured by HPLC (Shimadzu, Japan) using a reverse-phase column Chromolith Performance RP-18e (100–4.6 mm, eluent water-acetonitrile with acetonitrile gradient 0–100 vol%, flow rate = 1.0 mL min^{-1}). Firstly 200 μL of the drug loaded NPs were collected from the bulk sample, filtered (0.45 μm) and diluted to 150 μL with HCl (0.05 mol L^{-1}). Such a procedure led to a final pH ~ 3.0 and therefore a pH-induced NPs disassembly was achieved. Subsequently, the aliquot was diluted to a final volume of 1.0 mL by using acetonitrile (650 μL).[15] Afterwards, 20 μL of the final sample was injected through a sample loop. PTX was detected at 227 nm using ultraviolet (UV) detection. The retention time of PTX was 12.20 min under these experimental conditions. An analytical curve with linear response in the range (0.5–100 μg mL^{-1}) was obtained and used to determine the PTX content. The drug-loading content (LC) and the drug-loading efficiency (LE) were calculated by using the following equations:

$$\mathrm{LC}(\%) = \frac{\text{drug amount in NPs}}{\text{mass of NPs}} \times 100 \quad (5)$$

$$\mathrm{LE}(\%) = \frac{\text{drug amount in Nps}}{\text{drug feeding}} \times 100 \quad (6)$$

Release experiments

The release experiments were carried out at 37 °C in pH-adjusted release media (pH 7.4 and 5.0). Aliquots (500 μL) of PTX-NPs were loaded into 36 Slide-A-Lyzer MINI dialysis micro-

tubes with MWCO 10 kDa (Pierce, Rockford, IL). These microtubes were dialyzed against 4 L of PBS (pH 7.4 and 5.0).[16,23] The release media was changed periodically to reduce the possibility of drug-diffusion equilibrium. The drug release experiments were done in triplicate. At each sampling time, three microtubes were removed from the dialysis system and 0.1 mL from each microtube was sampled and the remaining drug was extracted by using the aforementioned methodologies. The reported data are expressed as the amount of released PTX relative to the total PTX content in the PTX-NPs.

Stability of the nanoparticles in blood plasma

The stability of the nanoparticles in blood plasma was monitored in real time while incubating them with diluted human plasma (10% v/v in PBS). Typically, 1 mg mL^{-1} of the block copolymer nanoparticles was added to a 10% v/v of diluted human plasma in PBS. The dynamic light scattering experiments were performed at intervals for a total incubation time of 36 h.[16,22,23,26]

Cytotoxicity assays

The HeLa cells were cultivated in Dulbecco's Modified Eagle's Medium (DMEM) supplemented with 10% fetal calf serum, 100 units of penicillin and 100 μg mL^{-1} of streptomycin (Life Technology, CZ). The cells were grown in a humidified incubator at 37 °C with 5% CO_2. For the cytotoxicity assay, 5000 cells per well were seeded in duplicates in 96 flat bottom well plates in 100 μL of media 24 h before adding the NPs. For addition of the particles the volume was calibrated to 80 μL, and 20 μL of the 5-times concentrated dilution of PTX or particle dispersion were added per well to obtain a final PTX concentration ranging from 10^{-5} to 5 μg mL^{-1}. All dilutions were made in full incubation medium with thorough mixing in each dilution step. The sample concentrations of the PTX-loaded particles were adjusted to contain the same total amount of PTX as the samples with free PTX. The cells were incubated with free drug or NPs for 24 h or 48 h. Then 10 μL of alamarBlue® cell viability reagent (Life Technologies, Czech Republic) were added to each well and incubated for a minimum of 3 h at 37 °C. The fluorescence of the reduced marker dye was read with a Synergy H1 plate reader (BioTek Instruments, USA) at excitation 570 and emission 600 nm. The fluorescence intensity of the control samples (with no drug or particles added) was set as a marker of 100% cell viability. The fluorescence signal of "0% viability samples" (all cells were killed by addition of hydrogen peroxide) was used as the background and subtracted from all values prior to calculations. The non-toxic character of the blank particles without the drug was shown by incubation of cells with 0.4 mg L^{-1} of blank particles. This corresponds to the amount of polymer that is contained in the samples of drug-loaded particles with a total PTX content of 5 μg L^{-1}. For the cell experiments the PTX-dilutions in incubation medium were made from a PTX stock solution of 120 μg mL^{-1} in PBS/DMSO ((96.5 : 3.5 v/v).[44] Precipitation of the hydrophobic PTX out of the cell culture medium can therefore be excluded because the PTX was previously fully dissolved in a PBS/DMSO solution (96.5 : 3.5 v/v) and subsequently diluted in the serum-supplied medium under thorough mixing. Consequently, even at a maximal PTX-concentration of 5 μg mL^{-1}, the final DMSO concentration in the incubation medium was below 0.2% and therefore had no effect on cell vitality in the applied setup.[45] All the results of the cell experiments are the average of at least 4 measurements ($n \geq 4$).

Acknowledgements

This research was supported by the Norwegian Financial Mechanism 2009-2014 under Project contract no 7F14009. C.R.-E. acknowledges the Grant Agency of the Czech Republic (GACR) under contract no. 15-09368Y and the project "BIOCEV – Biotechnology and Biomedicine Centre of the Academy of Sciences and Charles University" (CZ.1.05/1.1.00/02.0109), from the European Regional Development Fund. M. D. acknowledges BIMF (Bayreuth Institute of Macromolecular Research) and BZKG (Bayreuth Center for Colloids and Interfaces) for financial support. F. N. acknowledges support through the CNRS project PICS no. 06130.

Notes and references

1 J. Rodríguez-Hernández, F. Chécot, Y. Gnanou and S. Lecommandoux, *Prog. Polym. Sci.*, 2005, **30**, 691.
2 Y. Mai and A. Eisenberg, *Chem. Soc. Rev.*, 2012, **41**, 5969.
3 T. Smart, H. Lomas, M. Massignani, M. V. Flores-Merino, L. R. Perez and G. Battaglia, *Nano Today*, 2008, **3**, 38.
4 L. Zhang and A. Eisenberg, *J. Am. Chem. Soc.*, 1996, **118**, 3168.
5 L. Zhang and A. Eisenberg, *Polym. Adv. Technol.*, 1998, **9**, 677.
6 A. Blanazs, S. P. Armes and A. J. Ryan, *Macromol. Rapid Commun.*, 2009, **30**, 267.
7 G. Gaucher, M.-H. Dufresne, V. P. Sant, N. Kang, D. Maysinger and J.-C. Leroux, *J. Controlled Release*, 2005, **109**, 169.
8 V. P. Chauhan and R. K. Jain, *Nat. Mater.*, 2013, **12**, 958.
9 S. Petrova, E. Jäger, R. Konefał, A. Jäger, C. G. Venturini, J. Spěváček, E. Pavlova and P. Štěpánek, *Polym. Chem.*, 2014, **5**, 3884.
10 Q. Yin, J. Shen, Z. Zhang, H. Yu and Y. Li, *Adv. Drug Delivery Rev.*, 2013, **65**, 1699.
11 B. A. Webb, M. Chimenti, M. P. Jacobson and D. L. Barber, *Nat. Rev. Cancer*, 2011, **11**, 671.
12 E. G. Kelley, J. N. L. Albert, M. O. Sullivan and T. H. Epps III, *Chem. Soc. Rev.*, 2013, **42**, 7057.
13 E. S. Lee and Y. H. Bae, *J. Controlled Release*, 2008, **132**, 164.
14 K. Zhou, H. Liu, S. Zhang, X. Huang, Y. Wang, G. Huang, B. D. Sumer and J. Gao, *J. Am. Chem. Soc.*, 2012, **134**, 7803.

15 Y. Wang, K. Zhou, G. Huang, C. Hensley, X. Huang, X. Ma, T. Zhao, B. D. Sumer, R. J. DeBerardinis and J. Gao, *Nat. Mater.*, 2014, **13**, 204.
16 F. C. Giacomelli, P. Štěpánek, C. Giacomelli, V. Schmidt, E. Jäger, A. Jäger and K. Ulbrich, *Soft Matter*, 2011, **7**, 9316.
17 C. Pegoraro, D. Cecchin, L. S. Gracia, N. Warren, J. Madsen, S. P. Armes, A. Lewis, S. MacNeil and G. Battaglia, *Cancer Lett.*, 2013, **334**, 328.
18 J. Fang, H. Nakamura and H. Maeda, *Adv. Drug Delivery Rev.*, 2011, **63**, 136.
19 T. Riedel, Z. Riedelová-Reicheltová, P. Májek, C. Rodriguez-Emmenegger, M. Houska, J. E. Dyr and E. Brynda, *Langmuir*, 2013, **29**, 3388.
20 C. Rodriguez-Emmenegger, E. Brynda, T. Riedel, M. Houska, V. Šubr, A. B. Alles, E. Hasan, J. E. Gautrot and W. T. S. Huck, *Macromol. Rapid Commun.*, 2011, **32**, 952.
21 F. Surman, T. Riedel, M. Bruns, N. Y. Kostina and C. Rodriguez-Emmenegger, *Macromol. Biosci.*, 2015, **15**, 636.
22 E. Jäger, A. Jäger, T. Etrych, F. C. Giacomelli, P. Chytil, A. Jigounov, J. L. Putaux, B. Říhová, K. Ulbrich and P. Štěpánek, *Soft Matter*, 2012, **8**, 9563.
23 E. Jäger, A. Jäger, P. Chytil, T. Etrych, F. C. Giacomelli, B. Říhová, P. Štěpánek and K. Ulbrich, *J. Controlled Release*, 2013, **165**, 153.
24 B. Angelov, A. Angelova, S. K. Filippov, T. Naryanan, M. Drechsler, P. Štěpánek, P. Couvreur and S. Lesieur, *J. Phys. Chem. Lett.*, 2013, **4**, 1959.
25 B. Angelov, A. Angelova, S. K. Filippov, G. Karlsson, N. Terril, S. Lesieur and P. Štěpánek, *Soft Matter*, 2011, **7**, 9714.
26 F. C. Giacomelli, P. Štěpánek, V. Schmidt, E. Jäger, A. Jäger and C. Giacomelli, *Nanoscale*, 2012, **4**, 4504.
27 C. Giacomelli, L. Le Men and R. Borsali, *Biomacromolecules*, 2006, **7**, 817.
28 C. E. de Castro, B. Mattei, K. A. Riske, E. Jäger, A. Jäger, P. Štěpánek and F. C. Giacomelli, *Langmuir*, 2014, **30**, 9770.
29 H. Cabral, Y. Matsumoto, K. Mizuno, Q. Chen, M. Murakami, M. Kimura, Y. Terada, M. R. Kano, K. Miyazono, M. Uesaka, N. Nishiyama and K. Kataoka, *Nat. Nanotechnol.*, 2011, **6**, 815.
30 K. R. Whiteman, V. Šubr, K. Ulbrich and V. P. Torchilin, *J. Liposome Res.*, 2001, **11**, 153.
31 S. Kamei and J. Kopeček, *Pharm. Res.*, 1995, **12**, 663.
32 K. Cho, X. Wang, S. Nie, Z. Chen and D. M. Shin, *Clin. Cancer Res.*, 2008, **14**, 1310.
33 J. E. Liebmann, J. A. Cook, C. Lipschultz, D. Teague, J. Fisher and J. B. Mitchell, *Br. J. Cancer*, 1993, **68**, 1104.
34 X. Peng, F. Gong, Y. Chen, Y. Jiang, J. Liu, M. Yu, S. Zhang, M. Wang, G. Xiao and H. Liao, *Cell Death Dis.*, 2014, **5**, e1367.
35 D. Li, Y. Zhang, S. Jin, J. Guo, H. Gao and C. Wang, *J. Mater. Chem. B*, 2014, **2**, 5187.
36 F. Danhier, N. Lecouturier, B. Vroman, C. Jerome, J. Marchand-Brynaert, O. Feron and V. Preat, *J. Controlled Release*, 2009, **133**, 11.
37 J. Panyam, W. Z. Zhou, S. Prabha, S. K. Sahoo and V. Labhasetwar, *FASEB J.*, 2002, **16**, 1217.
38 S. K. Sahoo, J. Panyam, S. Prabha and V. Labhasetwar, *J. Controlled Release*, 2002, **82**, 105.
39 G. Gaucher, R. H. Marchessault and J.-C. Leroux, *J. Controlled Release*, 2010, **143**, 2–12.
40 W. T. Godbey, K. K. Wu and A. G. Mikos, *Proc. Natl. Acad. Sci. U. S. A.*, 1999, **96**, 5177.
41 K. Ulbrich, V. Šubr, J. Strohalm, D. Plocová, M. Jelínková and B. Říhová, *J. Controlled Release*, 2000, **64**, 63.
42 S. Perrier, P. Takolpuckdee and C. A. Mars, *Macromolecules*, 2005, **38**, 2033.
43 J. Jakes, *Czech J. Phys.*, 1988, **38**, 1305.
44 E. A. Dubikovskaya, S. H. Thorne, T. H. Pillow, C. H. Contag and P. A. Wender, *Proc. Natl. Acad. Sci. U. S. A*, 2008, **105**, 12128.
45 A. B. Trivedi, N. Kitabatake and E. Do, *Agric. Biol. Chem.*, 1990, **54**, 2961.

Journal Name

COMMUNICATION

Fluorescent boronate-based polymer nanoparticles with reactive oxygen species (ROS)-triggered cargo release for drug-delivery applications

Received 00th January 20xx,
Accepted 00th January 20xx

DOI: 10.1039/x0xx00000x

www.rsc.org/

Eliezer Jäger,[a,b,*] Anita Höcherl,[a,*] Alessandro Jäger,[a,b] Martin Hrubý,[a] Rafal Konefal,[a,b] Miloš Netopilik,[a] Jiří Pánek,[a] Miroslav Šlouf,[a] Karel Ulbrich[a] and Petr Štěpánek[a]

A new drug-delivery system of polymer nanoparticles (NPs) bearing pinacol-type boronic ester and alkyne moieties displaying triggered self-immolative polymer degradation in the presence of reactive oxygen species (ROS) with the capability of cellular imaging is presented. The NPs specifically release their drug cargo under concentrations of ROS that are commonly found in the intracellular environment of certain tumors and of inflamed tissues and exhibit significant cytotoxicity to cancer cells compared to their non-ROS-responsive counterparts.

Incorporation of selectively chemically degradable linkages into polymer-based nano (NPs)- and microparticulate drug-delivery systems allows to achieve external stimulus-triggered polymer degradation and triggered release.[1-3] This is a very useful feature both to release the therapeutic cargo and to eliminate the biomaterial from the body after the cargo is released and the carrier is no longer needed. Such stimulus may be an enzymatic removal of protecting groups, a pH change, light or more recently, the presence of reactive oxygen species (ROS) in the surrounding environment.[4-6] The ROS play a crucial role in human physiological and pathophysiological processes. An increasing amount of data indicates that ROS such as, *e.g.*, H_2O_2, is a component of cell signaling pathways that are necessary for the growth, development, and fitness of living organisms.[7] On the other hand, imbalances in H_2O_2 production lead to oxidative stress and inflammation events, which damage tissue and organ systems and are correlated with the onset and advancement of various diseases, including cancer, diabetes, cardiovascular and neurodegenerative diseases.[8-11] Several works suggest that many human cancer cells show higher H_2O_2 levels compared to their normal counterparts.[12-16] Specifically, H_2O_2 has become a common marker for oxidative stress playing important roles in carcinogenesis and is also linked to *e.g.*, apoptosis, cell proliferation and DNA mutations.[17-19] Thus the involvement of ROS in cellular signaling and disease states has motivated the construction of clever chemical tools as ROS-responsive micro- and NPs as drug carriers.[20-22]

The ability to generate a triggered NP carrier response (*e.g.*, release of cargo or polymer degradation) in ROS rich microenvironments is of particular interest, *e.g.*, for the targeted drug delivery to tumors and sites of inflammation.[4,5,21-24]

Herein, a biocompatible and biodegradable ROS-sensitive polymer backbone with the capability of cellular imaging to ROS-rich environment was synthesized by step-growth polymerization from monomers bearing a ROS-degradable pinacol-type boronic ester and alkyne moiety suitable for click chemistry-based attachment of active cargo (*see* Scheme 1).

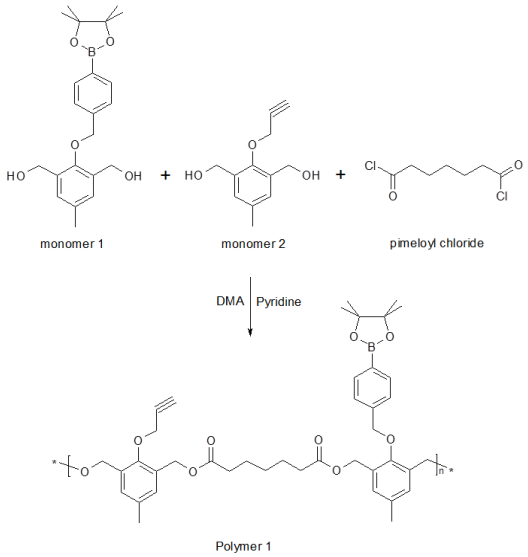

Scheme 1. Synthetic route of the ROS-responsive polymer 1 (P-1) bearing the alkyne group-containing monomeric unit 2 suitable for click reaction.

[a] *Institute of Macromolecular Chemistry v.v.i., Academy of Sciences of the Czech Republic, Heyrovsky Sq. 2, 162 06 Prague 6, Czech Republic.*
[b] *Charles University Prague, Faculty of Natural Sciences, Hlavova 2030, Prague 12840 2, Czech Republic.*
E-mail: jager@imc.cas.cz; hocherl@imc.cas.cz;

Electronic Supplementary Information (ESI) available: [details of any supplementary information available should be included here]. See DOI: 10.1039/x0xx00000x

Initially, monomer 1 was synthesized according to the previously reported procedure[21] (*see* ESI for synthetic route). Monomer 2 (Scheme 1) was synthesized by the protection of 2,6-bis-(hydroxymethyl)-*p*-cresol with tert-butyldimethylsilyl chloride generating the compound 2 that was then reacted with propargyl bromide to provide the protected alkyne compound 3 (Fig. S1, *see* ESI for synthetic route).

The monomer 2 (Scheme 1) was obtained in high yield (94 %) after the removal of the protecting groups from compound 3 (ESI, Fig. S2). The synthesized monomers 1 and 2 were further successfully copolymerized with pimeloyl chloride generating the ROS-responsive polymer 1 (P-1) (Scheme 1 and ESI). Successful polymer synthesis was confirmed by the ^{1}H NMR (Fig. 1) and by size exclusion chromatography (SEC) analysis (Fig. 2a). Weight-average molecular weight (M_w) of polymer P-1 was 21.5 kDa with reasonable polydispersity index PDI = M_w/M_n = 1.49 (where M_n is the number-average molecular weight) as determined by SEC (Fig. 2a – black lines). The ^{1}H NMR spectrum of P-1 shows characteristic signals for protons belonging to the repeating units of monomers. The signals from protons in monomer 1 and monomer 2 aromatic rings were detected at δ = 7.68 ppm (1 - *see* Fig. 1 for signal-structure assignment), δ = 7.41 ppm (2), and δ = 7.16 ppm (3). The methylene protons (4) of monomers 1 and 2 from the main chain of P-1 where observed in the same position at δ = 5.08 ppm, whereas the signals attributed to the methylene groups of side chains of monomers 1 (5) and 2 (6) appear at δ = 4.88 and 4.57 ppm, respectively (Fig. 1). The signal of the proton of the terminal alkyne group (7) is at δ = 2.51 ppm (spectrum of P-1 in d_6-DMSO is given also, *see* ESI, Fig. S3). Furthermore, the spectrum displayed signals of methylene groups (10) from pimeloyl chloride monomeric repeating unit at δ = 1.48 ppm, and peaks of the methyl with methylene groups (8 + 9, 12 + 11) with chemical shift at δ = 2.25 and 1.26 ppm, respectively. A ROS-insensitive counterpart to the P-1 polymer (polymer 2; P-2) was also synthesized to investigate the ROS response to the intracellular drug release efficiency. Spectra of the ROS-insensitive counterpart polymer 2 in $CDCl_3$ showed the characteristic peaks (Fig. S4, ESI), which also indicated successful polymer synthesis.

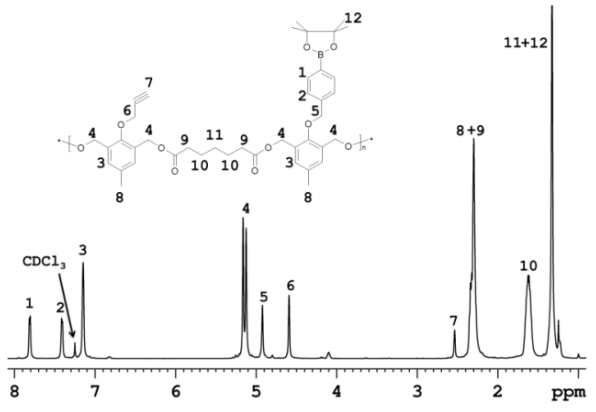

Fig. 1 ^{1}H NMR spectra of the synthesized ROS-responsive polymer (P-1) containing the monomer 2 units enabling the polymer modification by click reaction.

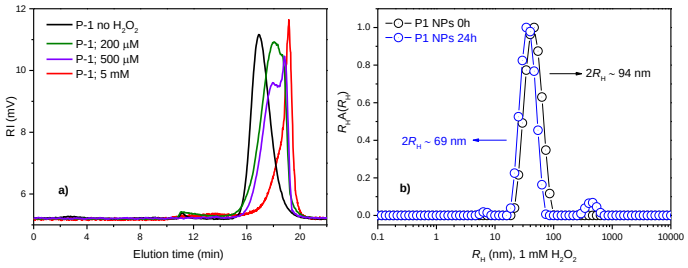

Fig. 2 SEC chromatograms of P-1 prior to the addition of H_2O_2 (black line) and after degradation in 20% PBS/DMF solutions containing 200 µM, 500 µM or 5 mM of H_2O_2, respectively (incubation at 37 °C for 1 day (a), and (b) distributions of R_H for P-1 (○) prior the H_2O_2 addition and (○) after 24h of incubation in 1 mM of H_2O_2.

The degradation of the P-1 polymer in presence of H_2O_2 was characterized by SEC analysis and ^{1}H NMR following the modified methodology according to Almutairi *et al*., 2012.[21]

In a typical experiment, the P-1 was incubated in a 20% PBS/DMF (*v*/*v*) solution containing different H_2O_2 concentrations and at predetermined time intervals aliquots were examined by SEC (*see* ESI).

The SEC chromatogram (Fig. 2) shows that P-1 degraded into small molecules and oligomers in a time- and H_2O_2-dependent manner. Polymer degradation proceeds more extensively with increasing incubation time and H_2O_2 concentration. P-1 was shown to be responsive to physiological levels of H_2O_2 (< ~ 1 mM)[25] after 1 day of incubation (Fig. 2a) while the non-ROS-responsive counterpart polymer (P-2) showed no degradation along the same time and conditions (data not shown). When degradation of both polymers was compared at higher H_2O_2 concentrations and for longer time (5 mM, 4 days), the degradation of P-2 polymer was only partial (Fig. S5). The degradation of the polymer P-1 evaluated with ^{1}H NMR was complete after 5 days of incubation (*see* ESI, Fig. S6) as broad peaks in ^{1}H NMR related to polymer are replaced by sharp peaks of the low-molecular-weight degradation products (monomers) confirming the depolymerisation of the P-1 triggered by the H_2O_2 (ESI, Fig. S6).

The NPs from the P-1 and P-2 polymers were prepared by a nanoprecipitation protocol (*see* ESI) and their behavior under different ROS concentrations was evaluated in detail by dynamic light scattering (DLS), static light scattering (SLS), transmission electron microscopy (TEM) and by *in vitro* drug model release experiments. Note that the NPs were prepared with hydrodynamic radius ($2R_H = D_H$ ~ 94 nm), *e.g.*, within a range known to be ideal for efficient tumor accumulation due to the enhanced permeability and retention (EPR) effect.[26] The ROS-responsiveness capability of the P-1 NPs was tested by DLS after 24 h of incubation with 1mM of H_2O_2. The Fig. 2b shows the distribution of R_H for P-1 NPs prior and after 24 h of incubation as measured by DLS. The distribution of R_H for P-1 NPs appears as only one single distribution of R_H relative to the presence of the single spherical polymer NPs in PBS solution with an average diameter of $2R_H$ ~ 94 nm (Fig. 2b, black circles). Furthermore, the polydispersity of the NPs is very low as estimated through the Cumulant analysis (μ/Γ^2 = 0.08 ±

0.007) (ESI). This is important for the homogeneous biological behavior of such NPs. However, after 24 h of H_2O_2 incubation, a trimodal distribution of R_H was observed. In addition to the NPs peak, the presence of molecularly dissolved copolymer chains as well as a peak of large aggregates with loose structure, could be noticed in the aqueous solution at 1mM of H_2O_2. Three well-defined peaks highlighting the three populations of the scattering polymer with average diameters of D_H ~ 11 nm, 69 nm and 1.9 µm were identified (Fig. 2b, blue circles). They can be attributed to free chains and their fragments, surface-eroded nanoparticles (decrease in D_H of ~ 25 nm) and polymer aggregates, respectively.[3,27] Further the polymer degradation-triggered cargo release was studied using the release of the fluorescent model of a drug, the Nile Red (NR). The NR-loaded ROS-responsive (from polymer P-1) and non-ROS-responsive (from polymer P-2) NPs were examined with fluorescence spectroscopy measurements along 24 h of incubation with 1 mM of H_2O_2 (Fig. S7 - S9). After 24 h the NR release from the ROS-responsive NPs was almost ~6 times faster than the NR release from their non-ROS-responsive counterparts, thus confirming the potential of the P-1 polymer NPs to release the model drug specifically in simulated ROS-rich microenvironments (Fig. S9, ESI).

The NPs degradation was also investigated by TEM microscopy (Fig. 3). The TEM microscopy showed particle size qualitatively comparable to that determined by DLS (Fig. 2b). Prior to incubation with H_2O_2, compact NPs of spherical morphology and narrow size distribution ($D_H \leq 85$ nm) were observed (Fig. 3a). After incubation with 1 mM of H_2O_2, the NPs showed diffuse irregular shapes and a very broad size distribution, with the smallest NPs well below 10 nm and the largest NPs above ~ 100 nm (Fig. 3b). This suggested that H_2O_2 caused decomposition of the NPs, and the decomposed parts were probably re-agglomerated due to their hydrophobicity. SLS data support the findings that the NPs underwent surface degradation as well as core decomposition, as the particles' D_H decreased (by 25 nm, *see* Fig. 2b) as well as the overall scattering intensity (Fig. S10a) followed by the increase in particles R_G (gyration radius), a characteristic of core hydration and swelling of the scattering particles in solution (Fig. S10b).[28-30]

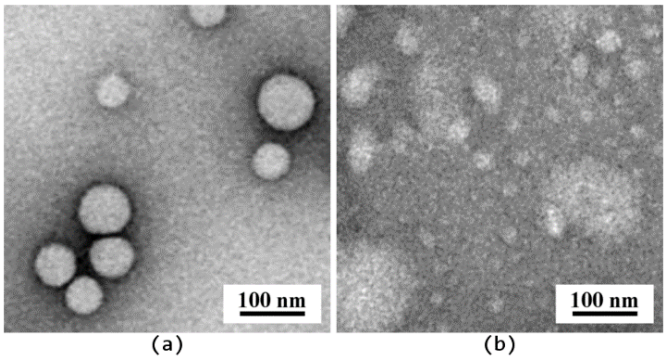

Fig. 3 TEM micrographs of polymer NPs from polymer P-1 prior to incubation with H_2O_2 (a) and after 2 days of incubation with 1 mM of H_2O_2 (b).

The decomposition was also in agreement with the observed low contrast for the incubated NPs (Fig. 3b). Compact NPs exhibited sharp edges and high contrast, whereas decomposed NPs, NPs fragments and their agglomerates showed only a vague interface.

The cellular uptake of P-1 and P-2 NPs loaded with NR (dye loading ~ 0.2 *wt*.%, *see* ESI and Fig. S7 and S8) and the intracellular NR release were followed *in vitro* in human prostate cancer (PC-3) cells (*see* ESI for method). The latter are known to produce high ROS levels.[31] While inside the particles the NR fluorescence is strong, upon ROS-triggered NPs degradation in cells the dye will be released and get quenched outside the NPs (due to polarity changes in the micro-surrounding). After 4 h both NPs displayed similar fluorescence intensity in the cells, however, after 20 h the fluorescence of P-1 was lower compared to P-2 NPs (*see* Fig. S11). This indicated faster ROS-triggered degradation of P-1 NPs after prolonged exposure in ROS-producing cells.

Based on the similar uptake rate of the NPs (as also confirmed by flow cytometry, *see* Fig. S12), the ROS-mediated fluorescence decay and cargo release of P-1 particles was further pursued *via* fluorescence lifetime microscopy (FLIM) and flow cytometry (FC). In a quantitative study *via* FC the NR quenching of the NPs was evaluated in PC-3 and human fibroblast (HF) cells (*see* ESI for methods). The latter are known for their low levels of ROS production contrary to *e.g.*, PC-3.[31-34] The cells were loaded with P-1 NPs, washed and incubated for 4 h, thus exposing the internalized NPs to intracellular ROS insofar as present in the cells. Data showed that after incubation the NR fluorescence was significantly reduced in PC-3 cells compared to the HF cells (Fig. 4). By the same experimental setup the Nile Red quenching of P-1 and P-2 NPs in PC-3 cells was compared. In line with the previous imaging data a lowered NR fluorescence of P-1, factor 0.7, compared to P-2 was observed.

In conclusion, the FC data acquired in PC-3 cancer cells and non-cancer HF cells indicated a ROS-induced degradation of P-1, and demonstrated the polymer's potential to specifically trigger the cargo release in ROS-containing intracellular environment. As the released NR inside the cells can interact with hydrophobic cell structures and partially recover fluorescence, released NR is never fully quenched and some residual fluorescence can be visualized in microscopy.

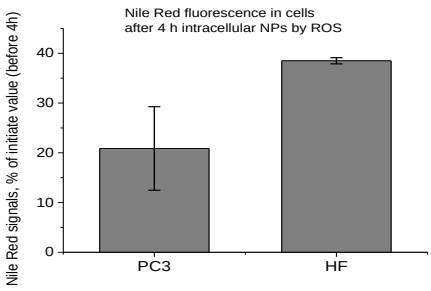

Fig. 4 Nile Red fluorescence signals from NR-loaded P-1 NPs in PC3 and HF cells after 4 h of incubation. At t0 prior to incubation, the cells had been loaded with P-1 NPs by a 2 h pre-incubation step, then the NPs were washed off (*see* ESI for methods).

To show the NR release *via* co-localization in FLIM microscopy, a second dye Alexa Fluor® 647 (Alx647) azide was covalently bound to the clickable alkyne linker of the P-1 *via* click reaction (*see* ESI, Fig. S13 and S14). NR was physically entrapped into the Alx647-labeled NPs as described previously. With two fluorophores the intracellular fate of cargo (NR) and the polymer (stained covalently with Alx647) could be tracked independently. The two dyes were visualized after separate excitation at 485 nm (NR), and 640 nm (Alx647). The co-localization of P-1 NPs and the NR cargo after 8 h incubation in PC-3 (Fig. 5a and 5b) and HF cells (Fig. 5c and 5d) was compared.

Analysis of lifetime τ (*see* ESI for method) clearly differentiated the free Nile Red (τ 4.2 ±0.3 ns, exc. at 485 nm) from the particles marked with Alx647 (τ 2.2 ±0.1 ns, exc. at 640 nm). In PC-3 cells the cytoplasm was nearly homogeneously colored with the released NR (Fig. 5a), while the polymer was clustered up in few locations (Fig. 5b). Oppositely in HF cells only little homogeneous NR fluorescence was visible outside the NPs (Fig. 5c), and the NR co-localized with the polymer to a high extent (Fig. 5d). However, after 8 h even in ROS-producing PC3 cells the NPs likely were not fully degraded and the cells still contained some Nile Red as well (*see* ESI).

In line with the findings after separate excitation, after simultaneous excitation at 485 nm and 640 nm the spread fluorescence of released NR was visible in PC-3 but barely in HF cells, and the co-localization of not-yet released NR with the particles was visible in HF but not in PC-3 cells (Fig. 6a and 6b). Furthermore, in FLIM analysis of PC-3 cells after only 1 h incubation with dual-marked P-1 NPs, NPs and Nile Red were highly co-localizing and only little released with freely distributed Nile Red was observed (Fig. S15).

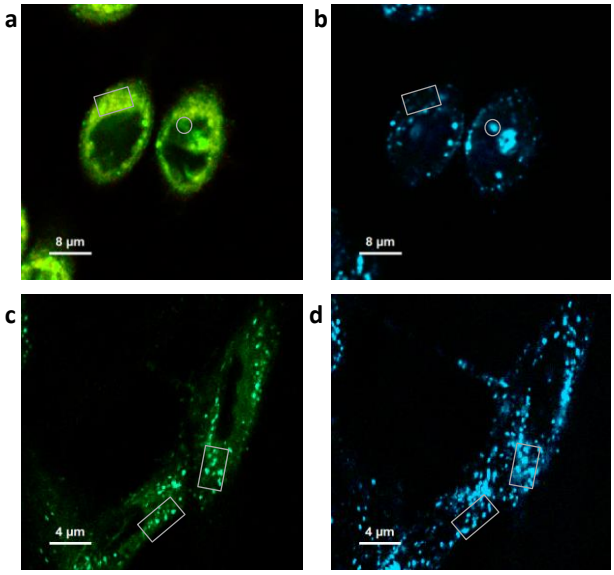

Fig. 5 FLIM microscopy of dual-marked P-1 NPs in PC-3 (a, b) and HF (c, d) cells after 8 h incubation, visualizing (released) Nile Red and polymer-bound Alx647. Fluorescence was detected after separate excitation at 485 nm (Nile Red, in a, c) and 640 nm (Alx647, in b, d). In a, b locations with high polymer content but little co-localizing NR are pointed out (circle), and *vice-versa* (square). In c, d the fluorescence patterns predominantly co-localize (squares).

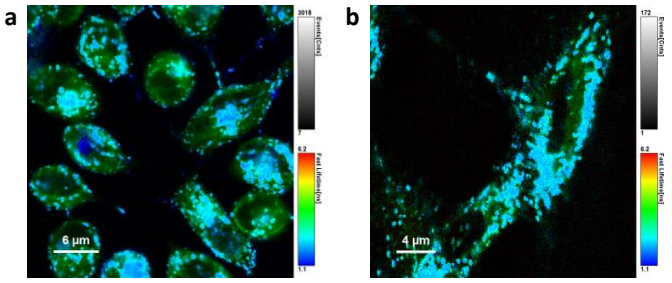

Fig. 6 FLIM images of PC-3 (a) and HF (b) cells after 8 h incubation with dual-marked P-1 NPs, color-coded by the averaged obtained lifetime per pixel. The localization of polymer (covalently bound Alx647, tau ca 2 ns, shown in blue) and of released Nile Red (spread throughout the cell, tau ca 4 ns, shown in green), and local overlap of lifetimes (turquoise tones) was visualized after simultaneous excitation at 485 nm and 640 nm.

This evidences that the P-1 polymer NPs can be used for selective cargo release to PC-3 cancer cells, with the release rate in non-cancer HF cells being lower than in the cancer cells with higher ROS levels.

Finally, to investigate the inhibitory effect on tumor cells, the ROS-responsive (P-1) and non-responsive counterpart (P-2) NPs were loaded with the antitumor drug paclitaxel (PTX) with an overall cargo content ~ 2.2 wt% and a loading efficiency of 94 % (*see* ESI). The alamarBlue® viability assay was used to evaluate the cytotoxicity of the PTX-loaded P-1 and P-2 NPs in cancer cell lines and in HF cells. For this study various cancer cell lines, which are known for increased ROS production, such as human cervix carcinoma (HeLa),[34] colorectal adenocarcinoma (DLD1)[35] and prostate cancer (PC-3)[31] cells were used and the NPs cytotoxicity compared with that found for the HF fibroblasts cells as low ROS controls (*see* ESI for methods). The drug-loaded NPs were incubated with the ROS-producing cells and with HF cells for 24 up to 72 h. Both NPs were at all times more toxic than the free drug (Fig. S17 and S19), which is generally attributed to the fact that the vast majority of freely administered drug molecules are binding to serum proteins.[36]

Tests after 24 h and 48 h comparing PC-3, HeLa and HF cells showed a roughly similar toxicity of P-1 and P-2 based NPs in the cancer cells (Fig. S17). In HF cells the ROS-responsive NPs caused a similar if not slightly lower toxicity than the P-2 NPs (Fig. S17a and S17c). Cytotoxicity of the polymer itself may be neglected at the concentrations used (*see* Fig. S18). As another test in HeLa cells had confirmed that NPs toxicity steeply increases with incubation time (raised from 12 h to 96 in HeLa cells, *see* Fig. S19), the difference in toxicity of P-1 and P-2 NPs could become more significant after longer incubation times *e.g.* under conditions of extensive ROS-triggered NPs degradation. Therefore the PC-3, HeLa and DLD1 cancer cells were incubated for 72h with P-1 and P-2 NPs, and in addition to standard cell culture conditions a second test with NPs incubated in a medium with a low serum content of 2% was performed (Fig. 7).

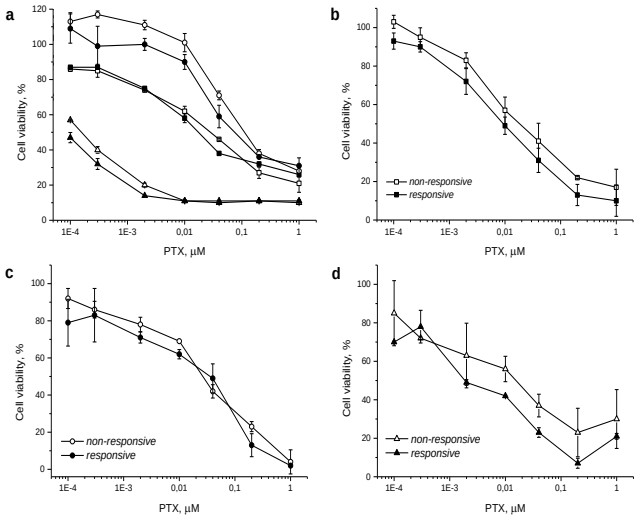

Fig. **7** Incubation of PTX-loaded ROS-responsive P-1 (filled marker) and non-responsive P-2 (hollow marker) particles with PC-3 (square), DLD1 (circle) and HeLa (triangle) cells for 72h in medium with 10% serum (a). Similar testing was done in medium with only 2% of serum, comparing again the cell lines PC-3 (b), DLD1 (c) and HeLa (d) cells after 72h incubation.

Reducing the serum content in the incubation medium is known to increase the overall uptake rate of NPs,[37] (as also observed by the authors, unpublished data), which in return might enhance the superior toxicity of P-1 NPs for cancer cells. It was found that the lower serum content caused no additional damage to the cells in Alamar Blue® assay (data not shown). In all three cancer cell lines including the experiments in medium with 2% and with 10% serum content, the toxicity of the responsive P-1 NPs was slightly higher than that of non-responsive P-2 NPs. The viability testing demonstrated herein that under the studied conditions the PTX-loaded ROS-responsive NPs appear more cytotoxic in tumor cells than their non-responsive counterpart NPs (Fig. 7).

In summary, we have shown evidence that fluorescent polymer NPs, bearing pinacol-type boronic ester linkers trigger self-immolative polymer degradation and subsequently release the cargo drug in the presence of ROS concentrations typically present in intracellular environment of certain tumor cells. Co-localization studies evidenced that the P-1 polymer NPs can be used for selective cargo release to PC-3 cancer cells, with the release rate in non-cancer HF cells being lower. Finally the drug-loaded ROS-responsive NPs were shown to be more cytotoxic to tumor cells compared to their non-responsive counterparts making the presented polymer a promising candidate for applications as delivery system and imaging agent (theranostics) aimed at inflamed microenvironments and cancer tissue.

Acknowledgements

Financial support of the Norwegian Funds (grant # 7F14009), Ministry of Industry and Trade of the Czech Republic (grant # FR-TI4/625) and of the Ministry of Education, Youth and Sports (grant # LH14292) is gratefully appreciated. The electron microscopy at the Institute of Macromolecular Chemistry was supported through grant TE01020118.

Notes and references

1 Y. Wu, D. Zhou, Y. Qi, Z. Xie, X. Chen, X. Jing and Y. Huang, *RSC Adv.*, 2015, **5**, 3523.
2 H. Cho, J. Bae, V.K. Garripelli, J.M. Anderson, H.-W. Jun and S. Jo, *Chem*. *Commun*., 2012, **48**, 6043.
3 S. Petrova, E. Jäger, R. Konefal, A. Jäger, C.G. Venturini, J. Špěváček, E. Pavlova and P. Štěpánek, *Polym*. *Chem*., 2014, **5**, 3884.
4 H. Chen, W. He and Z. Guo, *Chem*. *Commun*., 2014, **50**, 9714.
5 H.-L. Pu, W.-L. Chiang, B. Maiti, Z.-X. Liao, Y.-X. Ho, M. S. Shim, E.Y. Chuang, Y. Xia and H.-W. Sung, *ACS Nano* 2014, **8**, 1213.
6 D. Lee, S. Khaja, J.C. Velasquez-Castano, M. Dasari, C. Sun, J. Petros, W.R. Taylor and N. Murphy, *Nat*. *Mater*., 2007, **10**, 765.
7 B. D'Autréaux and M. B. Toledano, *Nat*. *Rev*. *Mol*. *Cell*. *Bio*., 2007, **8**, 813.
8 A. Mantovani, P. Allavena, A. Sica and F. Balkwill, *Nature* 2008, **454**, 436.
9 S. Reuter, S.C. Gupta, M.M. Chaturvedi and B.B. Aggarwal, *Free Radic*. *Biol*. *Med*., 2010, **49**, 1603.
10 N. Houstis, E.D. Rosen and E.S. Lander, *Nature* 2006, **440**, 944.
11 B. Uttara, A.V. Singh, P. Zamboni and R.T. Mahajan, *Curr*. *Neuropharmacol*., 2009, **7**, 65.
12 S. Toyokuni, K. Okamoto, J. Yodoi and H. Hiai, *FEBS Lett*., 1995, 358, 1.
13 T. P. Szatrowski and C. F. Nathan, *Cancer Res*., 1991, **51**, 794.
14 G.-Y. Liou and P. Storz, *Free Radic*. *Res*., 2010, **44**, 479.
15 G. Waris and H. Ahsan, *J*. *Carcinog*., 2006, **5**: 14.
16 P.T. Schumacker, *Cancer Cell* 2006, **10**, 175.
17 M. López-Lázaro, *Cancer Lett*., 2007, **252**, 1.
18 W. Dröge, *Physiol*. *Rev*., 2002, **82**, 47.
19 B. Kumar, S. Koul, L. Khandrika, R. B. Meacham and H. K. Koul, *Cancer Res*., 2008, **68**, 1777.
20 E. Lallana and N. Tirelli, *Macromol*. *Chem*. *Phys*., 2013, **214**, 143.
21 C. de G. Lux, S. Joshi-Barr, T. Nguyen, E. Mahmoud, E. Schopf, N. Fomina and A. Almutairi, *J*. *Am*. *Chem*. *Soc*., 2012, **134**, 15758.
22 M.S. Shim and Y. Xia, *Angew*. *Chem*. *Int*. *Ed*., 2013, **52**, 6926.
23 E.A. Mahmoud, J. Sankaranarayanan, J.M. Morachis, G. Kim and A. Almutairi, *Bioconjugate Chem*., 2011, **22**, 1416.
24 D. Jeanmaire, J. Laliturai, A. Almalik, P. Carampin, R. D'Arcy, E. Lallana, R. Evans, R.E.P. Winpeny and N. Tirelli, *Polym*. *Chem*., 2015, **5**, 1393.
25 A. Savina, A. Peres, I. Cebrian, N. Carmo, C. Moita, N. Hacohen, L.F. Moita, and S, Amigorena, *Immunity* 2009, **30**, 544.
26 E. Jäger and F.C. Giacomelli, *Curr*. *Top*. *Med*. *Chem*., 2015, **15**, 328.
27 F.C. Giacomelli, P. Štěpánek, C. Giacomelli, V. Schmidt, E. Jäger, A. Jäger and K. Ulbrich, *Soft Matter* 2011, **7**, 9316.
28 A. Jäger., D. Gromadzki, E. Jäger, F.C. Giacomelli, A. Kozlowska, L. Kobera, J. Brus, B. Říhová, M. El Fray, K. Ulbrich, P. Štěpánek, *Soft Matter* 2012, **8**, 4343.
29 T. Hu and C. Wu, *Phis*. *Rev*. *Lett*., 1996, **83**, 4105.
30 J. Fu and C. Wu, *J*. *Polym*. *Sci*., *Part B*: *Polym*. *Phys*., 2001, **39**, 703.
31 B. Kumar, S. Koul, L. Khandrika, R. B. Meacham and H.K. Koul, *Cancer Res*., 2008, **68**, 1777.

32 U. E. Martinez-Outschoorn, R. M. Balliet, Z. Lin, D. Whitaker-Menezes, A. Howell, F. Sotgia and M. P. Lisanti, *Cell Cycle* 2012, **11**, 4152.
33 M. P. Lisanti, U.E. Martinez-Outschoorn, Z. Lin, S. Pavlides, D. Whitaker-Menezes, R.G. Pestell, A. Howell and F. Sotgia, *Cell Cycle* 2011, **10**, 2440.
34 R.S. Bhimani, W. Troll, D. Grunberger and K. Frenkel, *Cancer Res*., 1993, **53**, 4528.
35 J.M. Lluis, F. Buricchi, P. Chiarugi, A. Morales, J.C. Fernandez-Checa, *Cancer Res*., 2007, **67**, 7368.
36 D.A. Smith, L. Di and E.H. Kerns, *Nat*. *Rev*. *Drug Discov*., 2010, **9**, 929
37 G. Baier, C. Costa, A. Zeller, D. Baumann, C. Sayer, P.H. Araujo, *Macromol*. *Biosc*., 2011, **11**, 628.

